PICKERING EMULSIONS AS TEMPLATES FOR SMART COLLOIDOSOMES

A Dissertation
Presented to
The Academic Faculty

by

Adriana San Miguel Delgadillo

In Partial Fulfillment
of the Requirements for the Degree
Doctor of Philosophy
in the School of Chemical & Biomolecular Engineering

Georgia Institute of Technology
December, 2011

PICKERING EMULSIONS AS TEMPLATES FOR SMART COLLOIDOSOMES

Approved by:

Dr. Sven Holger Behrens, Advisor
School of Chemical and Biomolecular Engineering
Georgia Institute of Technology

Dr. Yulin Deng
School of Chemical and Biomolecular Engineering
Georgia Institute of Technology

Dr. Carson Meredith
School of Chemical and Biomolecular Engineering
Georgia Institute of Technology

Dr. Eric Weeks
School of Physics
Emory University

Dr. Hang Lu
School of Chemical and Biomolecular Engineering
Georgia Institute of Technology

Date Approved: July 22, 2011

To my brother, for inspiring me; my parents, for supporting me; and my husband for encouraging me; to always reach further.

ACKNOWLEDGEMENTS

There are many people who have contributed and made an impact on the development of this work. I would like to thank every person that was part of the Behrens group during the last four years; each one of them has helped me learn in one way or the other. I would like to especially thank my lab mates Qiong Guo, Virendra Singh, Carlos Espinosa and Hongzhi Wang for many interesting discussions, not always about colloids. I would also like to acknowledge Dr. Jan Scrimgeour and Dr. Jennifer Curtis for their valuable help, which was crucial for the development of part of this work. Additionally, I would like to thank the members of my committee for their assistance, interest and time through the completion of this work.

I am very grateful to my advisor, Dr. Behrens, for sharing his enthusiasm for science and inspiring a bit in me, and for giving out all the knowledge possible every time. I would like to thank him for the patience, and for always trusting that I would make things work, eventually.

Finally, I would like to thank my family for their always unconditional support and freedom throughout the years, which has been essential in making difficult decisions that come with every undertaking. Especially, I would like to thank my husband, whose encouragement during hard times greatly helped me to keep perspective and move forward, for all the support given since the very beginning and until today.

TABLE OF CONTENTS

LIST OF TABLES

LIST OF FIGURES

LIST OF SYMBOLS

ε	Dielectric constant
θ	Contact angle
α	Weighing parameter in FRAP recovery curve
τ	Diffusion/permeation time constant
λ	Wavelength
ζ	Zeta Potential
Ω	Ohms
I_0	Bessel function of the 0^{th} order
I_1	Bessel function of the 1^{st} order
r	Roughness, ratio of surface area to projected surface area
Rms	Root-mean-squared roughness
R^2	Coefficient of Determination
f	Fraction of surface area in contact with liquid, in Cassie-Baxter wetting
Φ	Ratio of emulsion to separated phases remaining after centrifugation
γ	Interfacial tension
ΔG_{int}	Gibbs free energy of particle adsorption at a liquid-liquid interface
ρ	Density
g_c	Centrifugal field acceleration
V	Volume
A	Area
P_C^{max}	Maximum capillary pressure

LIST OF ABBREVIATIONS

wt/v	Weight/Volume
v/v	Volume/Volume
Da	Dalton
CV	Coefficient of Variance
MW	Molecular weight
PEO	Poly(ethylene oxide)
PPO	Poly(propylene oxide)
DCM	Dichloromethane
PVA	Poly(vinyl alcohol)
PEI	Poly(ethylene imine)
PDADMAC	Poly(diallyldimethylammonium chloride)
PMMA	Poly(methyl methacrylate)
PNIPAM	Poly-(n-isopropylacrylamide)
APTES	3-Aminopropyl triethoxysilane
FITC	Fluorescein isothiocyanate
FRAP	Fluorescence Recovery After Photobleaching
DLS	Dynamic Light Scattering
SEM	Scanning Electron Microscopy
AFM	Atomic Force Microscopy
W/O	Water-in-oil
O/W	Oil-in-water
W/O/W	Water-in-oil-in-water
pI	Isoelectric point

SUMMARY

Encapsulation is a widely used formulation tool in many areas where substances need to be delivered to a target medium while being protected from the surrounding environment until delivery conditions are reached. Some applications include drug delivery, taste and odor masking, fragrance encapsulation, and encapsulation for bio-active molecules and cells.

A novel type of microcapsules has been recently developed with great promise as a microencapsulation vehicle. This new type of capsules, known as colloidosomes, have a shell made up of individual colloidal particles as building blocks and are generated from Pickering emulsion templates. In this work, the first example for stimulus-responsive colloidosomes which completely dissolve upon a mild pH change is shown.

Stimulus-responsive nanoparticles that dissolve upon a mild pH increase are used as stabilizers for Pickering emulsions which serve as templates for the production of pH-responsive colloidosomes. Eudragit S-100, an enteric coating material, is used to synthesize the stimulus-responsive nanoparticles by a simple nanoprecipitation method.

These particles have been applied as sole stabilizers for a double water-in-oil-in water emulsion, where the middle phase is an easily extractable oil. The double emulsion-solvent extraction approach allows the generation of colloidosomes with a higher yield and encapsulation efficiency than typical single-emulsion methods. Removal of the middle oil phase by evaporation produces water-core colloidosomes that have a shell made of pH-responsive nanoparticles, which rapidly dissolve upon a mild pH change.

The permeability of these capsules, prior to the stimulus, was assessed by FRAP, whereby the diffusion of a fluorescent tracer through the capsule shell is monitored. In this work, a new model for a FRAP recovery curve is developed, which allows

significantly improved fits. Furthermore, this new model makes FRAP suitable for characterizing microcapsules of any size and permeability, greatly expanding its applicability for microcapsule permeability measurements.

In order to optimize the pH-responsive colloidosomes, three methods for tuning their permeability have been developed; these include ethanol consolidation, layer-by-layer assembly and the generation of PLGA-pH-responsive nanoparticle hybrid colloidosomes. The resulting colloidosomes have different responses to the pH stimulus, as well as different pre-release permeability values. The aforementioned permeability tuning methods provide a variety of pH-responsive colloidosomes, with varying degrees of pre-release permeability and different response to a pH-stimulus.

Previous examples of colloidosomes did not include the necessary characteristics for applying them as efficient microencapsulation vehicles: high yield, high encapsulation efficiency, stimulus-response, and high retention (low permeability). This work greatly advances the field of microcapsule generation from Pickering emulsion templates, by showing a variety of smart colloidosomes with a dissolution trigger, solving the lacking points of previously developed colloidosomes. With these developments, the application of colloidosomes as efficient microencapsulation vehicles can be made possible. Furthermore, this work can lead the way to generation of colloidosomes with new and multiple functionalities.

The generation of colloidosomes is still, however, a complex problem where many simultaneous requirements need to be met and where many fundamental mechanisms play a role. Some of these underlying physico-chemical mechanisms are studied on passing, such as the effect of ionic strength and pH on Pickering emulsions. With the purpose of increasing the knowledge in some of these areas, important not only for colloidosome generation but also for Pickering emulsification in general, an in-depth study regarding the role of particle surface roughness on Pickering emulsion stability is also developed. This topic is selected since it is lacking controlled experimental evidence.

Additionally, the pH -responsive nanoparticles synthesized and used as building blocks for the colloidosomes provided a unique opportunity to generate an experimental scheme that would allow this study in a systematic way.

The Eudragit S-100 pH-responsive nanoparticles were used as a coating for larger silica particles, producing rough raspberry-like particles. Partial dissolution of the nanoparticle coating allows tuning of the substrate surface roughness while retaining the same surface chemistry. Macroscopic flat substrates with the same coating and treatment as the silica particles were generated as models for quantifying surface roughness and contact angle. These data is representative of the roughness and wettability of the rough and smooth particles.

Interesting results regarding the effects of surface roughness on long-term emulsion stability were obtained by emulsion centrifugation studies. These results show that surface roughness increases the emulsion stability of decane-water systems (to almost twice), but only up to a certain point, where extremely rough particles produced less stable emulsions presumably due to a Cassie-Baxter wetting regime. Additionally, in an octanol-water system, surface roughness was shown to affect the type of emulsion generated.

These results are of exceptional importance since they are the first controlled experimental evidence regarding the role of particle surface roughness on Pickering emulsification, thus clarifying some conflicting ideas that exist regarding this issue. This work significantly advances the knowledge of Pickering emulsion stability regarding particle surface roughness, and provides a new parameter in Pickering emulsification. Certainly, many more studies that deal with the wetting regimes of particles at liquid-liquid interfaces, the dynamics of wetting and emulsification and the role of surface roughness on other systems are to be expected in the future, led by the work developed here.

CHAPTER 1

INTRODUCTION

Encapsulation is a widely used formulation tool in many areas where substances need to be delivered to a target medium while being protected from the surrounding environment until delivery conditions are reached. Drug delivery may be the most obvious example but there are many others. The most outstanding illustrations of encapsulation can be found in nature itself in such forms as egg shells, plant seeds and sea shells [*1*]. Microscopic examples of encapsulation by nature also exist, including diatoms, coccolithopores, radiolarian, pollen grains and bacterial spores [*1, 2*]. Cells themselves are examples of microencapsulation, where the membrane not only protects but also allows the passage of some molecules by selective permeability. Microencapsulation is useful for many applications; it can increase the effectiveness of delivery [*3, 4*], and ensure controlled or triggered release.

Micron-scale encapsulation finds use not only in the pharmaceutical field and in biology, but also in the food industry, textile treatment and laundering, in agriculture, cosmetics [*5*] and adhesives. Some examples include taste and odor masking, electronic ink paper, fertilizers and herbicides, fragrances, dyes, perfumes for textiles and scratch-and-sniff prints [*6*] as well as for applications involving advanced technology such as phase-change materials for thermal energy storage [*7*] and the encapsulation of enzymes, vitamins and plant or animal cells [*1, 8*]. The field of microencapsulation, which is only about 30 years old [*1, 9*], keeps growing along with the development of active ingredients and new materials.

The necessity of encapsulating a substance in some instances implies that it needs to be released at specific target conditions. Sometimes selective permeability is desired,

like in the case of cell or enzyme encapsulation. In this way, islets of Langerhans have been encapsulated with the intention of creating an artificial pancreas [*10*].

The conditions for release, either triggered or controlled, according to the target environment, can be engineered by choosing the shell properties. Initial encapsulation methods required the shell to be mechanically disturbed for the inner material to be released [*1, 9*]. Nowadays, the shell's constituents include polymers, inorganic materials, lipids, sugars and natural gums. Advances in material science allow us to use coatings which might respond to external stimuli, releasing the contents on demand. These triggers could be a change in pH, temperature, ionic strength (osmotic shock), or light intensity (irradiation) that causes a response in the material.

There are many methods of encapsulation and most of them rely on template-assisted self-assembly, where the shell material is assembled on a template such as a particle or an emulsion droplet. One such method uses solid-stabilized emulsions, so-called "Pickering Emulsions", as the template for producing a microcapsule whose shell is composed of colloidal particles. Typical emulsions are stabilized by surface active molecules (surfactants), while solid-stabilized emulsions rely on particles trapped at the interface to stabilize droplets against coalescence. These have the advantage of increased stability and of replacing potentially hazardous surfactants with inert particles. A variety of self-assembled particle structures from Pickering emulsions were developed in the pioneering work of Velev et al. [*11*], such as hollow microspheres composed of latex particles. Dinsmore et al. have called this type of capsules "colloidosomes" [*12, 13*] in analogy to polymersomes and liposomes. The idea of encapsulating substances in this type of structures appears to be very promising due to the potential advantages of using Pickering emulsion templates, which include: 1) increased capsule sturdiness, since the shell is constructed with solid particles as building blocks; 2) defined porosity, determined by the interstices between monodisperse particles forming the shell and 3) access to all the functionalities offered by modern particle technology.

The main focus of this work is geared towards developing microcapsules with a triggered response using solid-stabilized emulsions as templates, while understanding some of the fundamental underlying mechanisms that allow the generation of solid-stabilized emulsions in the first place. This objective is described in more detail in the following section. An overview of relevant scientific knowledge behind Pickering emulsification and encapsulation, as well as current developed methods for microencapsulation is included next.

1.1. Objective and Approach

The foremost objective of this work is to employ solid-stabilized emulsions as templates for fully functional stimulus-responsive microcapsules. Successful production of this type of microcapsules depends on many requirements. These considerations include stimulus-responsive materials and particles, Pickering emulsion stabilization with responsive particles, and the different routes that can be taken to generate microcapsules from emulsion templates.

In addition to the generation of fully functional stimulus-responsive colloidosomes, crucial fundamental mechanisms that allow Pickering emulsification, leading to a rational design of solid-stabilized emulsions and microcapsules, are also studied. Some of these, such as the role of charge and screening on emulsification, will be briefly touched on as the responsive colloidosomes are developed. However, many of the crucial fundamental mechanisms that allow Pickering emulsification and microencapsulation are far from understood. Specifically, the role that particle surface roughness plays on Pickering emulsification has been the least addressed by the scientific community due to the difficulty in generating an experimental method that allows systematic studies in this regard. Here, the role of particle surface roughness on Pickering emulsification is selected for an in-depth study not only due to its importance as a crucial

mechanism in solid-stabilized emulsions, but also since the pH-responsive nanoparticles used in the generation of stimulus-responsive colloidosomes provide a unique opportunity to create an experimental method for the systematic study of particle surface roughness and emulsification.

Thus, this work pursues two main research objectives:

1) Development of pH-responsive microcapsules from solid stabilized emulsions, as a proof of principle of Pickering emulsion-based fully functional microcapsules.
2) Fundamental study of a still widely unexplored crucial mechanism in Pickering emulsions: the role of particle surface roughness on emulsion stabilization.

An overview of relevant scientific knowledge behind Pickering emulsion stability, stimulus-responsive materials and particles, and surface roughness is presented next.

1.2. Scientific Background

1.2.1. Solid-stabilized emulsions and microencapsulation

1.2.1.1. Pickering emulsions

Although first described by Ramsden [*14*], solid-stabilized emulsions, were first studied by Pickering in 1907 with particles composed of lime, plaster, chalk, silica or alumina [*15*]. A wide range of particles has been applied for Pickering emulsions since then, such as metallic, glass and polymeric particles. These particles adsorb to the liquid-liquid interface formed upon agitating two immiscible liquids, and provide a barrier to droplet coalescence [*16*].

Particle adsorption to liquid-liquid and liquid-air interfaces results in a reduction in interfacial area, which is in turn replaced by particle-oil and particle-water interface [*17*]. The difference in surface energies determines the particle equilibrium position at the interface, which is described by the contact angle and is an indicator of the phase the particle is preferentially wetted by. When the particles have the right wettability, this adsorption results in a reduction in free energy.

By convention, the 3-phase contact angle formed by a particle and an oil-water interface is measured through the water phase, such that hydrophilic particles will have small contact angles ($\theta<90°$) and particles preferentially wetted by the oil have larger contact angles ($\theta>90°$). Bancroft proposed in 1913 [*18*], that hydrophilic particles tend to make oil-in-water emulsions, while hydrophobic particles tend to make water-in-oil emulsions [*19, 20*]. This is a still widely accepted idea, with recent theoretical support from the work of Kaptay [*21*]. This concept is better illustrated in **Figure 1.1**.

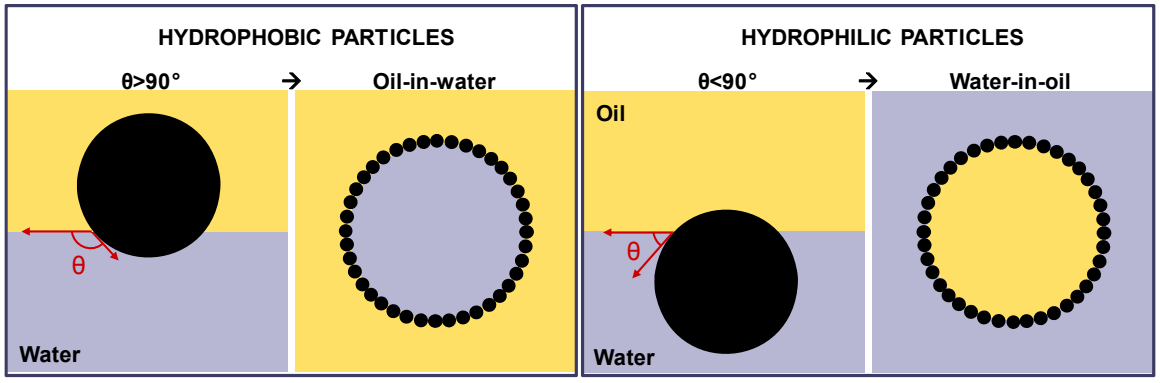

Figure 1.1 Particle contact angle and preferred emulsion type

The energy of attachment of a particle to the interface depends on the interfacial tension and contact angle, and it can be several orders of magnitude larger than thermal energy. The energy of attachment for a planar interface is given by [*16*]:

$$-\Delta G_{int} = \pi r^2 \gamma_{ow}(1 \pm cos\theta_{ow})^2 \qquad Eq.\ (1)$$

where r is the particle radius, γ_{ow} is the interfacial tension and θ_{ow} is the three phase contact angle. The positive sign in the bracket applies to desorption of the particles into the oil phase and the negative sign to desorption of the particles into the water phase (due to the typical convention of measuring contact angle through the water phase).

Even though true nanoparticles as small as 4.2 nm have been observed to attach to a water-toluene interface and stabilize droplets [*22*], the desorption energy is markedly decreased for small particles[*17*]. Lin et al. [*22, 23*] showed that larger particles will displace smaller particles exponentially with time. Particles of at least tens of nanometers in size, however, tend to be trapped irreversibly at the interface.

A micron-sized particle with $\theta_{ow} = 90^o$ at a typical non polar oil-water interface (γ_{ow}~50 mN/m) is trapped in an energy well of about 10^6 kT [*16*]. For a 10 nm silica particle at the water-toluene interface, $-\Delta G_{int}$ can vary from 2750 kT for $\theta_{ow} = 90^o$ to <10 kT for θ_{ow} between 0 and 20^o. The highest energy of adsorption will thus be accomplished when the contact angle of the particles is around 90^o.

The contact angle is important not only for the energy of adsorption, but also since the particle wettability determines the type of emulsion generated for a specific system, as previously mentioned. The type of emulsion (o/w or w/o) consistent with Bancroft's contact angle rule is known as the "preferred emulsion type", which is the emulsion type expected for 50:50 mixtures of the liquid phase. Emulsions of this type can have excellent long term stability and are insensitive to dilution with the continuous phase liquid. Increasing the volume fraction of the dispersed phase well above 50% under mixing, however, eventually leads to a so-called "catastrophic phase inversion" [*19, 20, 24-26*]. Asymmetric mixing ratios thus allow the formation of inverted, "disfavored type" emulsions [*19*], but these tend to be rather unstable against coalescence.

Alternatively, the (stable) emulsion type can be controlled by varying the contact angle. In a specific water-oil system, the contact angle can be modified through the particle surface properties, either by attaching molecules to the surface of by screening surface charges [*19*]. The oil type can also affect emulsification [*19, 26-28*] as the particle contact angle differs among oils. It has been shown that for the same type of particles, the type of emulsion created depends on the oil [*20*]. Binks et al. studied emulsification with hydrophobic silica particles and different oils. The work of adhesion, ($W_a = \gamma_{oa} + \gamma_{aw} - \gamma_{ow}$), as well as θ_{ow} consistently increased with oil polarity. Non-polar oils gave o/w, while more polar oils gave w/o emulsions, thus the particles behave more hydrophobic as the polarity is increased[*20*]. This is not surprising, if we take into account that the particles have hydrophilic SiOH groups on the surface, which should interact more favorably with polar oils than with non-polar oils. Read et al. [*27*] also observed a different behavior with polar and non-polar oils when charge-stabilized particles were used. Additionally, in the emulsions context, it has also been shown that the phase where the particles are first dispersed tends to be favored as the continuous phase [*19, 20*].

Surface charge is also an important factor. Particles that carry charge on their surface are electrostatically stabilized in aqueous environments. Thus, tuning the charge density of charge-stabilized particles either by pH or ionic strength can lead to changes in wettability (contact angle) and thus emulsion type [*19, 26, 27, 29*]. It has also been shown that highly charged states of negatively charged particles increase stability [*26, 27*].

Surface charge, though, is difficult to manipulate separately from charge screening. A change in pH or ionic strength should affect not only the surface charge of the particle, if chargeable groups exist, but also screen inter-particle interactions which can also lead to changes in emulsion behavior. It is known that the oil-water interface is negatively charged, at least for non-polar oils [*30, 31*], which sets up an electrostatic barrier for adsorption to the interface. Such barrier can be suppressed by the addition of electrolyte, which will also affect the wettability of the particles [*29*]. Above a certain

ionic strength it will also suppress the double-layer repulsion between particles, leading to particle aggregation [*32*].

Golemanov et al. [*32*] proposed that the phenomenon of particles going to the interface represents a kind of flocculation. They showed that the type of salt has an effect according to the Schulze-Hardy rule, which predicts that the critical coagulation concentration will go as $^{1}/_{z^{6}}$, where z is the valency of the salt. The presence of the electrolyte required to screen the charge at the interface, could also lead to particle aggregation, thus explaining why slightly flocculated particles have been found to be better emulsion stabilizers [*33*]. Surface charge and screening has also been suggested as a factor determining the extent of droplet coverage with particles by tuning inter-particle repulsion. For example, Gautier et al. [*34*] have found that emulsion droplet coverage can be tuned from highly covered to weakly covered by changing the pH.

For bulk emulsification, particle concentration has also been shown to play a role in the final droplet size. As the particle concentration is increased, the droplet size is decreased [*19, 26, 27*]. This is attributed to the fact that at lower particle concentrations, the particles do not immediately cover the droplets, and therefore some of the droplets will coalesce, increasing the average size.

1.2.1.1.1 Pickering emulsion stability

Typically, the most widely used expression to explain the high emulsion stability observed with solid-stabilized emulsions is the expression for the energy of adsorption shown before, Eq. (1). This equation alone suggests that larger particles with contact angles close to 90º are the best emulsion stabilizers.

In reality, there are additional considerations to be taken into account, which have been mainly overlooked in the Pickering emulsion studies. These considerations include the fact that droplet coalescence involves thinning and rupture of the continuous phase

between two approaching droplets. The stability of these films, has been described by various authors [*21, 35-41*] in terms of the maximum capillary pressure, P_C^{max}. This parameter represents the maximum pressure that a film stabilized by particles can be subjected to before breaking. **Figure 1.2** illustrates the breaking of a thinning emulsion film between two particle-stabilized droplets.

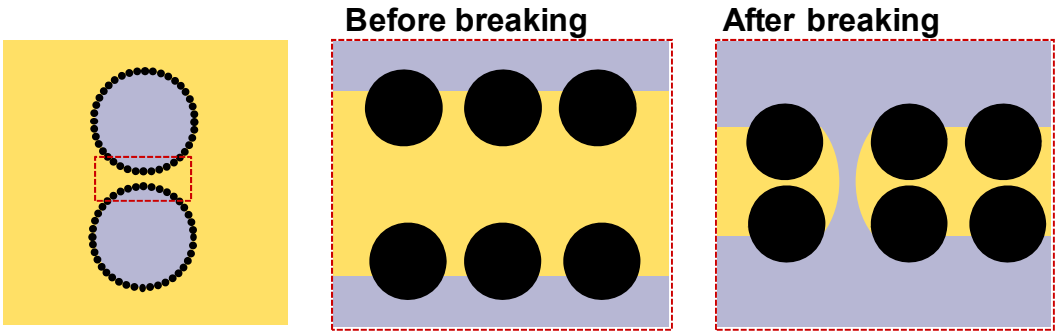

Figure 1.2. Thinning emulsion film between two particle-stabilized droplets before and upon breaking

Although several equations for P_C^{max} have been developed, depending on the packing and number of particle layers stabilizing the film (monolayer vs bilayer), the most general expression, derived by Kaptay [*21*] takes the form:

$$P_C^{max} = \pm p \frac{2\gamma_{ow}}{r} \cos(\theta \pm z) \qquad \textit{Eq. (2)}$$

where p and z are parameters describing the arrangement and packing of the particle layers; these values are typically constant for a specific situation (i.e., a range of contact angles and mono- or bi-layer of particles). The + sign is applied for o/w emulsions and the – sign is applied for w/o emulsions. In contrast to the predictions based purely on the energy of adsorption, the maximum capillary pressure predicts more stable films when smaller particles are used, and when the contact angles are further from 90º. In reality, emulsion stability should be described by a combination of both mechanisms. The

maximum capillary pressure becomes more important in the case where particles are expected to show contact angle hysteresis, as with rough particles [*41*]. As previously mentioned, this topic is described further in section 1.2.2 of this chapter.

1.2.1.2. Multiple Pickering emulsions

Multiple emulsions, or emulsions of emulsions, are systems where the dispersed phase of an emulsion is itself an emulsion. These systems require the presence of two different types of surfactant, one more hydrophobic and one more hydrophilic, to stabilize both type of emulsions. Double emulsions have been widely used as templates for microencapsulation and are thus important in this work.

One problem of multiple emulsions is that they tend to evolve into single emulsions by coalescence. Particles have been thus been applied to increase the stability of the outer emulsion [*19*]. Barthel et al. have successfully produced multiple emulsions stabilized solely by particles [*42*]. Examples are shown only for hydrophobized silica particles as stabilizers and oils such as toluene and triglyceride oil. Lee and Weitz [*43*] have also created double emulsions (w/o/w) stabilized by hydrophobic silica particles. In this case, the particles are dispersed in the oil phase (toluene). Even though the inner and the outer aqueous phase contain 2% Poly(vinyl alcohol), it is claimed that the emulsions are particle stabilized since the emulsions were not stable without the addition of particles.

Just as classical multiple emulsions, purely particle-stabilized multiple emulsions would require two different types of emulsifiers, with different degree of hydrophilicity/hydrophobicity for stabilizing the inner and outer emulsion. For those examples where both emulsions are stabilized solely by particles, different types of particles are used (silica of different hydrophobicity).

1.2.1.4. Colloidosomes: Pickering emulsion-based microcapsules

The production of colloidosomes was first introduced by Velev et al. [*11*] in a series of studies where different type of structures were made by taking advantage of the self-assembly properties of particles on droplets. The structures produced included microstructured hollow spheres [*11*] (i.e. colloidosomes). Such structures were created by making an octanol-in-water emulsion stabilized by latex particles. The particles were then locked together by flocculation adding HCl and $CaCl_2$. Upon interface removal by extraction of the oil with a co-solvent, empty spheres composed of latex colloidal particles were obtained [*11*]. The reversed system, water- in-oil, was also created and colloidosomes with some extra particles inside the capsules were generated [*44*]. Ball like aggregates of a defined size were also obtained after extracting the oil of a droplet phase containing dispersed particles [*45*]. This same structure was successfully coated with sulfate polystyrene particles to obtain a "composite supraparticle", which consisted of a shell of sulfate latex particles and a core of amidine latex particles [*45*] .

Dinsmore et al. [*12*], who coined the term colloidosomes, obtained this type of microcapsules by transferring particle-stabilized water droplets into oil. Additional locking methods were explored, such as sintering or the addition of a binding agent (poly-L-lysine). Hsu et al. [*13*] later tested different locking methods by measuring the mechanical strength of the capsules. Not surprisingly, sintering yield the most robust capsules.

From these first experiments, a large variety of colloidosome microcapsules have been developed [*4*]. Some of the most relevant examples include colloidosomes with sintered shells, gel-core and even monodisperse colloidosomes. Yow and Routh [*46*] have created colloidosomes with polystyrene particles from w/o and o/w Pickering emulsions. The particles were sintered, and different pore sizes were obtained depending on time and temperature of sintering, which permits tuning of the microcapsule's release profile. Monodisperse colloidosomes have also been created by Lee et al. [*43*] from

double emulsions by extracting the oil of a water-in-oil-in-water emulsion, where the particles are initially dispersed in the oil phase. In this case, hydrophobic silica and magnetic nanoparticles were used in a microfluidic device setup. Additionally, Paunov et al. created colloidosomes with a gelled aqueous core to trap the particles by gelation upon cooling [*47*]. Colloidosomes have also been accomplished with polymeric microrods made of photoresist (SU-8) [*48*] obtaining the so-called "hairy colloidosomes". Ao et al. [*49*] generated hybrid colloidosomes by integrating a dissolved polymer and particles in the middle phase of a double emulsion. Colloidosomes have been made from a wide variety of materials [*50*], such as inorganic silica particles [*51*], magnetic nanoparticles, polystyrene or PMMA particles [*11, 12, 43*].

Colloidosomes have been proposed as a microencapsulation technique with great promise [*4, 11-13, 52*] for controlled delivery applications. General advantages of this encapsulation route include the achievable sturdiness and defined porosity of the resulting capsule. Colloidosome shells can be very robust [*12, 13*], since their building blocks are solid particles instead of initially dissolved molecules. Moreover, the packing of same size particles in the capsule shell results in a defined pore size and size-selective permeability.[*12, 13*] Even some examples of stimulus responsive colloidosomes have been shown, [*53-56*] most of them responding to a temperature variation by a volume change. Although widely explored, and very promising as encapsulation vehicles, colloidosomes applied as efficient microencapsulation alternatives, with stimulus-triggered release and tuned permeability have not been shown yet.

1.2.1.5. Other encapsulation methods

Emulsion Solvent Extraction

This widely known method is based on producing an emulsion in which one of the phases is a solvent that can be extracted by evaporation or by dilution. This solvent should also be able to dissolve the polymer which will form the capsule shell or matrix. This method has mainly been studied for pharmaceutical applications and even for DNA loading for gene delivery [*57*] in PLGA-PEI nanoparticles. Solid-in-oil-in-water dispersions have also been used by Wang et al. [*58*], who encapsulated human immunoglobulin G (IgG) in PLGA to reduce protein denaturation.

This method has been used to a larger extent in double emulsions, as first described by Vrancken et al. [*59*], as double emulsion-solvent extraction. The method consists of a w/o/w emulsion, where a polymer is dissolved in the oil that can be removed by evaporation. Polystyrene capsules were produced encapsulating thiourea and dyestuff Acid Magenta A as the first examples. Later on, Ogawa et al. [*60*] modified the process and used only biodegradable polymers such as Poly(Lactic-co-glycolic acid), PLGA, and Poly(lactic acid), PLA, where Leuprolide Acetate was encapsulated [*3*].

This w/o/w method is suitable for encapsulating water soluble drugs like peptides, proteins and vaccines. In many cases, the shells are found to be porous [*58, 61-63*] due to fast solvent evaporation. Cayre and Biggs [*64*] found that the faster the rate of extraction, the larger the pores. This was also observed by Routh and Yow [*65*] who in this way obtained "colloidal buckets", where capsules have a single large hole in the shell. This method has also been applied to create microcapsules of pH-responsive polymers such as Eudragit, which dissolves at high pH but not at low pH. These capsules have been generated with the emulsion solvent extraction method by several templates like w/o [*61, 62*], w/o/o [*63*] , o/o [*66, 67*] and by w/o/w [*68, 69*]. In most cases, although the polymers dissolve at high pH, some of its content is released at very low pH [*61-63, 68, 69*].

Layer by layer assembly:

This method consists of coating a sacrificial template with a semipermeable membrane that is made of polyelectrolytes [*9, 70, 71*]. Layers of positively and negatively charged polyelectrolytes are assembled onto each other, creating the shell of the microsphere. The layer-by-layer assembly technique has been used Caruso et al. [*51*] to form hollow microspheres by alternating layers of silica and PolyDADMAC. Most of the times, the encapsulated material is used as a template, such as dye or enzyme crystals. Some examples include crystallized catalase [*72*] and ibuprofen [*71*]. This process requires thorough washings between the deposition of layers in order to obtain layering instead of coagulation.

Interfacial Polymerization and Precipitation:

In these methods, a solid material precipitates at the interface of emulsion droplets. Such material might come from phase-separation, complexation or a polymerization reaction, where one of the monomers is dissolved in the dispersed phase and the other is dissolved in the outer phase, at contact a polymer membrane is created [*6*]. Interfacial polymerization has been recently applied in a combination with Pickering emulsification [*73, 74*] to produce robust hybrid microcapsules.

Smaller scale structures, vesicles:

Amphiphilic molecules self assemble into structures such as micelles and vesicles, which include polymersomes, liposomes and peptosomes [*75*].The perfect example is the cell's membrane, which is made of a bilayer of natural amphiphiles of only a few nanometers [*76*]. The encapsulation procedure in vesicles is usually through solubilization by amphiphilic species. In this way, CdTe quantum dots, carotene, vitamin E and cancer therapy dugs have been solubilized in water [*75*] .

In all of these methods, the shell is composed of polymer molecules that assemble at the interface individually. Colloidosomes have the advantage that the building blocks of the shell are solid particles containing many macromolecules in a compact form, thus making capsules potentially more robust.

1.2.1.5. Stimulus-responsive systems in solid-stabilized emulsions

Stimulus-responsive systems have gained attention recently due to the potential applications in many areas such as sensors and actuators, triggered release vehicles and materials with switchable properties. In regards to Pickering emulsion-based responsive systems, some examples have also been developed.

Behrens et al. [*26, 77*] have created particle-stabilized emulsions of octanol-in-water with pH and temperature responsive particles. These particles were made of a poly(N-isopropylacrylamide), PNIPAM, microgel which also contained methacrylic acid groups. Emulsions prepared with these microgel particles at pH 6 could be de-stabilized alternatively by lowering the pH at room temperature, or by raising the temperature to 60° C. Microgel emulsifiers have also been used by Fujii et al. to produce stimulus-responsive emulsions[*78*]. Read et al. [*27*] used particles composed of a block copolymer of methyl methacrylate and 2-(dimethylamino)ethyl methacrylate. This polymer is charged at low pH and neutral at high pH. They showed that dodecane-in-water or water-in-undecanol emulsions could be demulsified by lowering the pH from 8 to 3.

Some efforts have also been made to accomplish responsive microcapsules. Some examples include capsules based on interfacial polymerization of PNIPAM, polymerization of poly(acrylic acid) on surfactant vesicles, and encapsulation of a microgel in a layer-by-layer assembly of polyelectrolytes[*6*]. Responsive colloidosomes with a temperature dependant size have been also been created [*53, 55, 56, 79*], by using microgel (PNIPAM) in the core or particles of the shell. Such colloidosomes respond to

temperature either by expanding or buckling, depending on the location of the microgel. Additionally, monodisperse magnetic, photocatalytic and piezoelectric colloidosomes have been recently generated by Sanders [*50*]

Nevertheless, responsive colloidosomes that allow triggered release from colloidosomes by complete shell dissolution upon a mild stimulus have not been realized. In the present work, a completely new class of colloidosomes is generated that allow for fast and complete release of an encapsulated cargo upon a mild pH stimulus.

1.2.2. Surface roughness effects relevant for Pickering emulsification

1.2.2.1. Surface roughness and wettability

Wetting of surfaces, mostly by water and in an environment of air or water vapor, has been a widely studied area in the last century. Interest in wetting and surface roughness has been fuelled by examples from nature which show water-repellency and even special adhesive forces, mainly the lotus leaf [*80-82*] and legs of insects such as the water strider [*83*], which due to their surface features allow them to carry out interesting processes, like walking on water or repelling water for self-cleaning purposes. These observations have led to the design of artificial superhydrophobic bio-inspired surfaces [*84, 85*]. Such artificial surfaces have found application as self-cleaning materials and non-adhesive surfaces [*84, 86*]. Furthermore, wetting is very important in many practical processes, such as spreading of paints, lubricants, inks, etc.

Most of the interest regarding wetting and roughness has been geared toward superhydrophobic surfaces [*82, 86-91*], whereas fewer examples have been shown for hydrophilic rough surfaces [*92-95*]). Other wetting regimes, such as superoleophobic surfaces [*96*], under-water superhydrophobic surfaces [*97*] and surfaces with a pH-responsive wetting [*98*] have also been studied. Most fabrication methods shown for

rough surfaces deal with etching, crystal growth, deposition of phase-separated materials or particles and other nanofabrication processes [*87*].

Clearly this research area is extremely active, and has been for some time. The surface roughness effect on wetting was first studied by Wenzel in 1936, [*99*] and has been scrutinized ever since. Extensive theoretical and experimental studies have been carried out with the aim of finding a comprehensive theory that fully describes wetting in terms of roughness, feature geometry and chemistry. Although no such theory has been developed, a fairly well-accepted consensus that recognizes different wetting regimes has been reached, which are referred to in honor of the field's protagonists as the Wenzel regime and the Cassie-Baxter regime [*86, 90, 92, 99, 100*].

In general, these basic models are regarded as the best, available way to describe the effect of surface roughness on wetting. These models are also referred to as homogeneous and heterogeneous wetting. The Wenzel wetting regime takes into account the surface physical heterogeneities, i.e. roughness, as a ratio of the real surface area to the projected surface area, due to its derivation which is briefly explained below. The Cassie-Baxter wetting regime, on the other hand, takes into account chemical or physical heterogeneities, as the fraction of the surface area that is actually wetted by the liquid, as opposed to the fraction not wetted by the liquid. Other models have been developed, that take into account the different length scales existing in the system [*101*]. Additionally, other wetting regimes and additional processes have been identified such as hemi-wicking, contact angle hysteresis, as well as surfaces that are sticky or slippy [*89, 95, 102*], to mention just a few.

As mentioned, more recent developments have shown that various length scales are also relevant for the roughness effect on wetting, such as the height of surface features, the height-to-width ratio, separation distance and geometry [*92, 103*]. Due to the ease of fabrication, most studies have focused on micrometer scale roughness, until recently [*84, 87, 103, 104*]. Nano-scale roughness has also been shown to be important in

wetting [*92-94, 105, 106*]. More recently, bio-inspired surfaces with hierarchical structures of multi-scale roughness have been generated and shown to exhibit extreme hydrophobicity [*84, 85, 107, 108*]. Additionally, nanoscale roughness has also been shown to modify slippage properties, tune the contact angle hysteresis and further enhance hydrophobicity [*89, 107*]. The importance of nanoscale roughness has thus become more evident [*89, 107*].

In order to fully describe the role of surface roughness on wetting, it is clear that many variables may need to be taken into consideration. Nonetheless, it is clear that micro- and nano-scale roughness on hydrophilic or hydrophobic surfaces have a profound effect on wetting. A brief theoretical background of the classical regimes considered in the description of wetting are presented next.

1.2.2.1.1 Ideal surface wetting – the Young equation

Young first described the wetting of a flat surface by the thermodynamic equilibrium resulting from the surface forces involved when a droplet is deposited on a surface, as shown in **Figure 1.3**.

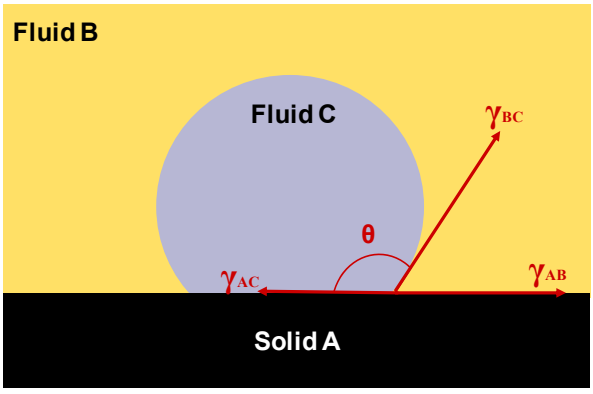

Figure 1.3. Equilibrium contact angle of an ideal surface

By establishing a force balance the thermodynamic equilibrium contact angle parameter is thus defined [*109*]:

$$\gamma_{AC} + \gamma_{BC} \cos\theta_i = \gamma_{AB} \qquad \textit{Eq. (3)}$$

Where γ refers to the interfacial energy between the touching surfaces, and θ_i is the thermodynamic equilibrium contact angle for an ideal surface, which is both chemically and physically homogeneous, where the interfacial tensions are constant and the surface area in contact with both phases is flat.

1.2.2.1.2. Wenzel Wetting Regime

Wenzel modified the Young equation to account for physical surface heterogeneities which result in an increased surface area. This regime assumes that the surface below the drop is completely wetted by the liquid, as shown in **Figure 1.4.**

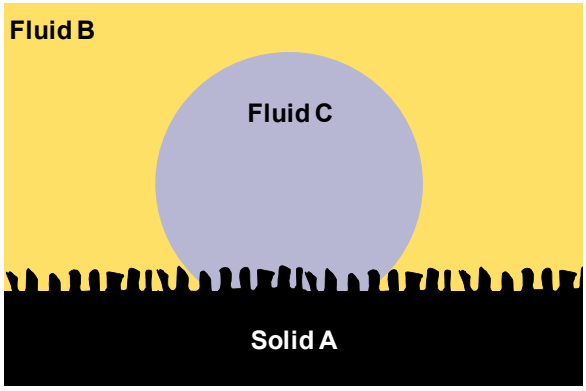

Figure 1.4. Wenzel wetting regime

In this case, the relation between contact angle and roughness has been described as [*99*]:

$$\cos\theta_W = r\cos\theta_i \qquad \textit{Eq. (4)}$$

Where θ_W is the Wenzel contact angle and r is the ratio of the real surface area to the projected surface area due to surface roughness. As r is always larger than 1, this equation states that the contact angle will be enhanced by surface roughness, making hydrophobic surfaces more hydrophobic and hydrophilic surfaces more hydrophilic. The further away the ideal contact angle of the flat material is from 90°, the larger the effect of the surface heterogeneities, while no effect is expected at 90°.

1.2.2.1.3. Cassie-Baxter Wetting Regime

The approach followed by Cassie and Baxter also follows the Young equation, by including the effect observed when the totality of the surface is not wetted by the liquid drop. In this case, pockets of air or other fluid remain in the grooves between the surface material and the liquid drop, as shown in **Figure 1.5**.

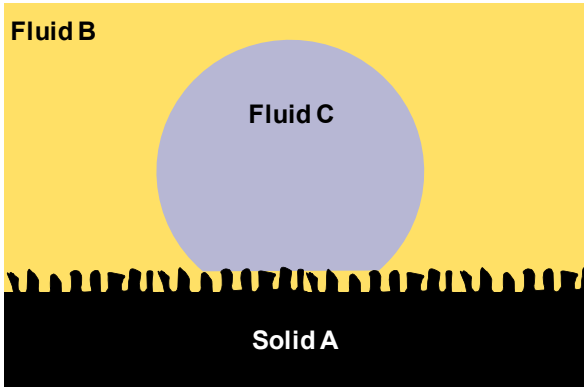

Figure 1.5. Cassie-Baxter wetting regime

In this case, the surface below the drop will consist of two different materials, which when accounted for, results in the following equation:

$$\cos\theta_{CB} = f_A \cos\theta_A + f_B \cos\theta_B \qquad \textit{Eq. (5)}$$

Where θ_{CB} refers to the Cassie-Baxter contact angle, f_A to the surface fraction below the drop occupied by surface A and f_B to that occupied by surface B, θ_A and θ_B are the ideal contact angles for surfaces A and B respectively. In the case where part of the surface (surface B) is air, the equation takes the form:

$$\cos\theta_{CB} = f\cos\theta_i + (1 - f) \qquad \textit{Eq. (6)}$$

Where f_A has been replaced by f.

It is clear from the first expression that when in the Cassie-Baxter regime the contact angle will tend to increase with rougher surfaces (larger values of f_A), if the interfacial energy between the drop fluid and the material trapped in the grooves (fluid or solid) disfavors spreading of such drop.

This is precisely the case of widely-studied superhydrophobic surfaces, where the liquid drop is typically water and the trapped fluid is air. Here, as more air is trapped, the spreading of the water drop is reduced, regardless of the ideal contact angle between the water and the surface material. The Cassie-Baxter state, is thus very interesting as the theory and experiments show that a hydrophilic surface can become hydrophobic by increased surface roughness [*82, 93, 106, 110*].

Although the Wenzel and Cassie-Baxter regimes should be applicable to any system, they have been mostly used to describe superhydro*phob*icity, where a water drop is repelled from the surface with air as the surrounding fluid, resulting in high contact angles. This wetting regime was become important especially for creating "self-cleaning" surfaces, where the water droplets roll-off on a surface [*89, 92*].

Other wetting regimes have been also developed to describe the wetting of a hydrophilic rough surface and to account for additional details that arise from specific surface features.

1.2.2.1.4 Wetting of rough hydrophilic surfaces and other surface feature considerations

Specifically, the scenario of wetting of hydrophilic surfaces has been far less explored than that of hydrophobic surfaces. The former scenario has been theoretically described by Bico [*95*], Martines et al. [*92*] and Netz et al. [*111*], among others.

In general, the wetting of a hydrophilic rough surface can follow the Wenzel equation, for certain degrees of surface roughness. In some cases, the surface roughness can induce wetting beyond the Wenzel regime. This case can be visualized if the surface roughness is thought of as a porous coating [*95*]. In this case, the features will promote the spreading of water on the surface, which can lead to an additional wetting regime: hemi-wicking, shown in **Figure 1.6**.

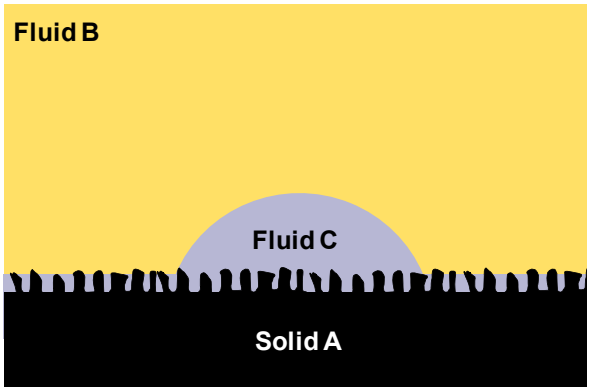

Figure 1.6. Hemi-wicking wetting regime

This case is similar to the Cassie-Baxter regime, except that the liquid composing the drop is also the fluid filling the roughness groves. The difference between this regime and the Wenzel wetting regime resides in the fact that the drop itself is in contact with a heterogeneous surface of liquid and solid, and the surface grooves are filled with liquid beyond the extent of the droplet cross-sectional area.

Other wetting phenomena have also been described, such as contact angle hysteresis, which is defined as the difference between the advancing and receding contact angle. This parameter expresses a dependence on the order in which the two fluid are brought into contact with the surface, and to the "sticky" or "slippery" nature of a surface [*89, 102*]. Generally, slippery surfaces are associated with Cassie-Baxter wetting and sticky surfaces are associated with Wenzel wetting [*86, 92*].The surface slip has been shown to be important to generate superhydrophobic surfaces, where not only high contact angles are expected, but also low contact angle hysteresis and low roll-off contact angles [*80, 89*]. Furthermore, nanoscale roughness on micro-scale features has been shown to be relevant in generating roll-off or slippery superhydrophobic surfaces [*89*].

From the shown wetting regimes, and the additional wetting considerations, it is easy to see how the shape, size and geometry of the surface features that create the roughness have a large effect on the wetting regime. Especially for Cassie-Baxter wetting, over-hangs or re-entrant sites have been shown to be relevant for trapping a fluid between the surface and liquid drop [*82, 96*], such as those shown in **Figure 1.7**.

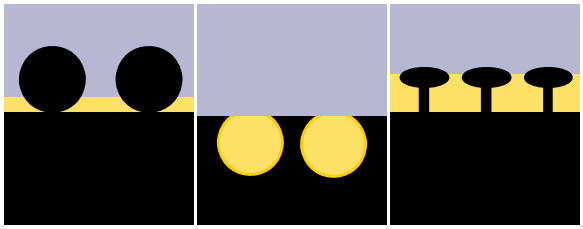

Figure 1.7. Re-entrant or over-hanging surface sites which promote Cassie-Baxter wetting.

1.2.2.2. Effect of particle surface roughness on Pickering emulsification

The effect of surface roughness on particle entrapment at the interface and on emulsification itself is a topic where information is scarce and conflicting ideas exist.
As previously mentioned, roughness magnifies hydrophilicity or hydrophilicity, at least in the Wenzel wetting state. If this concept is applied to rough particles adsorbed at the liquid-liquid interface of an emulsion droplet, one might expect emulsion stability to decrease, as the contact angle is shifted away from the ideal window near 90º, when considering only the particle adsorption energy as a component of emulsion stability. Indeed, one experimental example of the role of particle surface roughness on Pickering emulsification, developed by Vignati et al. [*112*], suggests that particle roughness decreases emulsion stability as well as droplet coverage. They proposed that the roughness affects the adsorption kinetics[*112*] as an explanation for decreased droplet coverage. In this study, however, the surface chemistry of the particles was not shown to be homogeneous.

Additionally, it has been suggested that particle roughness is associated with contact angle hysteresis and therefore explains the tendency of Pickering emulsions to choose as the continuous phase the liquid in which the particles are first dispersed [*19*]. It has also been suggested by Tadros and Vincent [*113*] that rougher particles are better stabilizers of emulsions due to contact angle hysteresis. This idea has been followed by a theoretical study by Denkov at al. where rougher particles also appear to be better stabilizers [*41*]. This study suggests that rough particles with contact angle hysteresis should exhibit larger maximum capillary pressures, i.e., the required pressure for rupturing of the film between two droplets.

In another current of ideas, it has been shown before that the emulsions are more stable with small particles when the dispersions used are weakly flocculated [*17, 19, 33, 114*]. Small aggregates of particles easily resemble a larger particle with surface roughness. As has been mentioned before, it has also been established that some

electrolyte concentration is required in order to overcome the barrier to adsorption to the negatively charged [*30*] interface and the process of particle adsorption has been thought of as a flocculation process itself [*32*]. It is unclear at this point, whether weakly flocculated particles make superior emulsifiers because of their aggregate's surface roughness or primarily because the salt ions responsible for their aggregation also remove the electrostatic barrier towards interfacial adsorption.

It is thus clear that particle surface roughness as a parameter in Pickering emulsification is in need of controlled experimental evidence. While very few theoretical or experimental studies have dealt either with particle surface roughness in emulsification, most studies have focused on the effects of surface roughness on particle adsorption at liquid-liquid interfaces.

Several investigations have been devoted to studying the effects of an ondulated contact line, caused by particle surface roughness, on capillary interactions between particles at interfaces. Stamou suggested that rough particles would create deformations at the liquid-liquid interface due to the protrusions in the contact line. These interface deformations would lead to roughness-induced capillary attraction[*115*]. Danov et al. have treated such interface ondulations as multipoles and developed a theory for their effect on capillary interactions [*116*]. Other studies have determined that this interaction is attractive except at very short distances [*117*]. Ironically, the idea that roughness should lead to a capillary attraction stems from the observation of an unexplained attractive interaction between interfacially adsorbed colloidal particles with *low* levels of surface roughness. Stamou [*115*] suggested that the deformations should be in the order of 50 nm, while Kralchevsky proposed that a minimal interface ondulation (2.2 Å) causes a significant capillary attraction between particles [*118*]. Oettel [*119*] on the other hand, has proposed that Stamou's analysis that predicts large attraction (~ 10^4 kT for 1 μm particles) cannot be generalized to charged particles.

Beyond the topic of capillary attractions at planar liquid-liquid interfaces, Nonomura et al. [*120-122*] have theoretically studied the adsorption of rough particles at liquid-liquid interfaces in terms of adsorption energy and contact angle. These studies predict that both the contact angle of the particles at the interface, as well as the adsorption energy, will be different for a smooth and a rough particle in the Wenzel wetting regime [*121*]. For extremely rough particles, it is suggested that the obtained wetting regime (Wenzel or Cassie-Baxter) will depend on the fluid the particles are first immersed in [*120*], and accordingly the influence of roughness on the contact angle will also depend on the order of wetting by the two liquids. For the Cassie-Baxter state, it was shown that the adsorption energy depends on the fraction of particle surface area that is in contact with the external liquid (analogous the value *f* for this wetting regime). In this case, the adsorption energy is smaller when less surface area of the particle is exposed (i.e., smaller *f* values). **Figure 1.8** is a representation of these possible wetting scenarios for a particle at a liquid-liquid interface; they are perfectly analogous to those for flat substrates, described earlier.

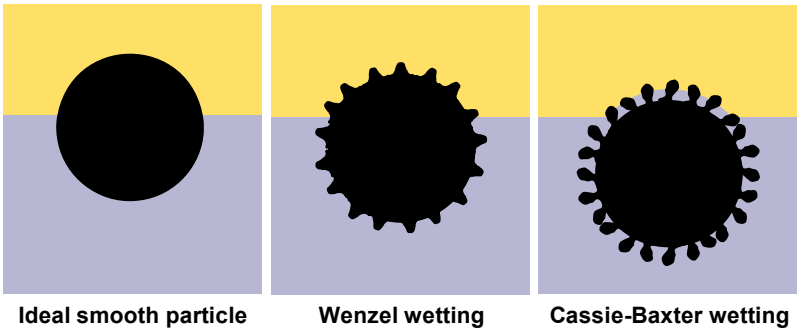

Figure 1.8. Wetting regimes of a particle at a liquid-liquid interface.

Overall, it appears that in theory surface roughness should have a strong effect on particle adsorption at liquid-liquid interfaces. Expected effects are alterations in the

equilibrium contact angle, the energy of adsorption and capillary interactions between particles. Furthemore, contact angle hysteresis due to particle surface roughness is also expected to increase the maximum capillary pressure for film rupture in emulsions. All of these are crucial parameters for Pickering emulsification, and therefore particle surface roughness must have a very important effect in Pickering emulsification. The present study is the first to investigate this effect systematically.

CHAPTER 2

PH-RESPONSIVE NANOPARTICLES

Parts of the following chapter have been published in references [123, 124] and have been reproduced by permission of The Royal Society of Chemistry.

As new developments in materials science arise, the generation of stimulus-responsive systems has become an area of ever increasing interest. These systems take advantage of a non-linear response, to a stimulus such as a mild change in the temperature, salinity or pH of a contacting medium, exposure to light or to an external electric field [*125, 126*]. Applications for stimulus-responsive systems include sensors and actuators [*127, 128*], vehicles for drug delivery [*125*], thermo-responsive surfaces [*129*], microfluidic devices, bioadhesion mediators [*126*], artificial muscles, chemical valves and responsive polymer matrices for the immobilization of enzymes and cells [*125*].

Stimulus responsiveness is especially useful for on-demand release of active ingredients in delivery systems, where the tuning of release profiles according to physiological needs is highly desirable [*125*]. Specifically in emulsification and microencapsulation studies, particles responsive to temperature and pH which make up the shell of a capsule or emulsion drop have been the most widely studied [*26, 27, 53, 55, 56, 77-79*].

Many examples of stimulus-responsive nanoparticles have been developed [*26, 54, 130, 131*]. Temperature-responsive nanoparticles have been most widely explored in the colloidal science field with PNIPAM hydrogels, which show a sharp, temperature-induced transition in volume. pH-responsive nanoparticles are generally made of polymers with chargeable groups, such as carboxyl, amine or amidine. The dissociation

of these groups induces a change in hydration with pH, which for cross-linked nanoparticles usually is manifested by a change in the degree of swelling.

In this work, pH-responsive nanoparticles are the base for the development of stimulus responsive microcapsules and for fundamental studies about Pickering emulsification. While some responsive particles have been used for stimulus-responsive emulsions and colloidosomes, [*26, 27, 53, 55, 56, 77-79*] colloidal particles made from materials that allow for complete triggered dissolution have not yet been applied in studies of Pickering emulsification or microencapsulation. The focus of this chapter is the generation of such responsive nanoparticles based on enteric coating polymers which completely dissolve upon a mild pH increase.

Enteric coatings are polymers resistant to low pH environments and are widely used in the pharmaceutical industry to protect ingested drugs from the harsh acidic environment of the stomach. As the active ingredients reach the higher physiological pH of the colon after their ingestion, the enteric coatings swell or dissolve thereby releasing the drugs to a milder environment.

Typically dissoluble polymers are random co-polymers with a hydrophobic component and an acid component. The hydrophobic part of the co-polymers chosen in our study are composed of poly(methyl methacrylate) or poly(ethyl acrylate) while the hydrophilic part is made of poly(methacrylic acid); the example of poly(MMA-co-MAA) is shown in **Figure 2.1**. The polymer dissolution is accomplished by the carboxylic acid groups in the polymer, which protonate at low pH and dissociate at higher pH, thus charging the polymer and leading to molecular dissolution. In this way, drugs are released at the higher pH of the colon, where the drugs can be absorbed without damage.

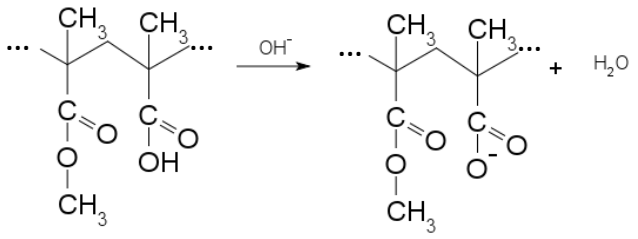

Figure 2.1 Enteric polymer dissolution.

The ratio of the acrylic acid groups to the hydrophobic groups determines the dissolution pH of the polymers, usually between 5 and 7. However, the nature of the acrylate group might have an impact as well. Examples of this type of polymers include Eudragit L-100 and Eudragit S-100, (Degussa-Evonik), as well as Kollicoat MAE (BASF). Some properties are shown in **Table 2.1.** Particles made of enteric coating polymers are proposed as building blocks for the generation of stimulus-responsive capsules because of their known response to a slight stimulus under mild solution conditions.

Table 2.1 Properties of enteric coating polymers

Polymer	pH for dissolution	Composition	MW
Eudragit S-100 [*132*]	7	Methyl Methacrylate:Methacrylic Acid 2:1	150,000
Eudragit L-100 [*132*]	6	Methyl Methacrylate:Methacrylic Acid 1:1	150,000
Kollicoat MAE [*133*]	5.5	Ethyl Acrylate:Methacrylic Acid 1:1	250,000

Eudragit polymers have been selected for generating pH-responsive nanoparticles, since they are commercially available as surfactant-free powder, whereas Kollicoat is available only with various surfactant additives [*133*] that make it unsuitable for fundamental scientific studies without extensive purification. Although surfactant-free, Evonik polymers are produced as particles of irregular shape and size (25 to 50 μm), as can be seen in the micrograph in **Figure 2.2**. It is therefore necessary to transform the polymer powder into colloidal particles suitable for Pickering emulsification.

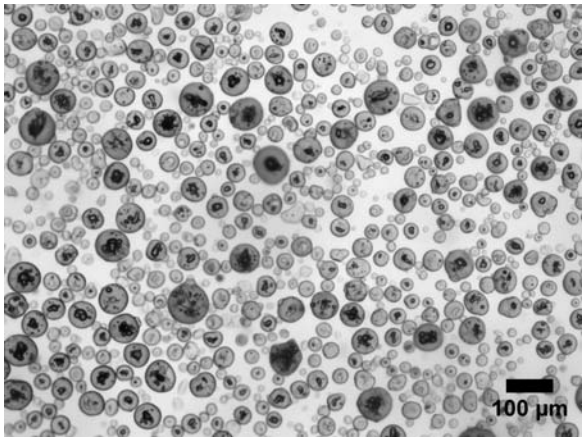

Figure 2.2 Eudragit S-100 powder micrograph

The transformation of the enteric coating polymers from powders to nanoparticles has been performed through a very simple nanoprecipitation method, which has also been called the "Ouzo" effect [*134-136*], because of its analogy to the effect produced by the phase-separation of anis oil in Ouzo liquor when in contact with water or ice.

The so-called "Ouzo effect" or nanoprecipitation method has been previously employed to create nanoparticles from various polymeric materials. This method has been described for the spontaneous formation of liquid oil droplets in water without the need for any agitation or mixing. The fundamental concept is the phase separation of oil or polymer that occurs upon mixing a water-miscible solution of oil or polymer with

water, whereby the oil or polymer supersaturates forming small oil droplets or polymer particles [*135, 136*]. This method has been employed not only with water, but with other substances used as the "non-solvent" [*137*]. It appears as a requirement that the solvent and the non-solvent are miscible, either polar or non -liquids [*137*]. Furthermore, if the solvent is to be extracted by evaporation, as is convenient in particle synthesis, it needs to be more volatile than the non-solvent. The requirements to remain inside this "Ouzo" region appear to be unrelated to the spinodal decomposition line [*134*] and are not well established yet according to recent studies [*134, 135, 138*] .

2.1 Nanoprecipitation with Eudragit Polymers

2.1.1 Nanoprecipitation of Eudragit Polymers in Water

Nanoparticles of Eudragit polymers have been created in water with and without stabilizers by nanoprecipitation, as previously reported [*135, 138, 139*]. The synthesis of Eudragit nanoparticles by other methods has also been shown, such as salting out and emulsification-diffusion [*138*], which involve the presence of large amounts of salt, surfactants or steric stabilizers, respectively. In the nanoprecipitation method, particles of different size can be synthesized by changing parameters such as polymer concentration in the initial solution and solvent to water ratio, as well as the solvent used. The particles synthesized with this method have been reported to have a polydispersity index of 0.1-0.4 [*139*].

In the specific case of Eudragit nanoparticles synthesis, the approach followed involved mixing an ethanol solution of the polymer with water in a 1:2 ratio. Evaporation of the solvent yields a particle dispersion in the non-solvent. No surfactants or stabilizers are required in the particle preparation step, since the dissociated carboxylic acid groups provide enough charge for electrostatic stabilization. This statement is supported by the

zeta potential of the particles, which is usually in a range between -40 and -60 mV at a 1mM background NaCl concentration, at slightly acidic pH values.

Based on previous results by other authors [*135, 138, 139*], several experiments were carried out with Eudragit S-100 and Eudragit L-100, in which the initial polymer concentration in ethanol was varied. Nanoparticles have been synthesized by preparing a solution of 0.5-4% (wt/v) of polymer in ethanol. This solution is added abruptly to twice the volume of water, stirring with a magnetic stirrer at 400 rpm. The mixture immediately turns turbid, and the solvent is evaporated by raising the temperature to 70º C for approximately 2 hrs. The suspension is then filtered through a 3 μm filter (Grade 6 Whatman qualitative filter) and cooled down to room temperature.

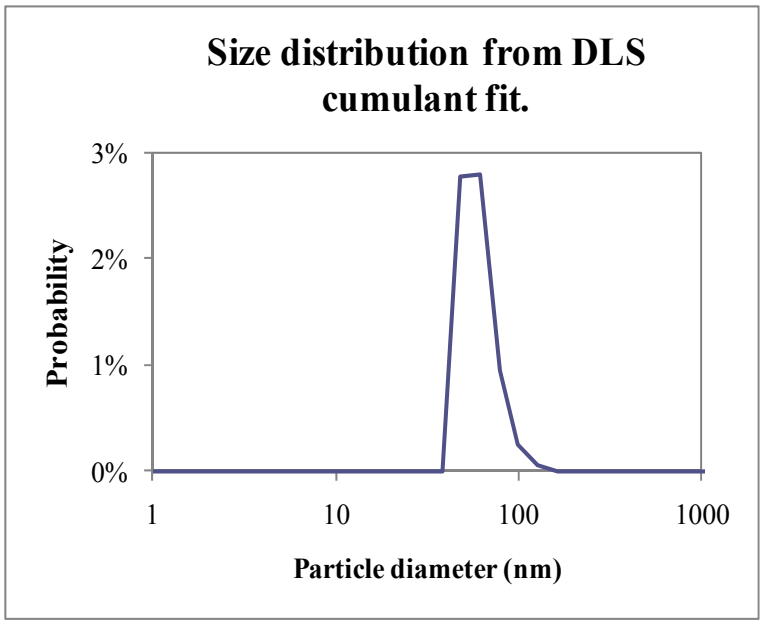

Figure 2.3 Size distribution of Eudragit S-100 nanoparticles obtained by nanoprecipitation from a 1% (wt/v) ethanol solution.

From these experiments it was found that the initial polymer concentration is a determining parameter in the final particle size. The obtained particle sizes range from 50

to 250 nm (obtained by Dynamic Light Scattering), with a fairly monodisperse size distribution, as shown in **Figure 2.3.** The size distribution shown in **Figure 2.3** represents the CONTIN analysis [*140*] for a particle batch prepared from a 1% (wt/v) polymer Eudragit S-100 solution in ethanol, with a resulting particle diameter of 83 nm and a CV of 8.6%.

The sizes obtained for polymers Eudragit-L100 and Eudragit-S100 are very similar, with a minimum average size of around 50 nm and a maximum average size of around 250 nm, as can be seen in **Figures 2.4 and 2.5**. The data presented are the intensity weighted diameters obtained from second order cumulant fits to the intensity-autocorrelation function obtained by dynamic light scattering. Polymer concentration refers to the polymer/solvent solution prior to precipitation with water.

The smallest particle size is limited by the solubility of the polymer in the mixture of solvents, where a polymer solution below a concentration of 0.5% (wt/v) Eudragit in ethanol, does not precipitate when mixed in a 1:2 ratio with water. There is also limit concentration of polymer above which nanoparticles do not increase the size, but large aggregates are formed along with the particles [*138*]; in this case that limit was found to be ~2.5% (wt/v). While these limits might be modified by using different ratios of ethanol-to-water or by varying the preparation temperature and pH, these options were not explored since the tested conditions yielded the pH-responsive nanoparticles in the desired size range.

While the nanoprecipitation method provided surfactant-free monodisperse pH-responsive particles, the first tests were carried out with the addition of stabilizers in the hope of obtaining stable dispersions. These tests provided interesting results which are also shown in **Figures 2.4 and 2.5.** As seen from the synthesis of nanoparticles from Eudragit S-100 and Eudragit L-100, the addition of Poly(vinyl alcohol) in the water phase has no effect on the size of the obtained nanoparticles, while the addition of the amphiphilic triblock copolymer Pluronic® F127 (BASF) appears to increase the obtained

size in all cases. The size of the particles increases monotonically with concentration of Pluronic® F127 (**Figure 2.5**). These results suggest that the amphiphilicity of the stabilizer allows the formation of larger droplets in water, potentially due to the existence of micelles that impose a preferred curvature and serve as templates for larger particles

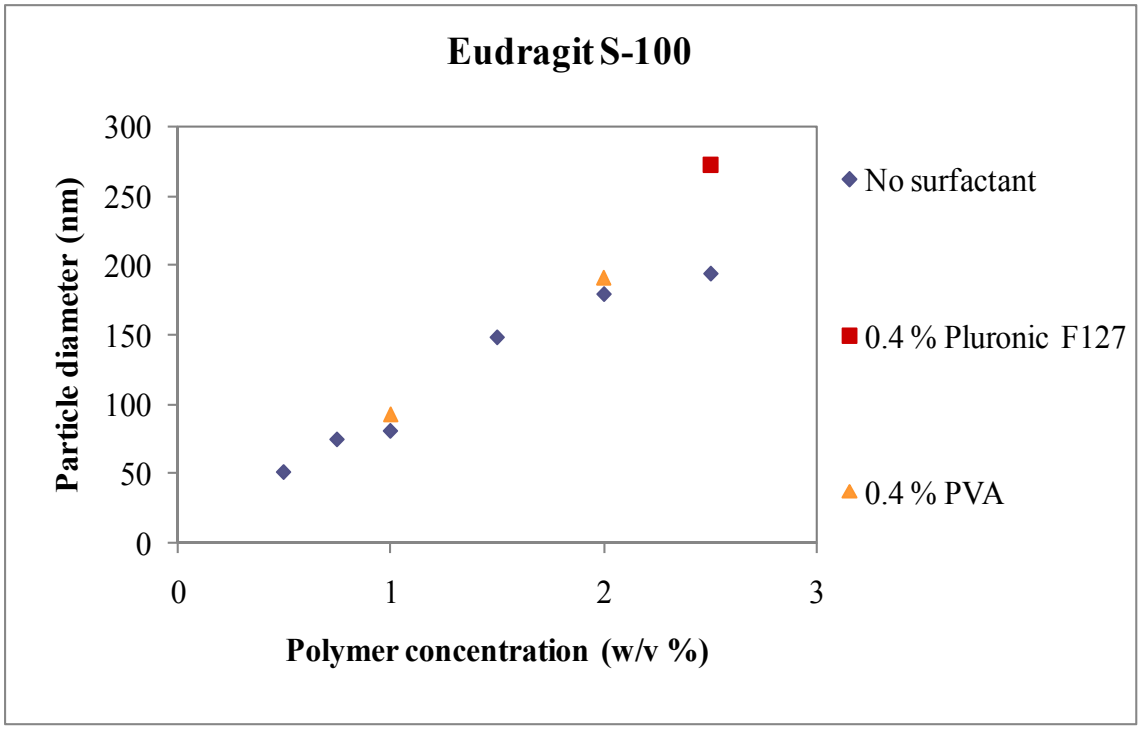

Figure 2.4 Eudragit S-100 nanoprecipitation synthesis size dependence on initial polymer concentration.

It is important to remark that the nanoprecipitation method provides the advantage of a very simple surfactant-free synthesis that results in fairly monodisperse nanoparticles. While the addition of amphiphilic polymers can potentially be used for generating particles larger than those obtained in the surfactant-free system, the work developed in this dissertation called for surfactant-free nanoparticles which would really act as sole emulsion stabilizers.

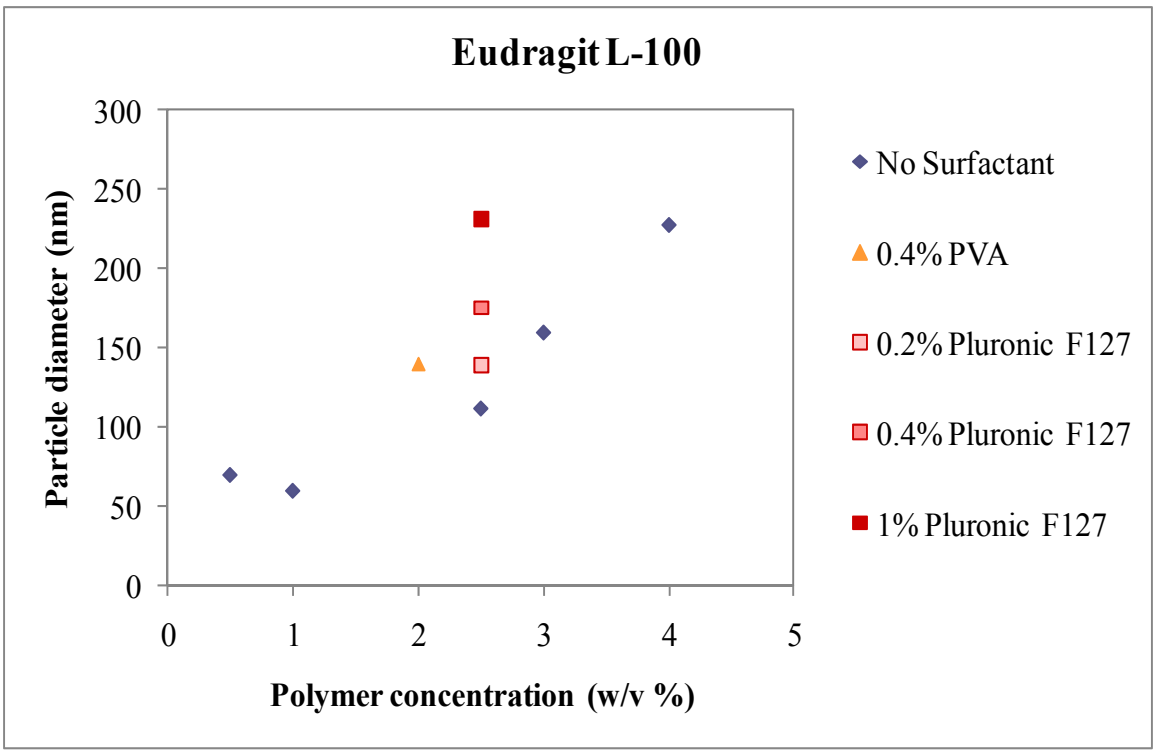

Figure 2.5 Eudragit L-100 nanoprecipitation synthesis size-dependence on initial polymer concentration.

2.1.2 Nanoprecipitation of Eudragit Polymers in Oil

Nanoprecipitation into a non-polar solvent poses a more difficult challenge, since the electrostatic stabilization will be absent. From this fact, it is to be expected that additional stabilizers are required. Although several examples of nanoprecipitation have been shown; very few deal with nanoprecipitation into oil [*137*].

An added complexity in this case is the solvent selection. Ultimately, the nanoparticles synthesized in oil are intended to be used as stabilizers of double emulsions of an extractable oil for capsule generation, as briefly introduced in Chapter 1 and further explained in Chapter 3. Therefore, while there is a wide variety of non-solvent oils, the synthesis trials were limited to those that could be used for the double-emulsion solvent-

evaporation method, i.e. oils with a higher vapor pressure than that of water (17.48 mm Hg at 25º C [*141*]) so that they can be extracted by evaporation.

The few choices available for oils that can serve as solvents and non-solvents are presented in **Table 2.2**, along with their vapor pressures. The solvent used for Eudragit should have a higher vapor pressure than the non-solvent, in order for the polymer solvent to be easily removed.

Table 2.2 Vapor pressures of solvents and non-solvents for Eudragit polymers

Non-solvents	**Pvap** (mm Hg)**	**Solvents**	**Pvap** (mm Hg)**
Dichloromethane	435	Acetone	231
Chloroform	197	Methanol	127
Toluene	28.3	Ethanol	44.4
		2-butanol	18.3

**Data @ 25ºC from reference [*141*].

Based on the information provided in table **Table 2.2,** dichloromethane was discarded as a potential non-solvent, since it has a higher vapor pressure than all the solvents. With the remaining solvents and non-solvents, a factorial experiment was carried out. In this case, a surfactant was required in the non-solvent, to provide stabilization to the particles. Non-ionic Pluronic surfactants were applied for this purpose, which are triblock co-polymers of PEO and PPO. Two of these surfactants were tested: Pluronic F127 and Pluronic 25R2. The former is more hydrophilic (HLB of 22) and has the form PEO-PPO-PEO, with a MW of 12,600 and 70% PEO; the latter is more hydrophobic (HLB of 4), having the form PPO-PEO-PPO, with a MW of 3,100 and 20% PEO [*142, 143*].

Table 2.3 shows the results of the factorial Eudragit S-100 nanoprecipitation experiment with the selected solvents and non-solvents. The stabilizers were dissolved in the non-solvent phase (toluene or chloroform) and the polymer was dissolved in the solvent (methanol, ethanol, 2-butanol or acetone) at a 1% (wt/v) concentration. The two solutions were abruptly mixed in a 1:2 ratio of polymer solution to non-solvent.

In most cases, the polymer did not precipitate upon mixture. Ideally, the polymer/non-solvent/solvent relative concentrations would be selected before-hand in the Ouzo region, or at least in the region where the polymer is solid. Since the three-phase diagram for solvent/non-solvent/Eudragit S-100 is unknown, the relative concentrations were kept constant at the aforementioned values. However, the results obtained for the experiment performed with acetone as the polymer solvent provides interesting insights into the best parameters for nanoprecipitation in oils.

Table 2.3 Factorial Experiment of Eudragit Nanoprecipitation in Oil.

	Toluene		**Chloroform**	
	0.5% Pluronic® F127	0.5% Pluronic® 25R2	0.5% Pluronic® F127	0.5% Pluronic® 25R22
Methanol	-	-	-	-
Ethanol	-	-	-	-
2-Butanol	-	-	-	-
Acetone	×	✓	×	×

(-) no precipitation, (×) precipitation in form of flocs and aggregates, (✓) stable nanoprecipitation, upon mixture of polymer solution and non solvent.

From the four options of non-solvent, the only one that resulted in stable nanoparticles upon mixing of the solvent and non-solvent is Toluene with Pluronic 25R2. As it would be expected, the more hydrophobic surfactant provided the means for stabilization of hydrophilic particles in a hydrophobic medium. As the typical theory for surfactant adsorption and colloidal stabilization suggests, a more hydrophobic stabilizer would be required for stabilizing a hydrophilic entity in a hydrophobic medium, which is the case here.

The exact geometry of Pluronic F127 adsorption onto the polymer nanoparticles is difficult to predict, and its explanation is beyond the scope of this work, but it appears logical that a polymer with two hydrophobic chains at the ends would be a better stabilizer than a polymer with a single hydrophobic chain in between two hydrophilic tails at stabilizing a hydrophilic particle in oil. It is thus easy to understand that Pluronic 25R2 appears to be an adequate option for the stabilization of Eudragit S-100 nanoprecipitates.

The nanoparticles obtained by precipitation from acetone into toluene had a mean hydrodynamic diameter of 334 nm, according to dynamic light scattering. Compared to particles precipitated in water, the particles synthesized in oil were characterized by an increased polydispersity, with a coefficient of variation (CV) of 31.58%. One reason for this difference can be the stabilization mechanism. In the case where precipitation occurs in water, electrostatic stabilization by the immediate creation of charged species on the polymer provides a uniform repulsion between nucleated droplets, whereas in the oil case the Pluronic diffuses from solution to the nucleating droplets where it adsorbs and provides steric stabilization against droplet coalescence. Also important, is the fact that, in water, the charge on the particle surface is high, since charge precursors (carboxylic groups) are present along the polymer chain, and thus electrostatic stabilization is expected to be very strong. Moreover, the time scale of the creation of charges vs. the

time scale for surfactant diffusion and adsorption can be relevant when compared to the time scale of droplet formation and coalescence.

It is thus suggested, that electrostatic stabilization occurs faster and more efficiently than steric stabilization provided by the surfactant. While upon initial mixing of the solvent and non solvent, the system appeared stable with Pluronic 25R2, aggregation was observed after some time upon complete extraction of the solvent by evaporation. The high polydispersity observed by DLS might also represent the initial stages of aggregation. Nanoprecipitation in oil did not yield a stable particle dispersion suitable for studying Pickering emulsification. Suggested future work in this area includes the study of stabilization when an oil is used as the non-solvent, in order to find the prerequisites for the formation of particle dispersions with good long term stability.

2.2 Nanoparticle Responsiveness

In order to assess the working window for the Eudragit-S100 nanoparticles, their pH-responsiveness was studied based on the dissolution threshold at different ionic strengths. In addition, the stability regime of the particles against aggregation was studied.

By means of Laser Light Scattering, three polymer states were distinguished:

(1) stable dispersed nanoparticles

(2) aggregated nanoparticles

(3) dissolved polymer.

In order to make the distinction between states, dispersions at the same solid concentration were prepared at different NaCl concentrations, and the pH was adjusted with HCl or NaOH. The sample at the given ionic strength and pH was studied by dynamic light scattering. The markers that provided information about the state of the polymer are: (a) the hydrodynamic radius obtained from a cumulant fit to the autocorrelation function, and (b) the average intensity of the scattered light measured as a

photon count rate (kcps). Stable dispersed nanoparticles were characterized by a known hydrodynamic radius, and a fairly low PDI value. In comparison, the dissolved polymer showed a notably reduced intensity by at least 1 order or magnitude. Aggregation of nanoparticles was identified by an increase in intensity and hydrodynamic size, eventually followed by sedimentation. In this manner, pH-ionic strength diagrams for the Eudragit polymers as well as for Kollicoat, were obtained and are shown in **Figures 2.6, 2.7 and 2.8**.

The lines represent only the farthest measured point (areas in-between are uncharted). Eudragit nanoparticles were synthesized as explained before, and Kollicoat was dialyzed to remove undesired surfactants. The pH for dissolution, as expected, is found to be lower for the polymers with more acid groups. As can be observed from the diagrams, the 3 regimes (aggregated particles, dispersed particles and dissolved polymer) are observed in order of increasing pH, which corresponds to an increase in the polymer charge.

At very low pH, the particles are essentially uncharged and aggregate while at high pH the particles dissolve. In the intermediate pH regime, the particles form a stable dispersion. In deionized water with little added salt, the “dispersed particle” regime is seen to span a fairly wide pH range, which narrows down with increasing ionic strength: added salt facilitates both particle aggregation and particle dissolution. This phenomenon is explained by charge screening due to the presence salt ions, where at low pH screening of particle charge induces aggregation, and at high pH screening the repulsion between charged sites along the polymer chain favors de-protonation, thereby facilitating further polymer charging at a given pH. Hence, the presence of salt promotes a sharp transition between states. It is thus concluded that the best control and most-sensitive pH-response can be expected for rather high salt concentration.

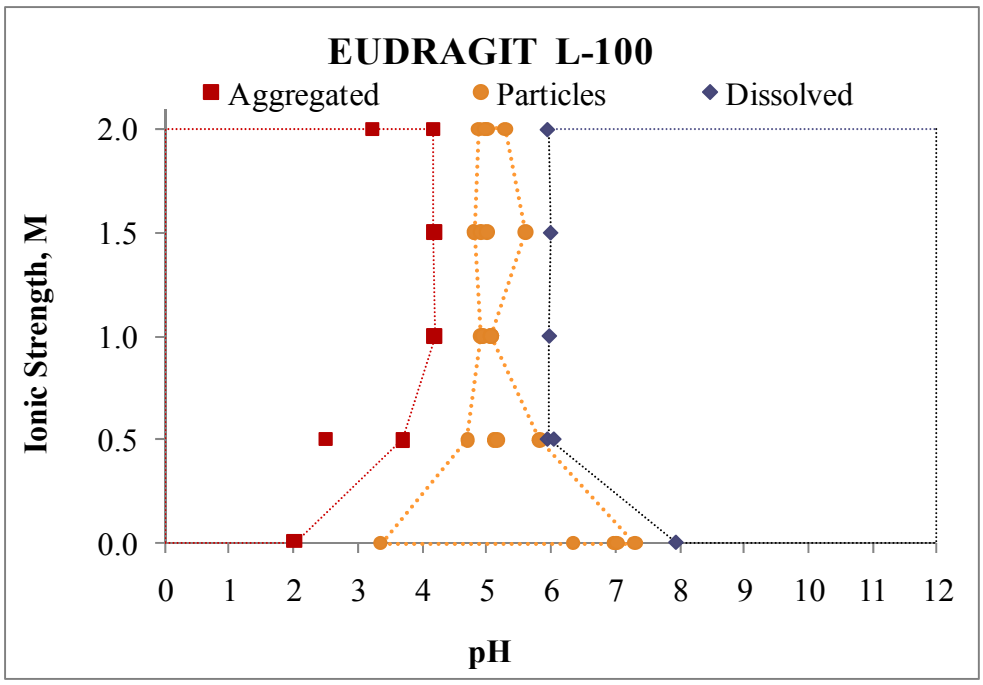

Figure 2.6 Eudragit L-100 pH-Ionic Strength Phase Diagram.

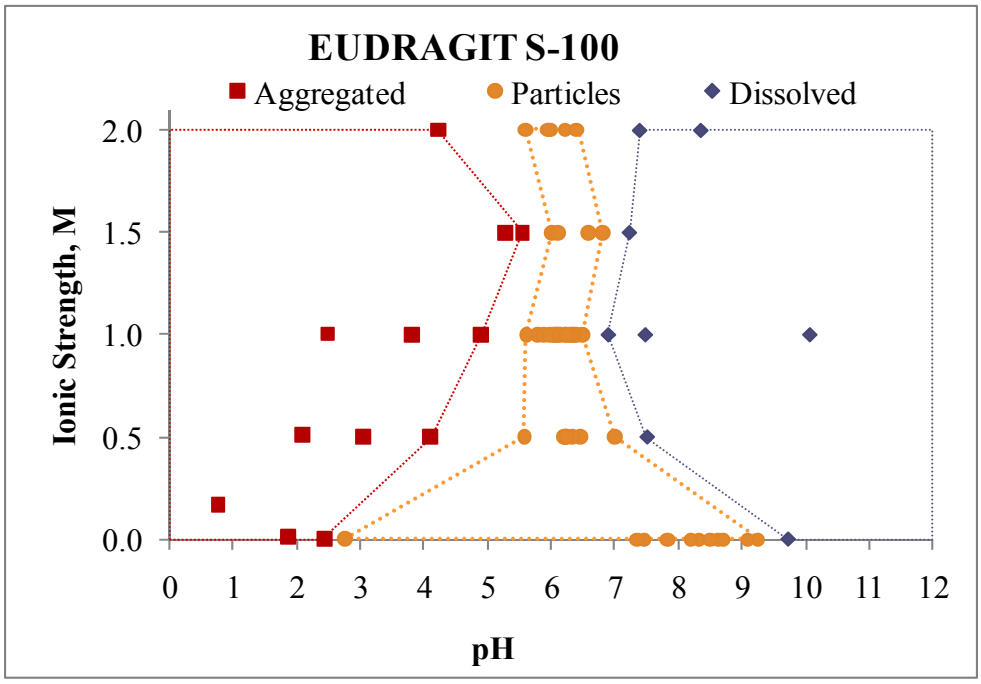

Figure 2.7 Eudragit S-100 pH-Ionic Strength Phase Diagram.

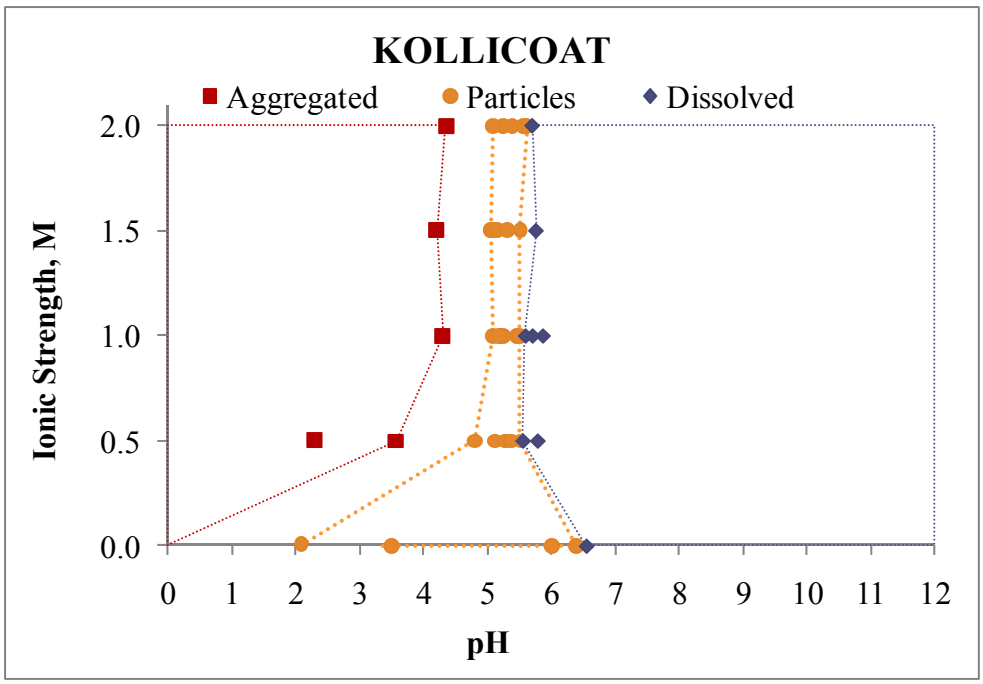

Figure 2.8 Kollicoat-MAE pH-Ionic Strength Phase Diagram.

CHAPTER 3

STIMULUS-RESPONSIVE MICROCAPSULES

Parts of the following chapter have been published in references [123, 124] and have been reproduced by permission of The Royal Society of Chemistry.

Microencapsulation techniques are very important formulation tools with widespread applications in the preparation of functional materials, chemically or biologically active agents, pharmaceuticals, cosmetics and even food [*1, 3, 7, 10*], as introduced in the first chapter. Pickering-emulsion based microcapsules, known as colloidosomes, are considered a promising alternative for microencapsulation [*4, 11, 12*], with the potential advantages of increased sturdiness, defined permeability and potential functionalities that colloidal particles can bring about.

In order to accomplish their purpose, microcapsules should retain and protect an encapsulated agent until delivery conditions are reached in the target environment. Release could be triggered by an external disruption of the system, such as mechanical stress or a non-target specific, externally activated stimulus: light, magnetism or temperature change, for example. Ideally, release would occur when the capsule encounters the inherent conditions of the delivery medium, which must differ in temperature, pH, or salinity from the surrounding environment. In this case, the delivery medium itself will exert a disturbance on the microcapsules. It is therefore desirable for the microcapsules to be responsive to the medium and release the contents on demand when a certain condition is triggered, such as a change in pH, temperature or salinity

Stimulus responsive Pickering emulsions whose stability depends precisely on these solution parameters have already been developed [*26, 27, 77, 78*], as have colloidosomes with a temperature dependent size [*53, 55, 56, 79*], but colloidosomes that

release their interior by complete shell dissolution in response to a mild triggering stimulus have not yet been realized.

3.1 Objective and General Approach

The objective of this work was to develop water-core colloidosomes that allow the release of their active ingredients by complete dissolution of the shell upon a mild stimulus which can be encountered in real systems. In reality, the generation of this type of microcapsules implies the simultaneous achievement of many different requirements:

1. Generation of responsive particles that completely dissolve upon a mild stimulus.

` 2. Stabilization of Pickering emulsions with stimulus-responsive particles. These emulsions should have an easily extractable oil phase that does not dissolve the particles, so that the emulsion droplets can be encapsulated in a shell of particles.

3. Fabrication of colloidosomes from such emulsions by extraction of the oil without disturbing the pre-formed particle shell.

4. Demonstration that the responsiveness of the particles is retained in the colloidosome.

This chapter describes a system that simultaneously accomplishes all the aforementioned requirements, and is also the first example of Pickering emulsion-based microcapsules that completely dissolve upon a pH change under mild solution conditions. These capsules combine the sturdiness and pore size control of colloidosomes with the option of triggered disassembly known from stimulus-responsive Pickering emulsions.

The first step, the generation of stimulus-responsive nanoparticles that completely dissolve upon a mild stimulus, has been accomplished and is discussed in detail in the

previous chapter. As a brief reminder, the generated pH-responsive nanoparticles are an unusual formulation of enteric coating polymers, which dissolve at high pH and remain solid at lower pH. The polymer used for the preparation of our pH-responsive particles is a 2:1 co-polymer of methyl methacrylate : methacrylic acid (Eudragit S-100, Evonik), with a dissolution threshold of pH 7. The particles were prepared, as previously described, by a nanoprecipitation method, also called the "Ouzo effect" [*136*]. This method has been applied previously for the synthesis of polymeric particles and is based on mixing a solution of the polymer with a miscible non-solvent, thus causing super-saturation and the formation of polymer droplets. Evaporation of the solvent yields a particle dispersion in the non-solvent. The solvent and non-solvent used for Eudragit S-100 are ethanol and water respectively. No surfactants or stabilizers are required in the particle preparation step, as chargeable carboxylic acid groups provide enough charge for electrostatic stabilization. These surfactant-free dispersions of pH-responsive nanoparticles are the basis for emulsion stabilization in colloidosome generation. While the stabilization of emulsions by the pH-responsive nanoparticles could be a goal itself, the ultimate purpose of emulsion-templated colloidosome capsules dictates further constraints for the emulsion architecture.

Here, it is noteworthy that most previously described colloidosomes rely on the self-assembly of particles at the oil-water interface of a simple emulsion [*11-13, 44*]. These particles are then connected by one of several methods: locking by Van der Waals attraction, sintering, addition of a binding polymer, or precipitation of additional polymer onto the particle shell [*12, 46, 49*]. Once these interfacial particles are connected into solid shells, the liquid interface is typically removed, either by extraction of the inner phase using a solvent miscible with both the oil and water phases of the emulsion, or by transferring the capsules *via* centrifugation into a different bulk phase composed of the same liquid as the emulsion droplets [*11-13*], as shown in **Figure 3.1**. It is easy to understand how either process can lead to capsule damage and a reduced yield [*43, 47*]

since thorough washings and solvent exchange steps are required. Exchange of the droplet phase also implies that any active cargo would have to be loaded into the capsule after completion of the fabrication and washing steps. Such a post-production loading, e.g. by diffusion from the continuous phase, typically results in very poor encapsulation efficiency, i.e. only a small fraction of the active ingredient in the system is actually encapsulated.

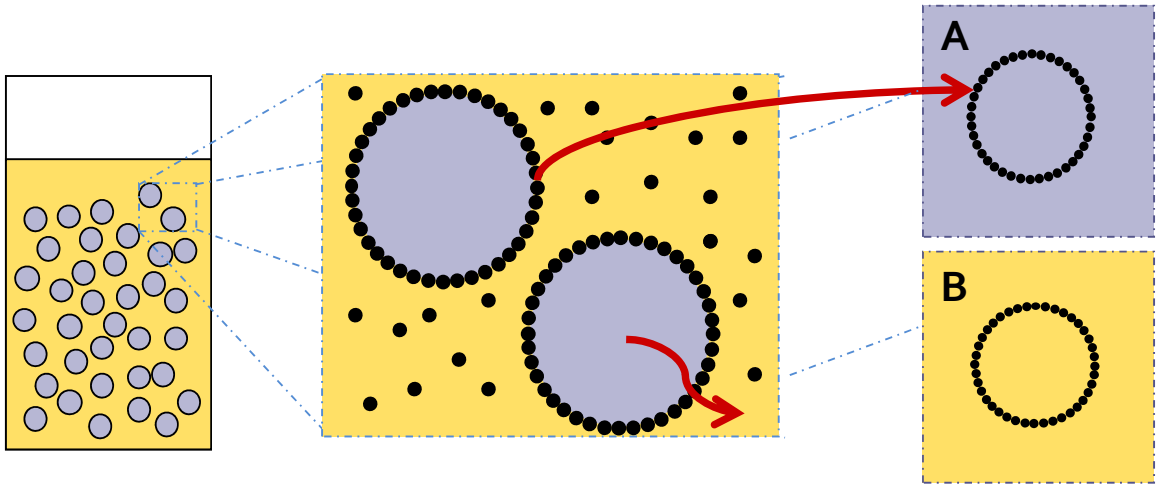

Figure 3.1 Colloidosome formation from single Pickering emulsions by interface removal. A) Transfer of droplets via centrifugation. B) Extraction of the inner phase and replacement with the outer phase.

A more recent method has been developed which uses a double emulsion template for the colloidosome assembly, [*43*] in analogy to a double emulsion/solvent extraction method widely used for microencapsulation by interfacial precipitation.[*60*] The advantage of encapsulating a droplet-in-a-droplet structure lies in the possibility of extracting the middle phase, thereby creating a capsule with the same liquid inside and out without the need of centrifugation or washing. Moreover, the encapsulated ingredient can be incorporated directly in the innermost emulsion phase, and thus higher encapsulation efficiencies can be expected.

Because of these advantages, the double emulsion approach has been selected for the assembly of particles with pH-dependent water solubility into similarly pH-responsive microcapsules. While this approach might seem as a superior route to take for colloidosome-type encapsulation, it is important to mention that double emulsion schemes suffer from a higher degree of complexity for several reasons. In the first place, there are two interfaces to be stabilized, one for the inner and one for the outer droplet, which typically requires two different types of stabilizers. Furthermore, there are three types of coalescence to be avoided. For instance, for a water-in-oil-in-water (W/O/W) emulsion, the oil droplets can coalesce with each other, while the inner water droplets in an oil drop can coalesce with each other or with the outer aqueous phase. Additionally, it is desirable to obtain a single drop in a drop for generating colloidosomes from double emulsions, since multiple drops in a drop would result in "connected microcapsules"; but classical emulsification techniques do not always favor this single drop in a drop structure. Nonetheless, the disadvantage of added complexity in the double emulsion approach is outweighed by the benefit of generating fully functional colloidosomes at high yields and encapsulation efficiencies.

The basic preparation scheme proposed is summarized in **Figure 3.2**. The process starts with creating a single water-in-oil (W/O) emulsion where pH-responsive particles self-assemble at the liquid-liquid interface and stabilize droplets against coalescence. Subsequently, this W/O emulsion is re-emulsified in water and is also stabilized by the pH-responsive nanoparticles. The middle phase is then removed by evaporation. As the two particle-covered interfaces of a W/O/W droplet combine, a pH-responsive solid shell containing at least two layers of particles held together by van der Waals forces, is formed.

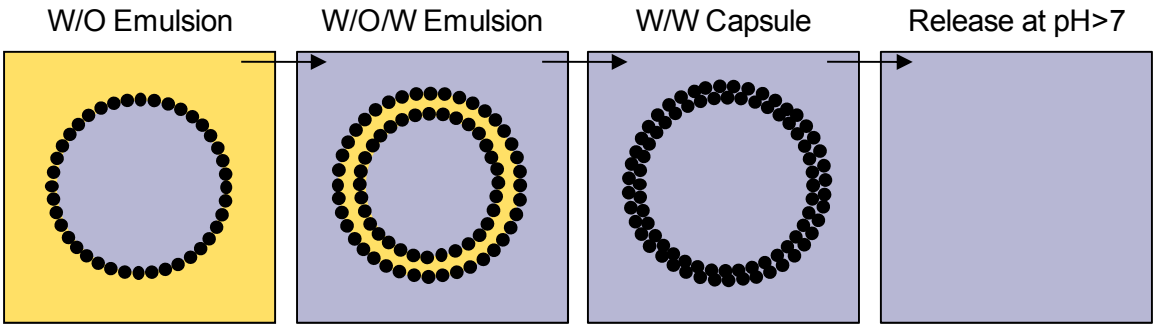

Figure 3.2 General approach for generation of pH-responsive colloidosomes by a double Pickering emulsion template. *Black dots represent pH-responsive nanoparticles.*

Once the preparation scheme has been established, the next step is naturally the oil selection for the generation of the double emulsions. As previously mentioned, the method of double-emulsion solvent extraction is widely known for the generation of microcapsules by interfacial polymer precipitation. Looking at previous examples of this technique [*3, 144*], several candidates to be employed as the middle phase of the water-in-oil-in-water emulsions have been selected, based on their potential for extraction, either by evaporation or diffusion into the water phase. Typical oils used in this process include: ethyl acetate, methyl acetate, isopropyl acetate, dichloromethane and even toluene in some cases of double emulsion solvent extraction for Pickering emulsions [*43, 50*].

While either of the aforementioned solvents appears as a feasible possibility for the generation of double emulsions due to their ease of extraction, there are additional requirements that need to be taken into consideration: 1) compatibility of the pH-responsive nanoparticles with the oils, avoiding dissolution or swelling of the polymer; and 2) the oil should be efficiently emulsified by the particles. The latter requirement is related to the wettability of the particles by both liquid phases. The particle wettability is quantified by the three-phase contact angle of the particles, as explained in the first chapter. The right contact angle has been proposed as a very important parameter in

Pickering emulsion stabilization [*17, 19, 21, 32, 145*] and it has been suggested to be the determining factor in the emulsion type obtained.

An ideal oil candidate would thus be one that is efficiently emulsified by the Eudragit S-100 nanoparticles, that is easily extracted and that is compatible with the particles. Several solvent candidates are shown in **Table 3.1**. The ease of extraction is judged by the potential for either evaporation or diffusion into the aqueous phase. These two characteristics are determined by the vapor pressure and the water solubility. Some water miscibility is required even for volatile oils since the solvent needs to go through the continuous water phase to be evaporated. The possible extraction method according to its vapor pressure and solubility in water is also listed, as well as some limitations that have been found for each of them. Based on these considerations, the solvents ethyl acetate, dichloromethane and toluene were selected. Looking at the solvent table, it seems that dichloromethane is extractable by evaporation while ethyl acetate appears to be extractable by diffusion into water. Toluene is another possibility, although extraction would be slower than with the other two mentioned solvents.

As can be seen in the table, methyl acetate in contact with water at very acidic or basic pH will hydrolyze to produce methanol. As previously mentioned, alcohols are good solvents for the Eudragit polymers, and thus the presence of methanol, or other alcohols, is to be avoided. The rest of the solvents seem to pose some difficulty in the extraction steps.

From these data, ethyl acetate appears to be the ideal candidate, not only for its ease of extraction, but also due to the fact that it seems to be the safest to be used for pharmaceutical applications. Although to a lesser extent, ethyl acetate will also hydrolyze in presence of water at low or high pH. While this process is not thought to occur to the extent where particle dissolution would become an issue, some swelling might occur. Furthermore, emulsification tests with ethyl acetate always produced oil-in-water emulsions.

Table 3.1. Properties of potential solvents for colloidosome preparation

	Solubility in H_2O @ 25°C (mg/g)*	**Pvap @ 25°C** (mm Hg)**	**ε*** **	**Extraction**	**Limitations**
Ethyl Acetate	73.72	92.52	6.081	E,D	-
Dichloro-methane	19.38	435.5	9.14	E,D	-
Toluene	0.54	28.31	2.385	E	-
Methyl Acetate	243.6	213.03	7.03	E,D	Hydrolysis
Heptane	0.002	45.5	1.921	E	Low water miscibility
Chloroform	7.5	4286.18	7.32	E	Very high volatility
Isobutyl Acetate	6.3	12.97	5.6	None	Difficult to extract
Octanol	0.54	0.084	10.3	None	Difficult to extract

* [*146*], **[*147*], ***[*148*]. *E= evaporation, D=extraction by dilution into water*

A few tests were also run with toluene, but no stable double emulsions were obtained. It is believed that high charging of the carboxylic acid groups throughout the polymer chain causes high particle hydrophilicity, which hinders emulsification, especially with a non-polar oil such as toluene. For toluene, which is less polar than dichloromethane (ε =2 .28 and 9.14 respectively) the inner emulsions are not stable, and the double emulsions evolve into simple oil-in-water emulsions. This result is similar to observations by Binks et al. [*17*] and Golemanov et al. [*32*] that charge-stabilized

particles behave “more hydrophobic” when in contact with polar oils than with non-polar oils.

Dichloromethane then seemed to be the best oil choice, as it was easily extracted and emulsified by Eudragit S-100 nanoparticles. Stable water-in-oil emulsions were obtained when high concentrations of NaCl were used. This is in accordance with experiments carried out by Golemanov et al. [*32*], where the required salt concentration for carboxylated latex particles to attach to the interface was between 0.3 and 0.5 M. In a series of experiments with Eudragit S-100 nanoparticles, the optimal NaCl concentration for a water-in-oil (dichloromethane) emulsion was found to be ~0.25M. At higher values, (≥0.5M NaCl), heavy aggregation is observed. At lower values, <0.25M NaCl for the inner aqueous phase, double emulsions were not stable and could not withstand extraction. Lower values of salt (0.025 M) were required for the outer aqueous phase where stable oil-in-water emulsions are obtained.

As a side note, Eudragit L-100 nanoparticles were also tested with the aforementioned solvents for emulsification, without success. This polymer has a 1:1 ratio of methacrylic acid and methyl methacrylate, and is therefore more hydrophilic than Eudragit S-100 which has a ratio of 1:2, respectively. It is concluded that high density of ionic groups makes this particle (Eudragit L-100) insurmountably hydrophilic for emulsification purposes. Therefore, the final selection for generation of pH-responsive colloidosomes from double emulsions was dichloromethane as the middle oil phase, and Eudragit S-100 nanoparticles as the shell building blocks.

Emulsification studies with dichloromethane and Eudragit S-100 particles, as well as the final colloidosome preparation, characterization methods and results will be discussed next.

3.2 Experimental Methods

3.2.1 Materials:

Eudragit S-100 polymer was obtained as a gift from Evonik and was used without further purification. Reagent alcohol (94-96% ethanol/methanol) was purchased from VWR. Dichloromethane, NaCl, NaOH and FITC-Dextran (500 kDa) were obtained from Sigma Aldrich and used as received without further purification. Deionized water (18.2 MΩ cm) was obtained with a Barnstead Easy PureII System.

3.2.2 pH-responsive particle synthesis:

The pH-responsive particles utilized in the generation of the pH-responsive colloidosomes, were produced by dissolving 2 g of Eudragit S-100 polymer in 100 ml of reagent alcohol. This solution was then abruptly added to 200 ml of deionized water (18.2 MΩcm) and the mixture becomes immediately turbid. The alcohol was then evaporated by stirring at 70°C for 2 hrs, and additional water was evaporated to increase the particle concentration until a final volume of 50 ml was obtained. The dispersion was left to cool to room temperature and filtered through a Whatman Grade 6 qualitative filter paper (~3μm retention) to remove particle aggregates. The particle concentration was determined by gravimetric analysis. Particle size as determined by DLS (Dynamic Light Scattering, ALV/DLS/SLS-5022F) was of 200 nm, and zeta potential was measured by electrophoresis (Malvern Zetasizer Nano ZS-90).

3.2.3 Microcapsule Preparation:

As previously explained, the colloidosomes were prepared by a double emulsion template. First, a single water-in-oil emulsion was prepared. This emulsion was created from 1.6% (w/v) particle dispersion at pH of 3.2 and a NaCl concentration of 25 mM. 1 ml of this dispersion was added to 2 ml of dichloromethane and homogenized at 30,000 rpm with an IKA T10 homogenizer. The obtained water-in-oil emulsion was then re-

emulsified in a 1.6% (w/v) particle dispersion at a pH of 3.2 and a NaCl concentration of 250 mM by adding 0.5 ml of the water-in-oil emulsion to 1.5 ml of the particle dispersion and shaken by hand. The double emulsion was then diluted in 10 ml of deionized water and stirred with an IKA RW-20 digital stirrer for 20 minutes for the oil evaporation. The capsules were observed in a Nikon Eclipse 50-i Microscope.

3.2.4 Capsule dissolution

The capsule responsiveness to a change in pH was studied by placing the capsules in a 0.2M ammonium chloride / hydroxide buffer at a pH 8 in a glass cell. The dissolution of the capsule was observed under the microscope and time series were recorded.

3.2.5 Contact angle of a macroscopic Eudragit S-100 film

A film of Eudragit S-100 was cast from an ethanol solution onto a polypropylene substrate; this film was submerged in water saturated with dichloromethane at the pH and NaCl concentrations used in the emulsification. A drop of dichloromethane was then deposited onto the film and contact angles measured with a Ramé-Hart Goniometer. The averages and standard deviations reported for each solution refer to 4 different droplets, each on a separately cast film, with both sides of the droplet measured independently.

3.3 Results and Discussion

3.3.1 Double emulsions of an extractable oil stabilized with Eudragit S-100 responsive nanoparticles.

Dispersions of the pH-responsive nanoparticles have been used to stabilize the double emulsions of water-in-dichloromethane-in-water. The stability of the particles made from Eudragit S-100 as a function of pH and ionic strength has been studied and

described in **Figure 2.7** of Chapter 2, and was considered for the emulsification with stable particle dispersions.

In this preparation scheme both types of emulsions are required: water-in-oil and oil-in-water. Typically, the creation of double emulsions requires two types of surfactants, one more hydrophilic for the O/W and one more hydrophobic for the W/O emulsion [*17*]. Similarly, particle-stabilized double emulsions usually require particles of different hydrophobicity [*42*], as represented in **Figure 3.3**. Surprisingly, the double emulsions could be prepared using the same type of particles in the inner (water-in-oil) and the outer (oil-in-water) interface.

It is well known that the emulsion type obtained is determined by several factors, including the particle wettability, as well as the volume ratio of inner-to-outer phase [*24, 25, 149*]. In order to assess the emulsification properties of a specific system, one of the basic parameters to look at is the *preferred emulsion type,* which is the emulsion type generated from a 50-50 mixture of oil and water and a surfactant or particle stabilizer, as mentioned in Chapter 1.

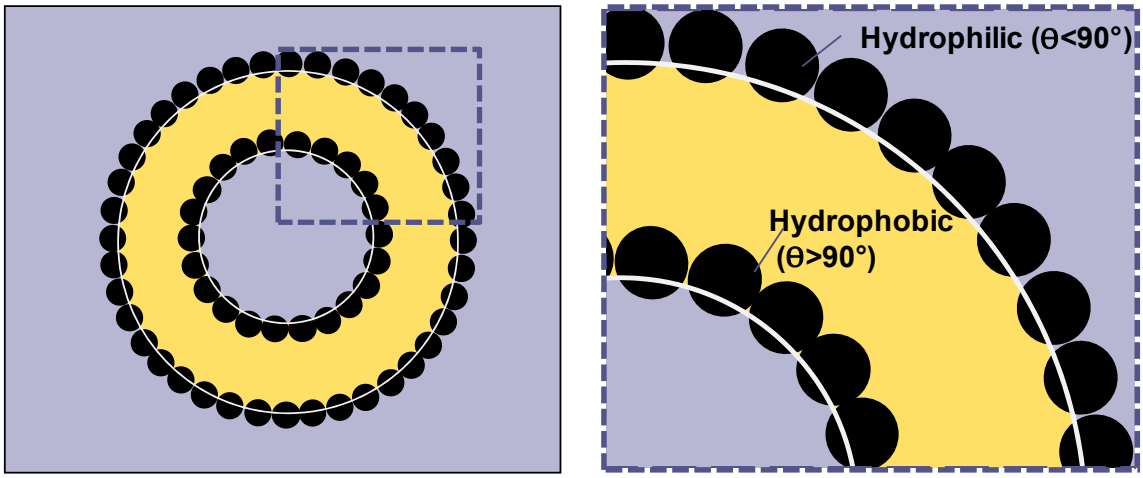

Figure 3.3 Double Pickering Emulsion Illustration

Stable emulsions of the non-preferred type can also be generated by changing the ratio of oil to water, a phenomenon known as "catastrophic phase inversion" [*24, 25, 149*], previously described. Changes in temperature, pH, or ionic strength can change the preferred emulsion type by shifting the relative affinity of the emulsifier for the two liquid phases and lead to a so-called "transitional phase inversion" [*27-29*].

Here, in order to stabilize both types of emulsions with the same pH-responsive particles, different amounts of charge screening by salt ions were used in the inner and outer aqueous phase. The extent of screening was assessed by measuring the particles' the zeta potential. It is believed that the extent of screening has an effect on the degree of particle hydrophobicity. Stability of the outer O/W emulsion required some screening (25 mM NaCl). More hydrophobic particles are needed in order to stabilize a W/O emulsion interface, and hence a higher degree of screening (250 mM NaCl) is required in the dispersion used for the inner emulsion phase. The higher ionic strength reduces the screening length and particles appear overall more neutral, showing a higher hydrophobicity. It was therefore possible to create double Pickering emulsions using a single type of particle, without the addition of stabilizers or surfactants.

In order to assess the actual change of particle wettability with ionic strengh, the contact angle of a dichloromethane droplet with a macroscopic Eudragit S-100 polymer surface was measured under an aqueous salt solution. The data is shown in **Table 3.2**, along with other properties of the particle dispersions. The measurement of contact angles of particles in liquid-liquid interfaces is very complicated. In some cases it has been shown, however, that the particle contact angle can be represented by the contact angle of a macroscopic surface made of the same material [*17, 150*]. In our case, since the material is a random co-polymer with carboxylic groups throughout the chain, it is expected that a macroscopic film cast from this polymer will have exactly the same surface chemistry as the particles. Furthermore, the polymer films, like the particles used for emulsification, are first exposed to the aqueous medium and then to the

dichloromethane. Therefore, it is reasonable to expect that contact angle of the macroscopic film is representative of the contact angle of the particles at the oil-water interface.

Table 3.2 Properties of the particle dispersions used for double emulsion and contact angle of a macroscopic Eudragit S-100 film under the same conditions.

Particle dispersion	**Inner**	**Outer**
Particle conc. [wt/vol%]	1.6	1.6
NaCl [mol/l]	0.25	0.025
pH	3.25	3.39
Zeta potential [mV]	−7.8	−34.2
Electrophoretic mobility [μm.cm/V.s]	−0.61	−2.68
Contact angle [°]	75.1 ± 2.5	64.9 ± 2.3

The data shown in **Table 3.2** indicates that the particles have a smaller zeta potential (in magnitude) for a higher degree of screening, which is expected. The pH drops slightly due to the increase in the ionic strength, which promotes deprotonation of the carboxylic acid groups. Moreover, it can be seen that the particle surface indeed becomes more hydrophobic when exposed to a higher ionic strength solution.

While the data shows that the particle does indeed become more hydropohobic as more salt is added, the contact angle data for both dispersions is below 90º. As previously explained, it is a fairly well-accepted theory that the particle contact angle determines the preferred emulsion type, where hydrophobic particles ($\theta>90º$) stabilize water-in-oil emulsions and hydrophilic particles ($\theta<90º$) stabilize oil-in-water emulsions [*17, 19, 32*].

Indeed, the preferred emulsion type of Eudragit S-100 dispersions (in a 50-50 mixture of oil and water) has been found to be oil-in-water for both ionic strength conditions (0.25 M and 0.025 M), which is consistent with the measured contact angles below 90º (**Table 3.2**). As explained in the experimental section, for the inner W/O emulsion, the aqueous particle dispersion (1ml) was added in a drop-wise fashion to dichloromethane (2ml) and homogenized at 30,000 rpm. In this case, the final ratio of water to oil was 1:2. The W/O emulsion (0.5 ml) was added to the outer particle dispersion (1.5 ml) and shaken by hand. Thus for the water-in-oil (W/O) emulsion interface, the stabilizing particles are supplied from the inner phase, whereas the outer (O/W) interface is stabilized by particles adsorbed from the outer phase.

From this information it can be seen that the particle wettability was tuned by different degrees of charge screening, and the oil/water ratio was set to a point where obtaining a water-in-oil emulsion was made possible. It is still important to mention that the same ratio of water to oil at lower charge screening resulted in very unstable emulsions. Therefore, we believe that both mechanisms (particle wettability tuning and water-to-oil ratio) helped in successfully obtaining a double emulsion which would withstand oil extraction without any type of coalescence.

Additional parameters to take into account in the generation of the double emulsions are the droplet size and the number of water drops in the oil drops. These are important since they will determine the final capsule size, and whether connected or individual capsules are obtained. While the level of control that can be attained by batch emulsification is small in terms of droplet size monodispersity and number of water drops in the oil drops, the parameters used for the second emulsion step seemed to be adequate to obtain mostly single drops in the oil droplets. In reality, a few oil droplets contained more than one water droplet, and even some oil droplets without any water droplets were observed. Nevertheless, most of the observed droplets were a single drop in a drop. It

appears as if a small volume of emulsion aids in the efficient dispersion of individual drop-in-drops into the outer aqueous phase.

There are other possibilities to attain precise control over the drop size and number of drops in the oil droplets. One of them is glass capillary microfluidics [*43, 151, 152*], which are systems that allow tuning of the droplet size and number of droplets produced in an oil drop. These devices have been applied for several emulsification studies, as well as for some Pickering emulsions and even colloidosomes, and are certainly a possibility for improvement for these double emulsions stabilized with pH-responsive nanoparticles. In fact, we carried out a few tests to generate the double emulsions with the aforementioned system. Unfortunately this system posed additional complications from typical microfluidics-based emulsions since the oil used, dichloromethane, has a very low viscosity, which is a crucial parameter for the break-off of the inner water droplets. In microfluidics, it is important to attain apporpriate wetting of each wall and conduit used, as the surface effects are extremely large. Dichloromethane showed particular wetting difficulties with the typical glass and silanized glass surfaces used. While the additional challenges posed by this system on typical glass capillary microfluidic devices can certainly be solved, this goal was not pursued further as it was not crucial for the main purpose of this work. Nonetheless, microfluidic devices are a great possibility to improve on the double emulsions and microcapsules obtained with this approach, and would certainly present opportunities for future expansion of this work.

3.3.2 pH-Responsive colloidosomes from a double emulsion by oil extraction

Once the double emulsion is formed as explained in the previous section, the oil is extracted by dilution in deionized water and solvent evaporation at room temperature. This is done by diluting the double emulsion with water and allowing the

dichloromethane to evaporate at room temperature by stirring the diluted double emulsion under the hood. Stirring is important since the double emulsion droplets tend to sink, as dichloromethane is heavier than water, thus retarding the evaporation. By microscopic observation it was determined that evaporation was completed in 15-30 minutes, which is to be expected as dichloromethane is a very volatile solvent.

Once the oil is extracted, particles assembled on the original interface remain connected by van der Waals forces. No additional locking methods were required for the particles to remain as a closed shell since the van der Waals forces are enough to keep the capsules stable. The ionic strength of the inner aqueous phase of the double emulsion is sufficient to induce particle aggregation. We suspect that some particle aggregation seen outside the capsules is due to ion transport across the solvent phase. Deposition of particle aggregates onto the nascent capsules further enhances the shell thickness. The typical capsule size reproducibly ranges from 25 to 60 μm in radius. An example of the obtained microcapsules is shown in **Figure 3.4**.

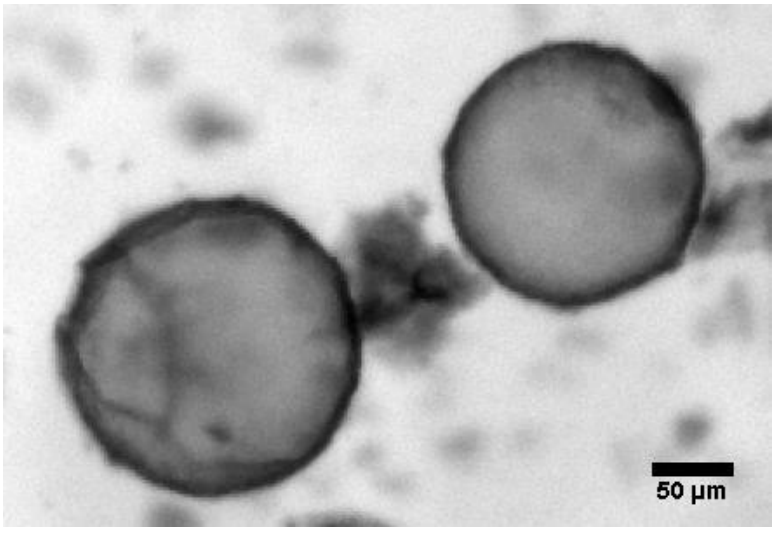

Figure 3.4 pH-responsive colloidosome

In order to corroborate the capsule's responsiveness to pH, the capsules, which were initially prepared at pH 4.5 and were stable up to pH 7, were dispersed into a buffer medium at pH 8 by depositing a drop of capsule dispersion at pH 4.5 into a glass cell filled with a 0.2 M ammonium chloride / ammonium hydroxide buffer and monitoring a capsule under the microscope. Dissolution is shown in **Figure 3.5**, where the time series illustrates the complete disintegration of a microcapsule within seconds. This confirms that a swift release of the capsules' contents can be triggered by a mild change in the pH of the medium. In reality, the initial encounter with a higher pH occurred before the time zero shown in **Figure 5.3 d**ue to the method used for following capsule dissolution, the time elapsed, however is only of a few seconds.

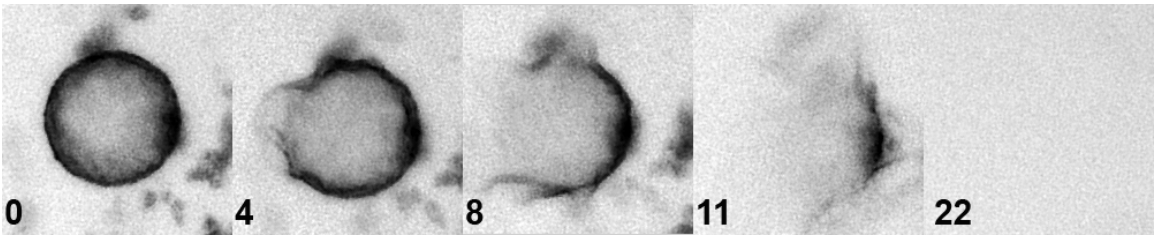

Figure 3.5. Capsule dissolution time series in a 0.2M ammonium chloride / ammonium hydroxide buffer at pH 8. Numbers are seconds after pH change.

In order to study the retention of encapsulated materials prior to capsule dissolution, the capsules' permeability was studied using Fluorescence Recovery After Photobleaching (FRAP), a method that has been shown to be useful for assessing diffusion through a hollow shell [*43, 153*]. FRAP measures the mobility of fluorescent tracers by monitoring their diffusion into a previously photobleached volume.

In this case the interior of the capsule is bleached and the time for recovery is observed. After the capsule interior is bleached, the kinetics for the recovery of the fluorescence intensity represents the time scale for transport of fluorescently-labeled

molecules through the capsule shell. The development of a mathematical model that best describes permeability through a spherical capsule has been developed, as well as additional methods for permeability tuning of the pH-responsive colloidosomes. This work is presented in detail in the next chapter.

3.4 Conclusions

The work presented shows a novel technique for microencapsulation of aqueous droplets in pH-responsive colloidosomes. The colloidosome shells are comprised of nanoparticles made from enteric coatings by a nanoprecipitation method. The pH-responsive nanoparticles are surface active and efficiently emulsify both W/O and O/W emulsions when wettability is modified through charge screening and the water-to-oil ratio is chosen judiciously. Colloidosomes are generated by a double W/O/W Pickering emulsion template via a double emulsion solvent evaporation technique. The resulting microcapsules show a response to a slight pH change, and immediate dissolution is triggered by changing the solution conditions from pH 6 to pH 8. The next chapter presents work focused on developing a mathematical model to study capsule permeability as well as optimization strategies for this parameter by exploring additional particle locking methods.

CHAPTER 4

COLLOIDOSOME PERMEABILITY TUNING AND MEASUREMENT BY FRAP

Parts of the following chapter have been published in references [123, 124] and have been reproduced by permission of The Royal Society of Chemistry.

4.1 Introduction

The combination of microencapsulation techniques and stimulated release mechanisms is particularly appealing for the controlled delivery of any active substance that requires protection against chemical degradation before the target environment or desired time of action has been reached, and for actives that need to be ‘‘camouflaged’’ for improved uptake or to mask a bad taste. Good performance in these applications obviously implies low microcapsule permeability for the active ingredient prior to the release stimulus, and a significant permeability increase in response to it. Apart from the specifications regarding cargo retention and release, economic viability also calls for high encapsulation efficiency and high capsule yield.

As it has been previously mentioned, colloidosomes have been proposed as microencapsulation technique with great promise due to the potential advantages that come from utilizing particles as building blocks of the capsule shell. These include increased sturdiness, defined permeability and the option of functionality introduced by the particles themselves.

Despite all of the recent advances in colloidosome assembly, the practical use of colloidosomes as delivery vehicles has been extremely limited so far, arguably because the known colloidosome systems fail to satisfy simultaneously all of the previously

mentioned demands (regarding retention, release, and efficiency) dictated by typical controlled release applications.

The pH-responsive colloidosomes that have been developed and described in detail in the previous chapter are intended to function as microencapsulation systems that integrate all of the aforementioned requirements. Some of these have already been accomplished: they show stimulus-response by completely dissolving upon a slight pH change, while high yield and encapsulation efficiency are requirements that are optimized by the approach taken for formulation: the double emulsion-solvent extraction route.

An additional parameter to be considered is the colloidosome shell permeability; as a low permeability means the encapsulated ingredients are retained in the colloidosome until the shell is dissolved. A microcapsule shell permeable to the encapsulated cargo will release the ingredients before the stimulus is triggered, thus defeating the purpose of the stimulus-responsive material. This chapter focuses on the technique for measurement of colloidosome permeability as well as methods developed to tune this parameter while retaining a stimulus-responsiveness, with the intent of generating fully functional stimulus-responsive colloidosomes.

4.2 Capsule Permeability Measurement with FRAP

Fluorescence Recovery After Photobleaching is an optical technique typically used to measure diffusion in 2D systems [*154-156*]. This technique is based on photobleaching fluorescent molecules by a brief exposure to a high intensity focused laser beam. Subsequent recovery of the fluorescence intensity due to diffusion of unbleached molecules is monitored by confocal microscopy using the same laser in a strongly attenuated form [*156*]. Since permeability accounts for the diffusion of a molecule through a membrane or wall, FRAP can be applied as a method to measure this parameter in microcapsules [*43, 153*]. **Figure 4.1** shows a series of images taken from a

FRAP experiment performed on a microcapsule. Initially, the capsule has been equilibrated with a solution of fluorescent molecules, which are visible in the inside and on the outside of the shell. The next frame shows the capsule immediately after photobleaching with no fluorescence in the interior. As time passes, unbleached molecules from the outside diffuse to the inside of the capsule, thus recovering the intensity.

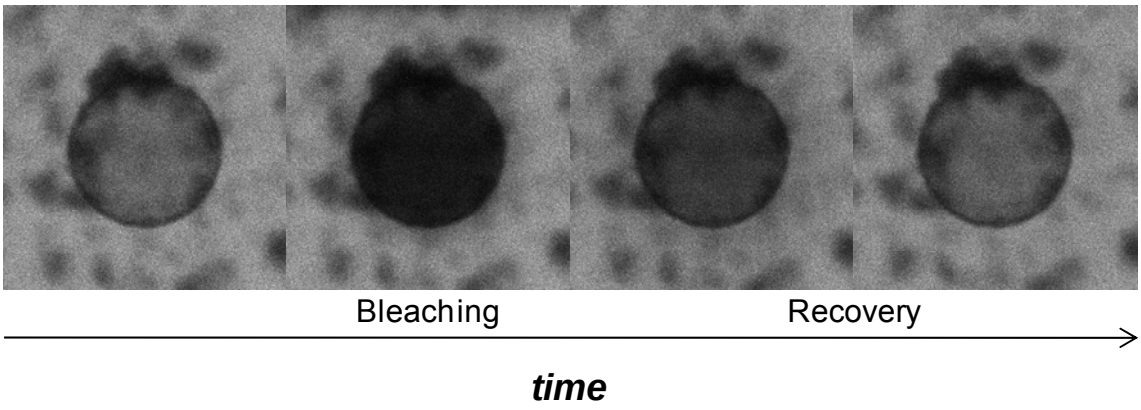

Figure 4.1 FRAP on a microcapsule with 500 kDa FITC-dextran.

A theoretical description of fluorescence recovery developed by Soumpasis works well for many systems, representing unconfined 2D [*154, 155*] and 3D [*157*] geometries. An alternative analysis is necessary for confined systems such as the interior of a microcapsule.

In the fully bleached interior of a small microcapsule, tracer transport is limited by permeation through the capsule wall [*153*]. In the previous studies where FRAP has been applied to measure capsule permeability, the recovery of intensity was modeled with an exponential recovery [*43, 153*]. This is expected for a system where only diffusion of the tracer through the wall is to be accounted for intensity recovery [*153*].

The normalized intensity recovery is thus modeled by the following expression [*43, 153*], referred to, in the following, as the "Möhwald" equation[*153*]:

$$f(t)_{Möhwald} = \left[1\text{-}\exp\left(-\frac{t}{\tau}\right)\right] \qquad \textit{Eq. (7)}$$

where *f(t)* represents the normalized fractional intensity, τ is the adjustable parameter representing the diffusion timescale and *t* is time.

The fractional intensity is given by:

$$f(t) = \frac{I(t) - I(0)}{I_\infty - I(0)} \qquad \textit{Eq. (8)}$$

where $I(t)$ is the fluorescence intensity, $I(0)$ is the intensity upon photobleaching $(t = 0)$, and $I_\infty = lim_{f\to\infty} I(t)$ is the fluorescence at full recovery.

In the larger capsules considered here, only a subvolume of the capsule interior is bleached, determined by the bleaching area and the extent of the optical system's point-spread function, as illustrated in **Figure 4.2**. This figure exemplifies one potential cause of non-perfect bleaching. Additional factors affect bleaching, which are later discussed.

In this case, two mechanisms will contribute to fluorescence recovery in the bleached region: permeation of the tracer through the capsule wall and the free diffusion of unbleached tracer in the capsule. Permeation is expected to contribute an exponential recovery [*153*], as with the Möhwald expression, whereas the recovery due to free diffusion is best described by Soumpasis' expression involving the modified Bessel functions I_0, I_1: [*155*]

$$f(t)_{Soumpasis} = \exp\left(\frac{-2\tau}{t}\right) \cdot \left\{I_0\left(\frac{2\tau}{t}\right) + I_1\left(\frac{2\tau}{t}\right)\right\} \qquad \textit{Eq. (9)}$$

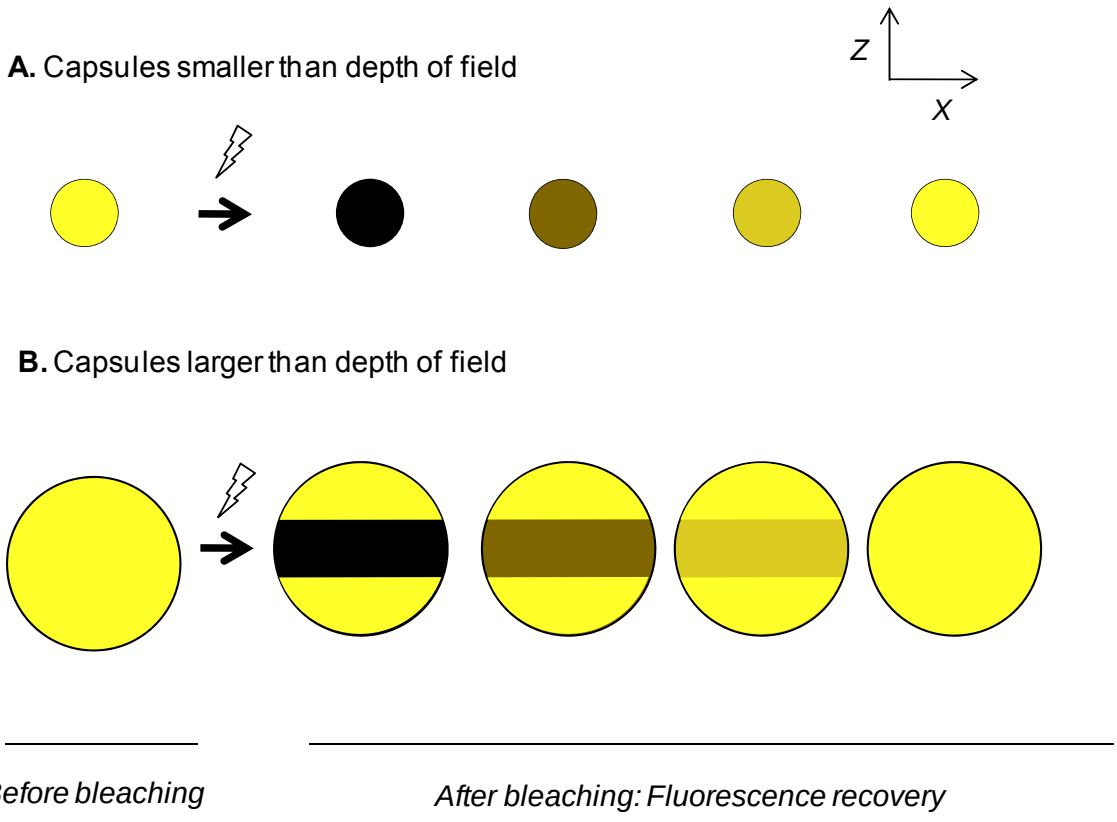

Figure 4.2 FRAP for small capsules with complete bleaching and for large capsules with partial bleaching. *Sideview*

While Möhwald´s expression might be suitable for modeling fluorescence recovery for fully bleached capsules (generally very small capsules), we have developed a more general model, which is useful for the measurement of capsules of any size and permeability values [*123, 124*]. Both mechanisms, permeation and diffusion, are therefore taken into account by a weighted expression that captures the main features of the fluorescence recovery:

$$f(t)=\alpha\left[\exp\left(\frac{-2\tau_1}{t}\right)\cdot\left\{I_0\left(\frac{2\tau_1}{t}\right)+I_1\left(\frac{2\tau_1}{t}\right)\right\}\right]+(1-\alpha)\left[1-\exp\left(-\frac{t}{\tau_2}\right)\right] \qquad \textit{Eq. (10)}$$

In this case, τ_1 represents the free diffusion time constant, τ_2 represents the permeation time constant and α is the weighing parameter determined by the fraction of

the fluorescent molecules bleached inside the capsule. By finding the time constant for diffusion through the capsule wall, τ_2, the permeability can then be obtained by [*153*]:

$$P = \frac{R}{3\tau_2} \qquad \textit{Eq. (11)}$$

where *R* is the capsule radius.

In order to validate the model, some FRAP experiments performed on different capsules are presented. These experiments were carried out by equilibrating a solution of a fluorescent molecule overnight with the capsule dispersion, in order for the molecules to diffuse into the capsules. The solutions used were: fluorescently labeled dextran (FITC-dextran, 500kDa) at 0.25 mg/ml or a fluorescein solution at a 4mM concentration prepared in a pH 6 phosphate buffer. FRAP was performed in a confocal microscope, Zeiss LM510 with an Argon laser at 488 nm wavelength with a 10x objective. The inside of the capsule was bleached and time series images were recorded. The images were then analyzed with MATLAB (Mathworks) and the average intensity of the capsule interior was determined.

A typical recovery curve for a pH-responsive colloidosome, is presented in Figure 4.3. This figure also shows a control recovery curve, which represents the intensity recovery of FRAP performed on free solution of the same fluorescent molecules. The recovery time-scale for the control is thus associated with the free diffusion of the molecules. The difference observed between the capsule and the control is due to hindered diffusion of the fluorescent molecules to the capsule's interior through the shell. Quantification of these timescales can be related to the capsule's wall permeability. The values for the adjustable parameters of the weighed expression are obtained by a least squares approximation with MATLAB software.

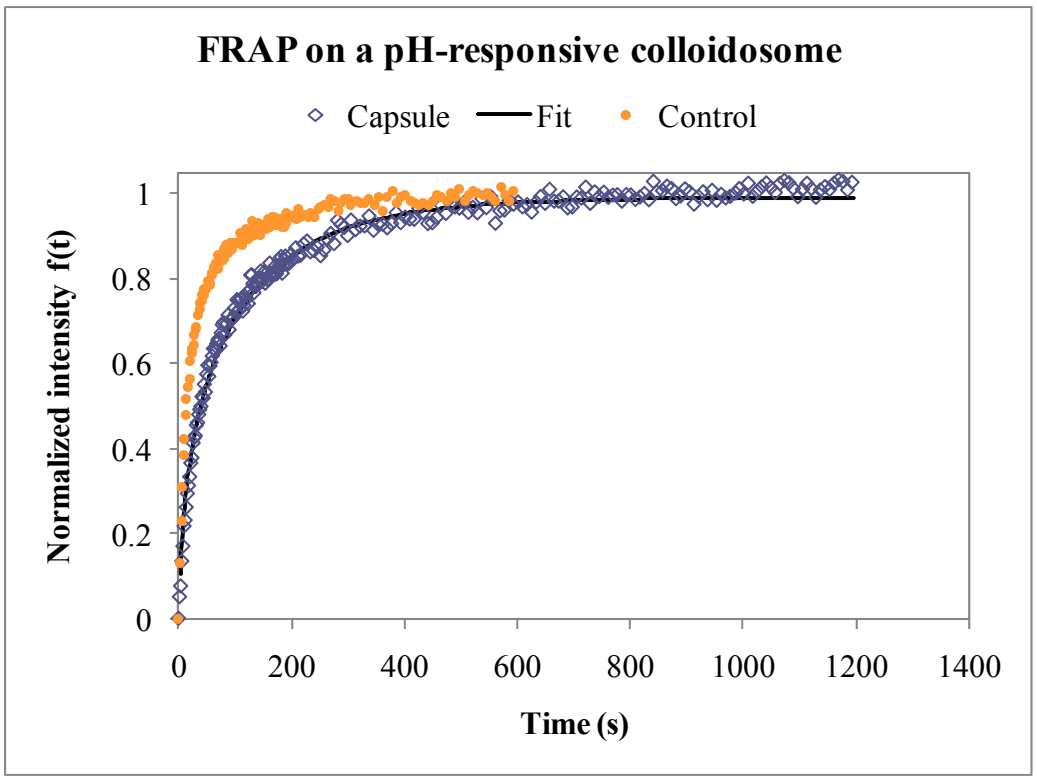

Figure 4.3 Fluorescence Recovery curve for free-diffusion and hindered diffusion through a pH-responsive colloidosome shell of 500 kDa FITC-Dextran.

For this specific case, the values obtained are:

- Capsule's radius: 24 μm
- α=0.57
- τ_1=18 s
- τ_2=138 s
- Coefficient of determination for the fit, R^2=0.985
- Permeability = 0.06 μm/s

The capsule's intensity recovery is fit well by the weighted expression. In these experiments, the capsules were incubated with 500 kDa FITC-dextran prior to measurements. The bleached area was a circular region with a perimeter corresponding to

the capsule equator. The existence of the longer time constant, τ_2, is evidence that the capsule wall acts as a diffusion barrier.

The inclusion of parameter α makes the weighed expression applicable to capsules of any size and permeability. Ideally, α would be determined only by the volume of the capsule under observation and that out of the focal plane. These dimensions are quantified by the capsule's radius and the objective focal depth. This would certainly be true for instantaneous, perfect photobleaching, where 100% of the molecules in the capsule slice under observation are darkened and the bleached volume is identical in size and shape to the capsule interior, where fluorescence recovery is recorded. In reality, there are some factors that affect the efficiency of bleaching.

One important aspect is the time required for photobleaching the region of interest, in this case, the capsule's cross-sectional area. This time will be determined by two main parameters: capsule size and laser velocity. Since the laser sweeps the image with a single laser spot, the photobleaching time will be affected by the velocity at which the capsule image is completely scanned by the laser. Evidently, larger capsules will take longer to be scanned.

The laser velocity will itself be determined by the pixel dwell time, i.e., the time the laser remains in a single spot. This time should be long enough to bleach the molecules under the laser. By using fluorophores that are easily bleached, this time can be reduced. Fluorescein, a fluorescent molecule that is easily bleached, is thus a widely used molecule for FRAP experiments. This photobleaching time scale becomes relevant when it is comparable to the diffusion timescale of the fluorescent molecules. In this case, the longer the time for photobleaching, the more non-bleached molecules will diffuse into the observation volume. This will cause non-efficient bleaching, which can be quantified by the percentage of intensity lost. There are other variables that can affect the bleaching efficiency, such as the laser power, which are not under control.

As mentioned, a loss in bleaching efficiency is thus related to the diffusion of non-bleached molecules back into the observation molecules. These molecules can be diffusing from the un-bleached capsule volume, or permeating from the outside of the capsule. The diffusion of non-bleached molecules during bleaching into the observation volume will therefore depend on: 1) the free diffusion coefficient of the non-bleached molecules, 2) the un-bleached volume, and 3) the permeability of the capsule.

As can be deduced from this information, larger capsules will have smaller α values, not only because the volume ratio of the bleached to non-bleached volume is smaller, but also because larger capsules have longer photobleaching times.

Furthermore, for the same capsule, α can be different if molecules of different size are used in the frap experiment; where larger, slower diffusing molecules would result in smaller α values. Even more, for two capsules of the same size, but different permeability, α would be larger for the more permeable capsule, because fluorescence recovery is determined to a lesser extent by capsule permeation and more by the unhindered diffusion of tracer molecules.

From our experiments performed on capsules with different permeability, it has been found that capsules with low permeability have much higher bleaching efficiency. This can be explained by the fact that even un-bleached molecules that diffuse back into the observation molecules still have the opportunity of being bleached. In the case of low permeability capsules, the molecule exchange will occur mainly between the observation volume and the rest of the capsule. For highly permeable capsules, this exchange will occur with the equilibrium media surrounding the capsule. As the exchange volume of low permeability capsules is much smaller, the probability of bleaching molecules is higher than for the highly permeable case.

In the ideal, perfect and instantaneous bleaching case (which is represented in **Figure 4.2**) one could set the α value only by knowing the capsule dimensions and the

objective focal depth. In reality, for the reasons explained before, α is necessarily an adjustable parameter, which is related to the bleaching efficiency.

FRAP experiments performed on high permeability and low permeability capsules of roughly the same size are shown in **Figures 4.4 and 4.5[i].**

Fluorescein has been used in both experiments. As is shown by comparing both figures, the α values are very different for both capsules, which are roughly of the same size. The obtained numerical values for these experiments are shown in **Table 4.1**.For capsules of very different permeability, the proposed model with weighing parameter α is a considerably better fit for the intensity recovery curve. As is to be expected due to the more efficient bleaching in low permeability capsules; the highly permeable capsule's recovery resembles more closely the Soumpasis' fit for free diffusion, while the low permeability capsule's recovery resembles more closely the Möhwald's approach where recovery is limited entirely by permeation.

---

[i] The microcapsules used for the experiments shown in Figures 4.4, 4.5 and Table 4.1 have been generated by tuning the permeability of the pH responsive colloidosomes described in Chapter 3. The approach for permeability tuning as well as FRAP experimental details will be described extensively in the next section of this chapter.

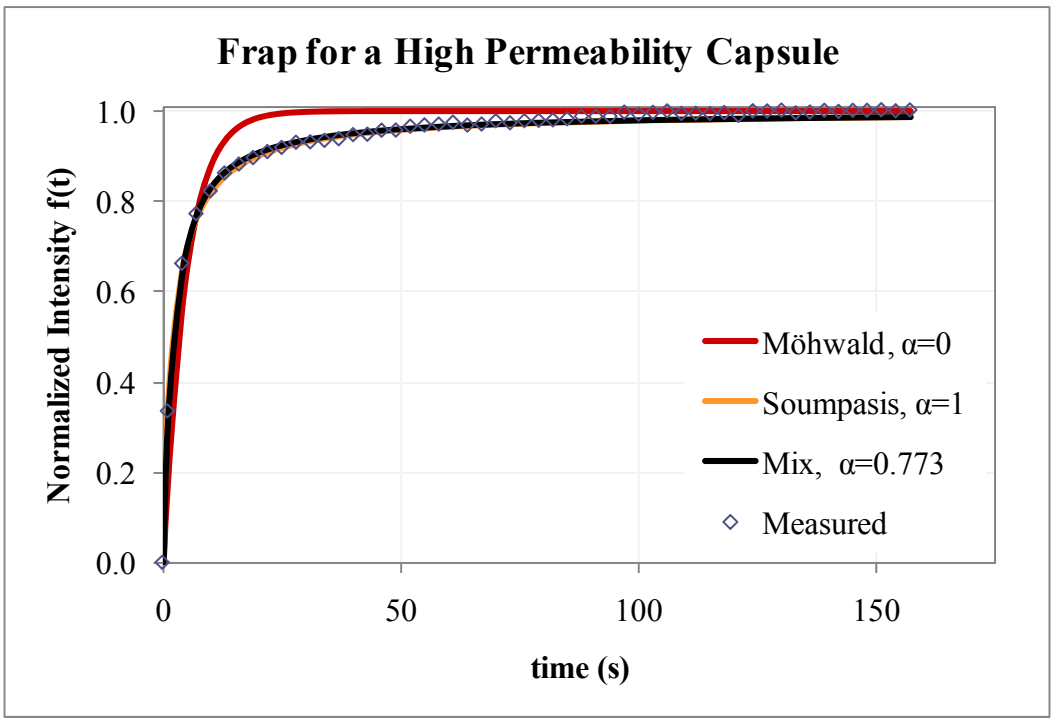

Figure 4.4. Comparison of fit models for FRAP performed on a highly permeable capsule.

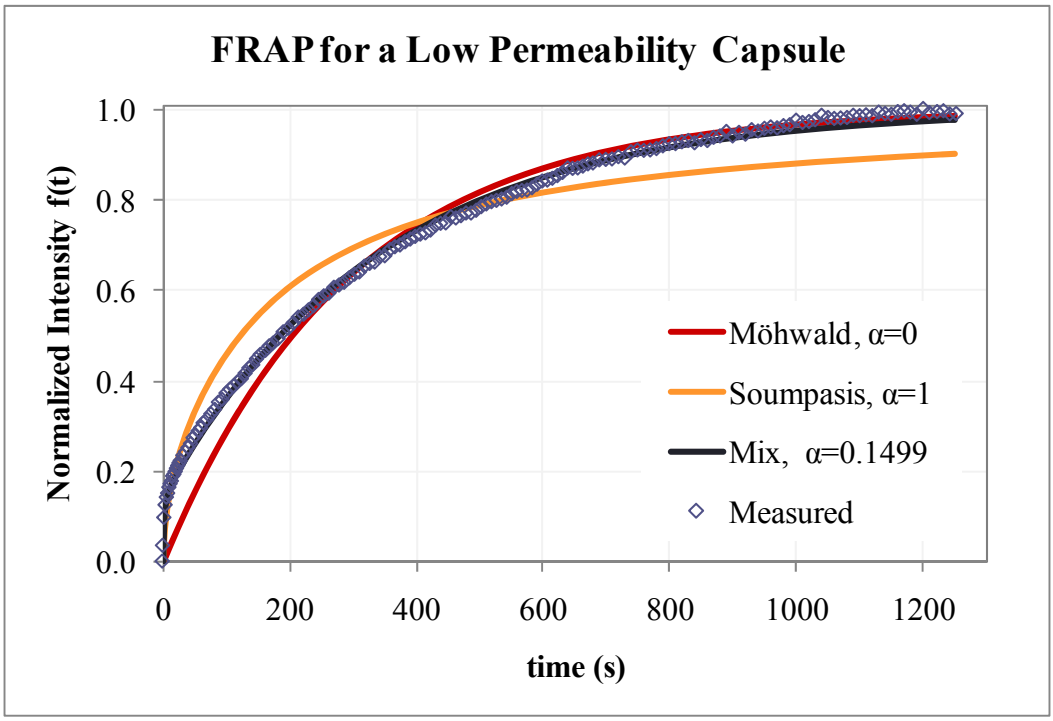

Figure 4.5. Comparison of fit models for FRAP performed on a low permeability capsule

Table 4.1. Numerical values from FRAP experiments with a fluorescein tracer (MW = 332 Da) for high and low permeability capsules.

		High Permeability	Low Permeability
	Capsule radius (μm)	31	28
Möhwald, α=0	τ	5	256
	R^2	0.93	0.96
Soumpasis, α=1	τ	2	113
	R^2	0.995	0.91
Mix, 0<α<1	α	0.77	.19
	τ_1	3	2
	τ_2	3	320
	R^2	0.997	0.999
	Permeability (μm/s)	3.4	0.03

It is important to mention that for capsules of very high permeability, such as the one shown in **Figure 4.4**, the values obtained for the permeation characteristic time are very similar to the free diffusing timescale. In this case, with a high α, the precision of the obtained value for τ_2 is smaller, as the fit has a reduced sensitivity to this time scale. Therefore, for this type of capsules, the high permeability value obtained comes with a comparatively large error margin (~ 0.3 μm/s for the example shown in Table 4.1) By contrast; a precise permeability value will be obtained when there is a significant difference in the free diffusion and permeation timescales, τ_1 and τ_2. In the case of high permeability capsules, this can be accomplished by using larger fluorescent molecules, such as FITC-labeled dextrans.

Nonetheless, as shown in **Figures 4.2**, **4.4** and **4.5**, the proposed model for fluorescence recovery in a microcapsule works well for capsules of any permeability values and size. The inclusion of the weighing parameter to account both for free diffusion and permeation expands the applicability of FRAP for permeability measurement to a wider range of microcapsules. It is believed that the proposed mixed model is a better approach even for very small capsules where mainly permeation is to be taken into account, since introducing a small α value will allow a more precise fitting of the exponential time constant to be related to permeability, since both recovery modes will be present in all cases.

4.3 Permeability Tuning of pH-Responsive Colloidosomes

The model developed to measure capsule permeability has been applied to determine the permeability of the pH-responsive colloidosomes. Although endowed with good processing properties and an efficient release trigger, these responsive colloidosomes show high permeability values prior to dissolution. As briefly mentioned in the previous section, the capsule used to take the data shown in **Figure 4.3**, has a permeability of 0.06 μm/s for a 500k Da FITC-dextran. The figure shows complete recovery after 1200 seconds, which would imply that a very large molecule, such as a 500 kDa dextran is retained for far less than half an hour. Such a capsule is of no practical use because its permeability prior to dissolution is already so high that a cargo of lower molecular weight would already be lost by diffusion through the capsule wall long before the intended triggered release.

In this section, a solution to this last crucial deficit is provided, by demonstrating three methods of controlling the capsule permeability prior to release while maintaining the intended response to the release trigger. The applied methods include: (a)

colloidosome consolidation by partial dissolution and sintering, where the solvent conditions are changed after the colloidosome assembly, (b) deposition of additional polyelectrolytes and responsive particles via layer-by-layer adsorption onto the original colloidosomes, and (c) inclusion of the water-insoluble poly-(lactic-co-glycolic acid), PLGA, in the middle oil phase of the double emulsion at the time of the capsule preparation, resulting in pH-responsive PLGA–nanoparticle composite microcapsules. Each of these approaches leads to a marked reduction in permeability without sacrificing the ability of triggered release by (complete or partial) capsule dissolution. The presented composite microcapsules are the first colloidosomes to combine the benefits of high yield and encapsulation efficiency with good cargo retention and triggered release upon a mild pH stimulus. The different approaches are taken to reduce the permeability of these capsules, while retaining their pH-responsiveness are presented next.

4.3.1 Experimental Methods

4.3.1.1 Particle synthesis and characterization

Particles were synthesized as previously described in Chapter 2 [*123*]. Particles of two different sizes were prepared, one (180 nm) for all the capsule preparation and another (74 nm) for the layer-by-layer reinforcement. For the large particles, 2 g of Eudragit S-100 (received as a gift from Evonik and used without further purification) are dissolved in 100 ml of hot reagent alcohol (BDH, purchased from VWR). This solution is abruptly added to 200 ml of deionized water (obtained from a Barnstead Easy Pure II System, resistivity: 18.2 MΩ cm) and mixed at 400 rpm with a magnetic stirrer. The solution immediately turns turbid, indicating particle precipitation. Alcohol and water are then evaporated under continued mixing at 70°C until the volume is reduced to ~35 ml. After passing the particle dispersion through a Whatman Grade 6 qualitative filter, a

particle concentration of 5% (w/v) is found by gravimetric analysis. The particle size in diluted samples was measured by Dynamic Light Scattering (DLS) using a goniometer setup (ALV/DLS/SLS-5022F). The (intensity weighted average) size for these particles is 180 nm in diameter with a coefficient of variance (CV) of 2.8%, as determined from a second order cumulant fit to the measured intensity autocorrelation function. In the case of the smaller particles, 2.25 g of Eudragit S-100 is dissolved in 300 ml of reagent alcohol and this solution is added to 600 ml of deionized water. The dispersion is evaporated at 70°C to 50 ml. The resulting particle concentration is 1.5% (w/v), with a mean particle diameter of 74.2 nm and a CV of 11.6%.

4.3.1.2 Capsule preparation

4.3.1.2.1 Regular dissoluble capsules.

These capsules are prepared as previously described in Chapter 3 with some minor modifications that help reduce the capsule size. First, a single emulsion is prepared by adding in a dropwise fashion 0.5 ml of a 4% (w/v) particle dispersion at 0.4 M NaCl into 2 ml of dichloromethane (Sigma) and homogenizing at 30 000 rpm with an IKA T10 Ultraturrax Homogenizer. The emulsion is left to rest for approximately 30 seconds and homogenized again at 30 000 rpm for another 30 seconds. Next, 0.7 ml of this w/o-emulsion is added to 1.5 ml of a 3% (w/v) particle dispersion at 0.2 M NaCl and emulsified at 14 500 rpm. The resulting double emulsion is then diluted to 10 ml in deionized water and left to evaporate for 30 min in an IKA RW20 digital stirrer at 150 rpm. This dilution and evaporation step leads to the extraction of the solvent phase and the formation of pH-responsive colloidosomes.

4.3.1.2.2 Ethanol consolidation.

Microcapsules prepared in the same manner as described above are treated as follows: 0.2 ml of the capsule dispersion are mixed with 0.1 ml of reagent alcohol. The capsules are left to rest for 30 minutes to allow for partial dissolution. Next they are placed in an oven at 77.5ºC to allow for ethanol evaporation and heat treatment. The capsules are removed from the oven after 20 minutes and left to cool. Mild sonication for 20 seconds was required to reverse capsule aggregation.

4.3.1.2.3 Layer-by-layer reinforcement.

Regular dissoluble capsules are reinforced by alternate deposition of a polycation and Eudragit nanoparticles. The chosen polycation was polyethyleneimine (Sigma Aldrich) in one case, and PDADMAC (Sigma Aldrich, 20% solution) in another. The polycations are adsorbed from a 2.5 mg/ml polyelectrolyte solution at pH 6 and 0.5 M NaCl, the negatively charged (74 nm) particles from 1.5% (w/v) particle dispersion (also at pH 6 and 0.5 M NaCl). The pH is adjusted with 0.1 M HCl or 0.1 M NaOH. For each layer, 2.5 ml of the capsule dispersion is added to 10 ml of the polycation solution or particle dispersion, and left for 30 minutes to ensure polymer/particle adsorption. This is followed by 3 washing cycles that involve centrifuging at 400 rpm for 8 minutes, removing 10 ml of supernatant, and replenishing with a 0.5 M NaCl solution at pH 6. Four complete layers (4 positive and 4 negative layers) were deposited in total. The ζ-potential of the capsules with each new layer was measured with a Malvern Zetasizer Nano. Even though the values might not be accurate because of the very large size of the capsules, they provide a reliable indication of the charge inversion experienced in each adsorption step.

4.3.1.2.4 Particle–PLGA composite capsules.

The capsules are prepared in exactly the same manner as the regular capsules, with one exception: the oil phase in this case is a poly(DL-lactide/glycolide) 50 : 50 (Polysciences) solution in dichloromethane instead of pure dichloromethane. The PLGA concentration was varied between the values of 7, 14 and 28 mg/ml.

4.3.1.3 Capsule imaging

Microscopy images were taken using a Nikon Eclipse TE 2000-E microscope with a 60X oil immersion objective. Scanning Electron Microscopy images were taken with a Zeiss Ultra 60 SEM at a voltage between 1 and 5 kV. In this case, the capsule dispersions were dried at room conditions on aluminum stubs with carbon tape; the samples were then coated with gold using an EMS 350 sputtering system.

4.3.1.4 Permeability studies

4.3.1.4.1 FRAP.

Fluorescein is initially dissolved in reagent alcohol at a 4 mM concentration. 12.5 ml of this solution is added to 1 ml of the capsule dispersion in a 0.2M phosphate buffer solution at pH 6. The sample is placed in a glass cell fabricated with a no. 1.5 coverglass spacer between two coverglasses of the same thickness. The measurements were made in a Zeiss LSM 510 Confocal Microscope with an argon ion laser (λ=488 nm, 10X 0.3 NA objective). The samples were bleached at a laser intensity of 100% and the recovery observed at 0.3%. Images were acquired at 2–3 second intervals until saturation was reached. MATLAB Software (Mathworks) was used for image analysis as well as for curve fitting.

4.3.1.4.2 Microfluidic dialysis cell for pH switch.

In order to study the exact same capsule under a pH-induced permeability jump, a microfluidic dialysis cell developed by Sato and Breedveld [*158*] was used. The design developed by Breedveld's group was applied for measuring capsule permeability with the initial help of Dr. Jan Scrimgeour.

This cell, made from PDMS and a glass observation compartment, includes a nanoporous membrane (20 nm pores) between the observation compartment and the flow conduits. Using this cell allows for pH change by flowing buffers at different pH values and in situ observation of the same capsule in different solution conditions. **Figure 4.6** shows a digital picture of a typical microfluidic dialysis cell utilized for this purpose. This image clearly shows an inlet and outlet connection. The porous membrane can also be observed through the clear PMDS as a white circle in the center of the cell.

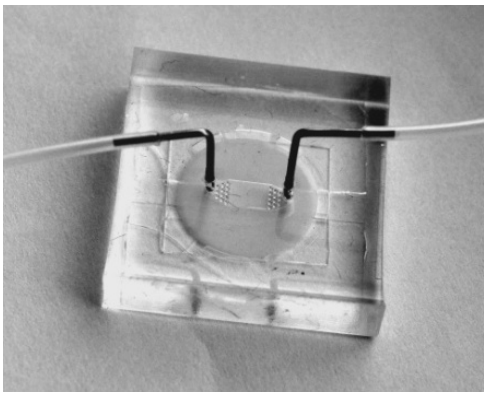

Figure 4.6 Microfluidic dialysis cell for performing FRAP measurements on the same capsule at different solution conditions.

Initially, a 0.2 M phosphate buffer solution at pH 6 with 0.05 mM fluorescein is pumped through the flow chamber. After the first FRAP measurement, the pH is raised by flushing with 0.2M ammonium chloride/ammonium hydroxide buffer at pH 8, again containing 0.05mM fluorescein. The pH change is confirmed by an expected increase in

the bulk fluorescence intensity. Once the intensity stabilizes, the next FRAP measurement is initiated. Finally, the pH is switched back to pH 6 by flushing with the initial solution, and, after stabilization of the fluorescence intensity, the FRAP measurement is repeated one more time.

4.3.2 Results and Discussion

As previously mentioned, three different approaches were taken to tune the permeability of the pH-responsive colloidosomes: 1) ethanol consolidation, 2) layer-by-layer assembly and 3) hybrid PLGA-nanoparticle colloidosome formation. The different approaches taken to tune the permeability of the pH-responsive colloidosomes helped to improve this parameter to different extents. In some cases the capsules completely dissolve upon a pH increase, whereas in other cases the capsules remain intact, but show an abrupt increase in permeability.

The pH-responsive colloidosomes, previously introduced, which dissolve above pH 7 and have a high permeability at lower pH [*123*] serve as a base case for the present study and will be referred to as ‘‘regular’’ dissoluble capsules from here on. Previously, a value of 0.06 μm/s for permeability to 500 kDa FITC-dextran has been presented. In the present study, a smaller molecule has been applied as a fluorescent tracer for the FRAP permeability experiments, so that lower permeabilities obtained with the mentioned colloidosome consolidation approaches can be monitored in a reasonable amount of time.

In all of the cases presented, the permeability of the capsules for a small tracer molecule (fluorescein, Mw: 332 g /mol) was studied using FRAP. The reported values correspond to the permeability at pH 6 unless noted otherwise. In the case of measurements done in the microfluidic dialysis cell, the permeability of the same capsule was measured before (pH 6) and after (pH 8) dissolution of the Eudragit particles from

the capsule shell. Finally, the solution was switched back to pH 6 and the permeability measured once again. The different approaches taken to tune the colloidosome permeability and the results obtained with each method will be presented next.

4.3.2.1. Regular dissoluble capsules and consolidation with ethanol

Regular dissoluble colloidosomes with high permeability were prepared from the pH-responsive Eudragit particles as described in the previous Chapter. **Figure 4.7 A** shows the preparation scheme of the regular capsules, along with micrographs of a capsule before and after dissolution by a pH increase.

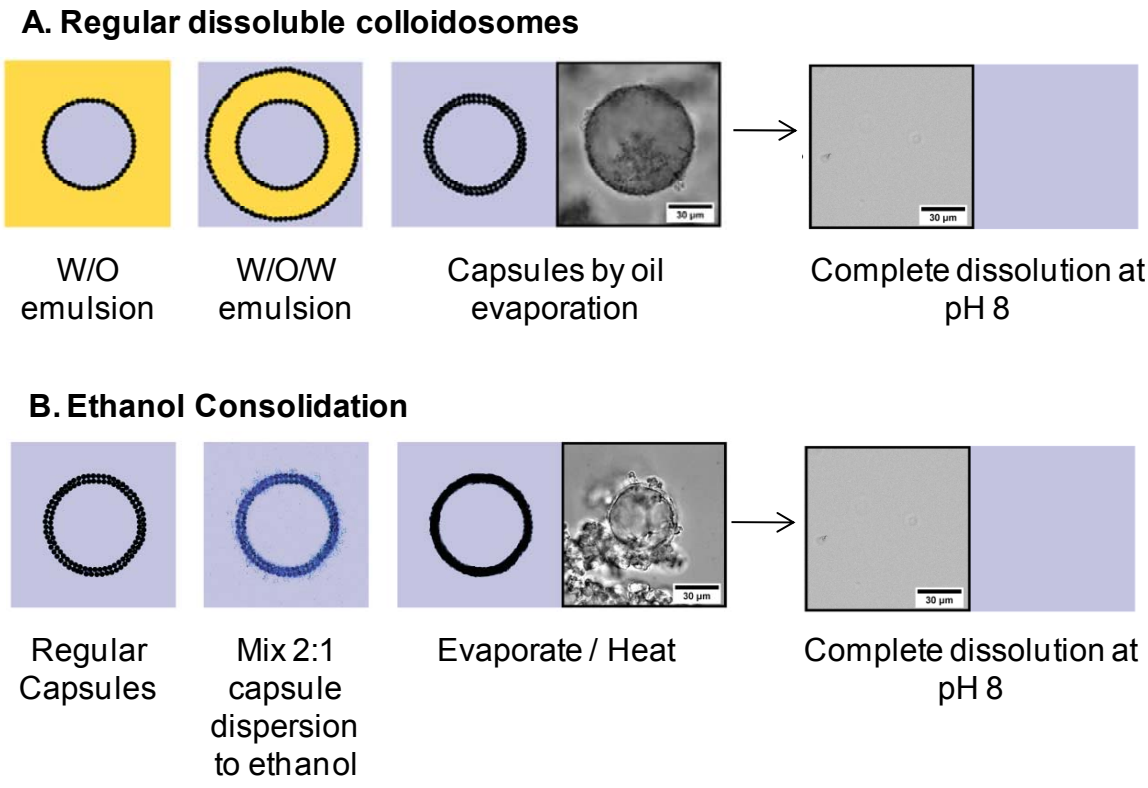

Figure 4.7 (A) Preparation of regular dissoluble colloidosomes. (B) Ethanol consolidation approach for tuning permeability, starting from regular dissoluble colloidosomes. *Microscope images (in frames) show the generated capsules at pH 6 and after raising the pH to 8 with a 0.2 M NH4OH/NH4Cl buffer. Scale bars are 30 μm.*

Many capsules show broken areas or openings as seen in **Figure 4.8 A** below, presumably as a result of damage during capsule drying. An excess of individual particles deposited on the capsule and imaging substrate process is also visible. In order to seal and strengthen these regular capsules, a capsule dispersion is mixed with ethanol. After brief incubation, during which the particles are believed to dissolve partially, the alcohol is removed by heating. A capsule generated with this approach is shown in **Figure 4.7 B**.

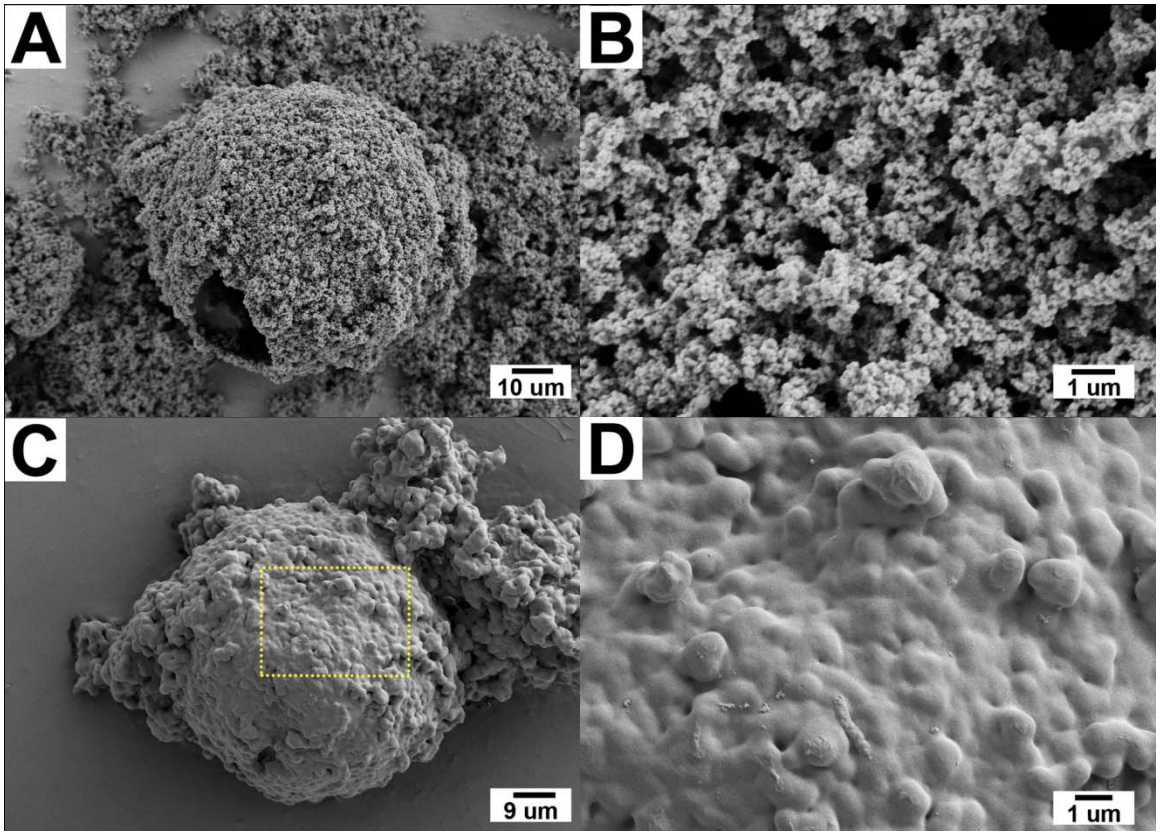

Figure 4.8 SEM images of: (A) regular capsule with high permeability, (B) close-up of surface shown in A, (C) capsule after ethanol consolidation, and (D) close-up of surface shown in C.

We propose that this combined solvent and heat treatment leads to a plasticization and fusion of particles in the capsule shell and to a closure of capsule pores (ethanol

consolidation). **Figure 4.8 C and D** show a capsule treated in this way: particles indeed appear to have partially fused with each other. The large openings regularly observed in the untreated capsules after drying (**Figure 4.8 A**) are not seen after ethanol consolidation, which suggests an improved structural integrity of the treated capsules under stress.

Most importantly, the proposed ethanol/heat treatment leads to a marked reduction in the capsule permeability as one might expect. As presented in **Figure 4.9**, the regular capsules have a high average permeability for fluorescein of 1.5 μm/s. The consolidated capsules, by contrast, have a permeability of only 0.11 μm/s on average, which represents a 13.5-fold reduction.

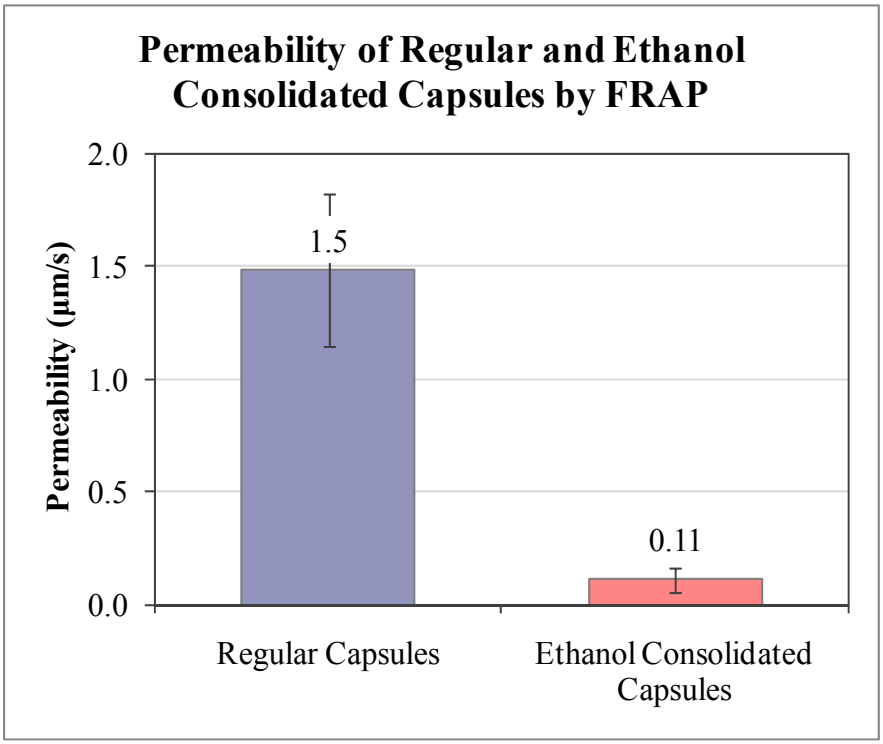

Figure 4.9 Permeability of regular capsules and capsules after ethanol consolidation. *Reported values represent averages over 14 individual measurements for regular capsules and 5 individual measurements for ethanol capsules.*

A statistic analysis (not shown) of permeability values measured for different capsules within the same sample showed good agreement with a log-normal distribution. The fitted width of this distribution is indicated by the error bar in the figure. Capsule-to-capsule variations notwithstanding, the consolidated capsules clearly show a significantly lower permeability for fluorescein or similarly sized capsule cargoes. Ethanol consolidation colloidosomes therefore represent one feasible route towards pH-responsive colloidosomes with improved retention of the active ingredients. Since the shell of the consolidated capsules is still composed entirely of the dissoluble enteric coating polymer, these capsules fully retain the benefit of complete and fast dissolution upon a pH increase above pH 7.

4.3.2.2. Layer-by-layer reinforcement

Another approach explored to generate pH-responsive colloidosomes with low initial permeability applies the well-known method of layer-by-layer assembly, [*51, 72, 159-161*] using a regular dissoluble capsule as template for the deposition of a multilayer adsorbate. Following earlier examples of multilayer assemblies involving polyelectrolytes and nanoparticles of opposite charge [*159*], we alternately deposit layers of a polycation and of negatively charged, dissoluble Eudragit S-100 particles. The schematic representation of layer-by-layer reinforcement is shown in **Figure 4.10**.

Two different polycations were tested, one a high molecular weight (Mw: 200–350 kDa), linear polymer, poly(diallyldimethyl ammonium chloride) (PDADMAC), and the other a branched polymer of lower molecular weight (Mw: 25 kDa), polyethyleneimine (PEI). The deposited anionic particles have a diameter of 74 nm and are chemically identical to the (180 nm) particles used in forming the templating regular capsule; the smaller particles were chosen for the adsorbate layers in order to achieve

high area coverage. Four polycation layers and four particle layers were deposited in total. In order to test the efficient adsorption of each layer, ζ-potential measurements documenting the capsules' charge reversal in each adsorption step are shown in **Figure 4.11**

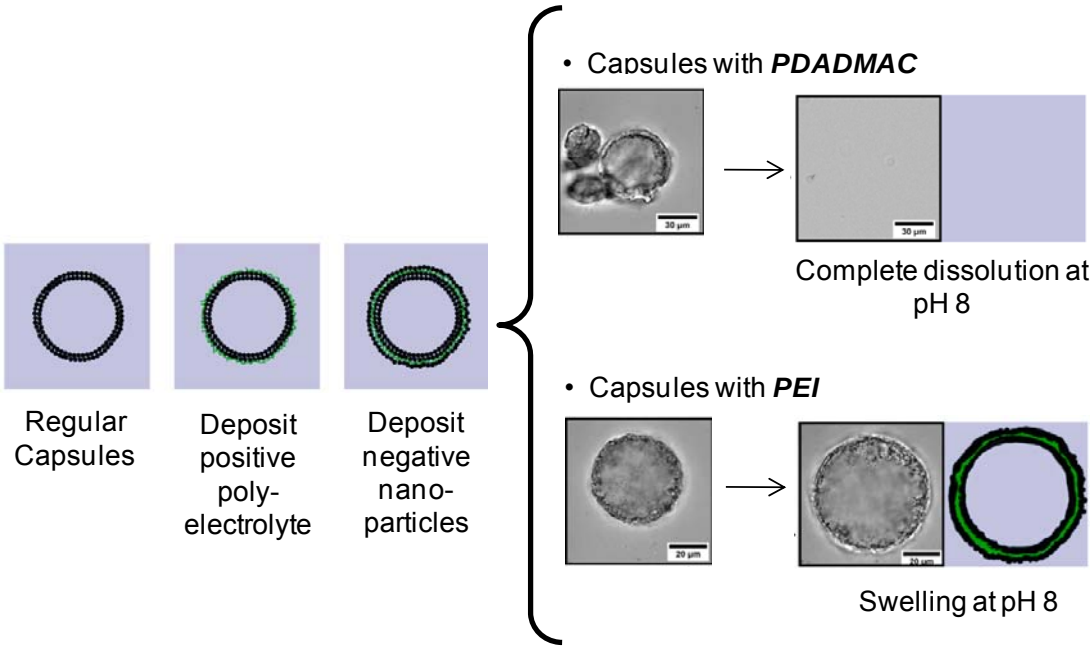

Figure 4.10 Permeability tuning of regular dissoluble colloidosomes by layer-by-layer assembly. *Microscope images (in frames) show the generated capsules at pH 6 and after raising the pH to 8 with a 0.2 M NH4OH/NH4Cl buffer. Scale bars are 30 µm. Shown capsules with layer-by-layer reinforcement contain 4 added layers of polycation and 4 layers of nanoparticles*

Representative microscope images of these capsules are included in **Figure 4.10**, and SEM images are shown in **Figure 4.12**. The SEM images suggest that capsule surfaces have a somewhat different morphology depending on the type of polycation used in the reinforcing layers: capsules obtained with PDADMAC consistently appear smoother than those obtained with PEI.

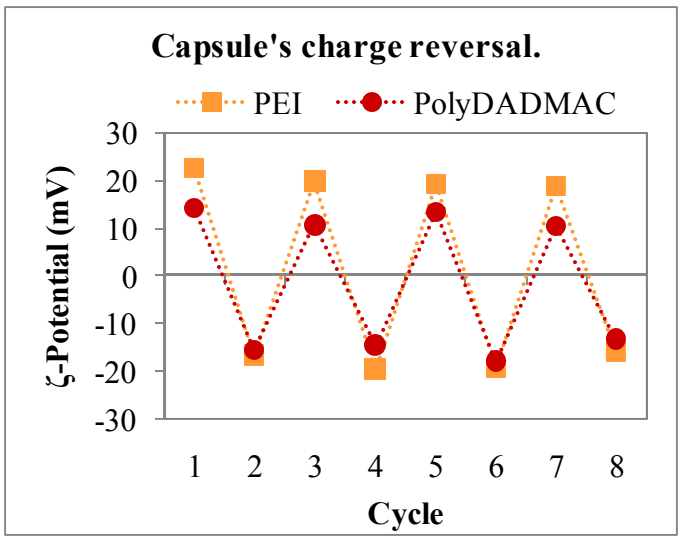

Figure 4.11. Zeta Potential measurements of layer-by-layer reinforced capsules after each adsorption cycle.

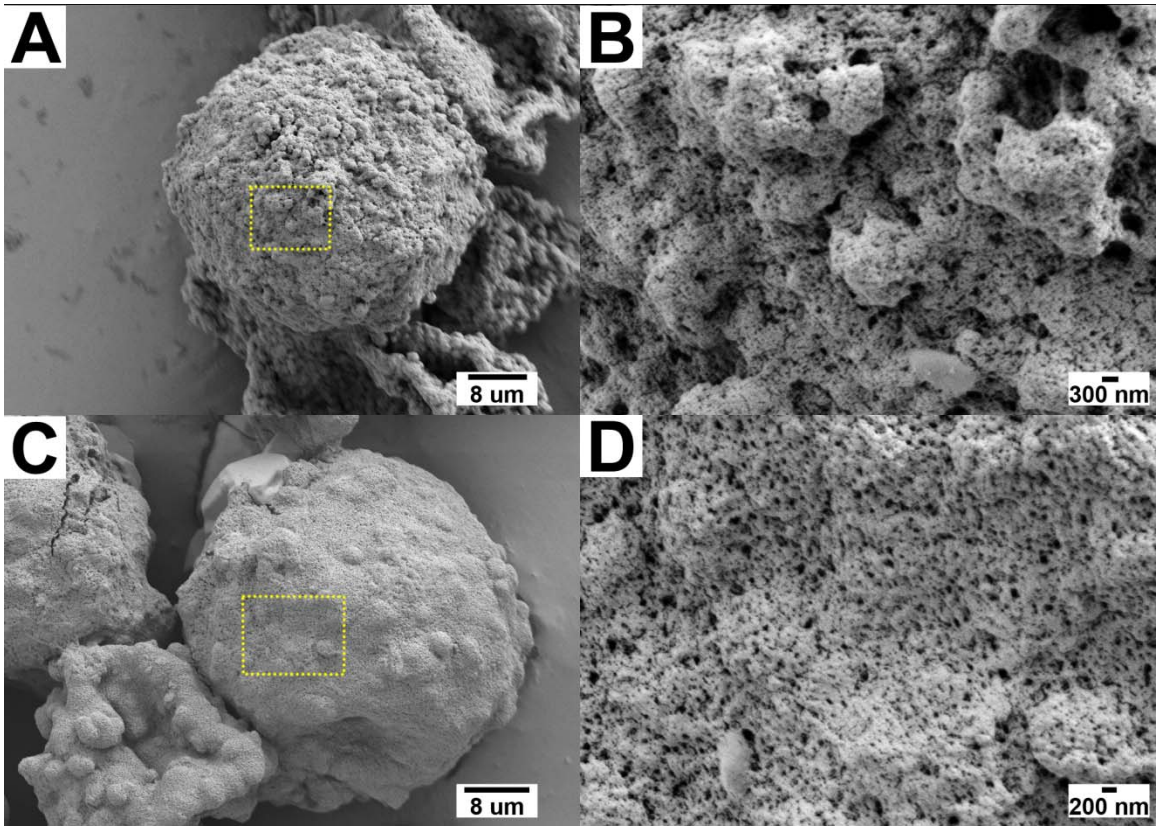

Figure 4.12 SEM images of: (A) microcapsule with layer-by-layer reinforcement using PEI and nanoparticles, (B) close-up of A, (C) capsule with LbL reinforcement using PDADMAC as the polycation, and (D) close-up of C.

When exposed to a pH 8 buffer, the capsules obtained with PDADMAC dissolve completely whereas those obtained with polyethyleneimine remain intact, although in a swollen state. Without investigating the issue further, it is conjectured that the integrity of the capsules containing polyethyleneimine stems from the branched architecture of this polycation, which promotes complexation of the anionic copolymer in a more cross-linked (insoluble) structure.

The effect of the layer-by-layer reinforcement on capsule permeability is presented in **Figures 4.13 and 4.14**. As shown **Figure 4.13**, the addition of four PDADMAC/nanoparticle layers only reduces the permeability by about a factor of 2 on average, whereas a 6-fold reduction is observed on average when polyethyleneimine is used as the polycation.

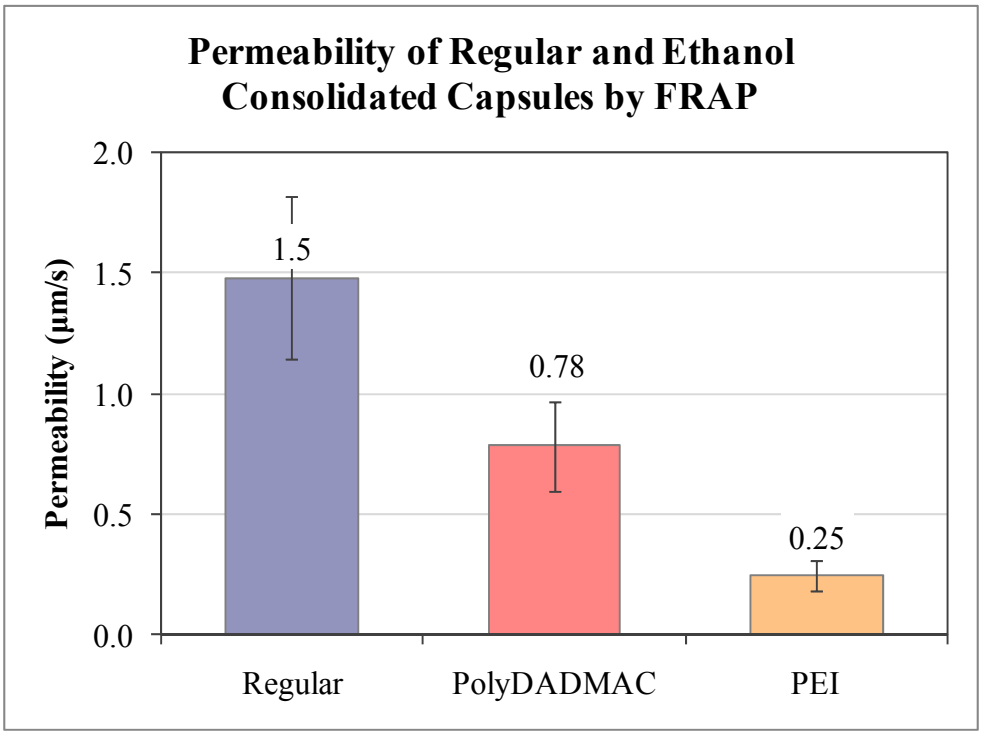

Figure 4.13. Permeability of capsules with layer-by-layer reinforcement, and comparison with regular capsules.

An individual capsule with such polyethyleneimine/nanoparticle reinforcement was studied in a microfluidic dialysis cell. When the pH is raised from 6 to 8, a capsule expansion to more than twice the original volume is observed, and the permeability increases beyond the typical values for the untreated regular capsules. As one might expect, this permeability increase, associated with the dissolution of particles in the capsule wall, cannot be reversed by switching the pH back to 6 (see **Figure 4.14**), instead the capsules remain in a highly permeable state. This property of requiring only a temporary, short term pH stimulus to induce a more permanent state of release can potentially be valuable for on-demand delivery.

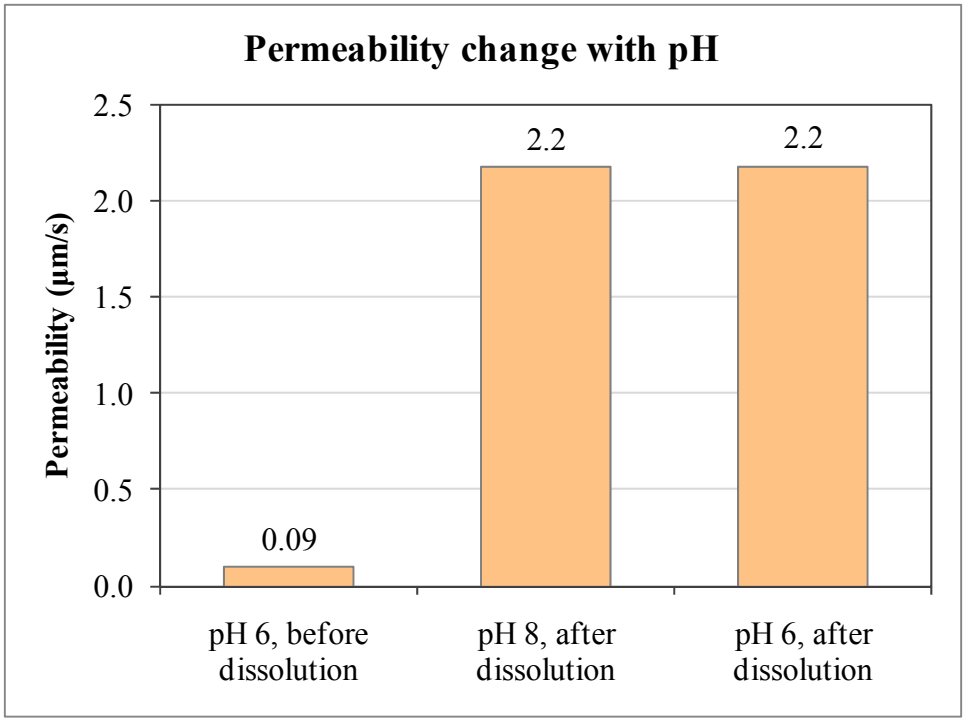

Figure 4.14. Permeability of one capsule with PEI/nanoparticle layer-by-layer reinforcement before and after particle dissolution, measured inside a microfluidic dialysis cell.

As it has been previously explained, it is important to note that FRAP measurements of the capsule permeability become less precise when the permeability is very high, because the rapid exchange of tracer molecules through the capsule walls prevents a complete and uniform bleaching of the capsule interior. In consequence, the observed fluorescence recovery is mediated to a larger extent by free diffusion and to a smaller extent by capsule permeation (corresponding to a larger value of the weighing factor, α), which makes the fit of the experimental data less sensitive to variations in the permeation time constant τ_2 and decreases the precision of the inferred permeability. Therefore, the high permeability values found after dissolution of the Eudragit particles can be taken as an indication for the capsule being ‘‘open’’ or in a release state, but should not be taken as exact values.

From the results shown, layer-by-layer reinforcement of pH-responsive colloidosomes appears as yet another viable route for the generation of pH-responsive colloidosomes with low pre-release permeability. An obvious disadvantage of both the layer-by-layer reinforcement and the ethanol consolidation, however, is that low permeability is only achieved in a post-assembly treatment, which takes some time and bears a risk of cargo loss or degradation. A more radical improvement may therefore be expected from the following strategy, which improves the capsules’ retention properties at the level of the very first assembly step.

2.4. PLGA composite capsules/inverse colloidosomes

In this third approach, a second, water-insoluble polymer is added in the middle phase (solvent phase) of the particle stabilized double emulsion; it binds the particles together once the oil is extracted and, if enough polymer is added, forms a continuous film, in which the particles are embedded. This approach has been previously explored in

non-responsive colloidosomes [*49*]. The preparation scheme and representative microscope images of these capsules are shown in **Figure 4.15.**

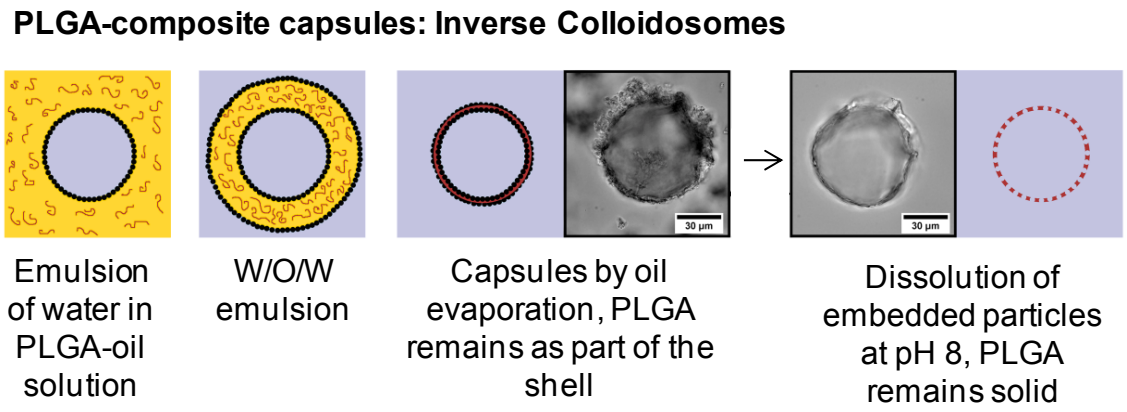

Figure 4.15. Preparation of PLGA-composite pH-responsive capsules. *Microscope images (in frames) show the generated capsules at pH 6 and after raising the pH to 8 with a 0.2 M NH4OH/NH4Cl buffer. Scale bars are 30 µm. The imaged capsule was prepared with 7 mg/ml PLGA in dichloromethane as the middle phase of the double emulsion.*

Here a biodegradable polymer, PLGA, was dissolved in the middle oil phase; as the oil is extracted, the polymer remains as the majority component of a solid shell, with embedded pH-responsive particles. During the oil extraction, the particles are believed to ensure continued, uniform wetting of the inner water droplet by the oil phase, and promote the formation of a solid polymer film with fairly uniform thickness. The same principle of particle-assisted wetting has been applied to the spreading of oil on macroscopic water surfaces and utilized to produce uniform, free-standing porous membranes [*162, 163*]; in this case, the emerging capsule shells can be thought of as ‘‘membranes’’ surrounding the templating water droplets.

As the pH is increased, the particles embedded in these spherical membranes dissolve and leave behind a pure PLGA shell with holes in the original particle locations. The resulting porous capsule wall can be thought of as the negative shape or inverse of a

classical colloidosome with holes instead of particles assembled in a spherical shell. This can be seen more clearly in **Figure 4.16**, where SEM images of this type of capsule before and after dissolution are presented.

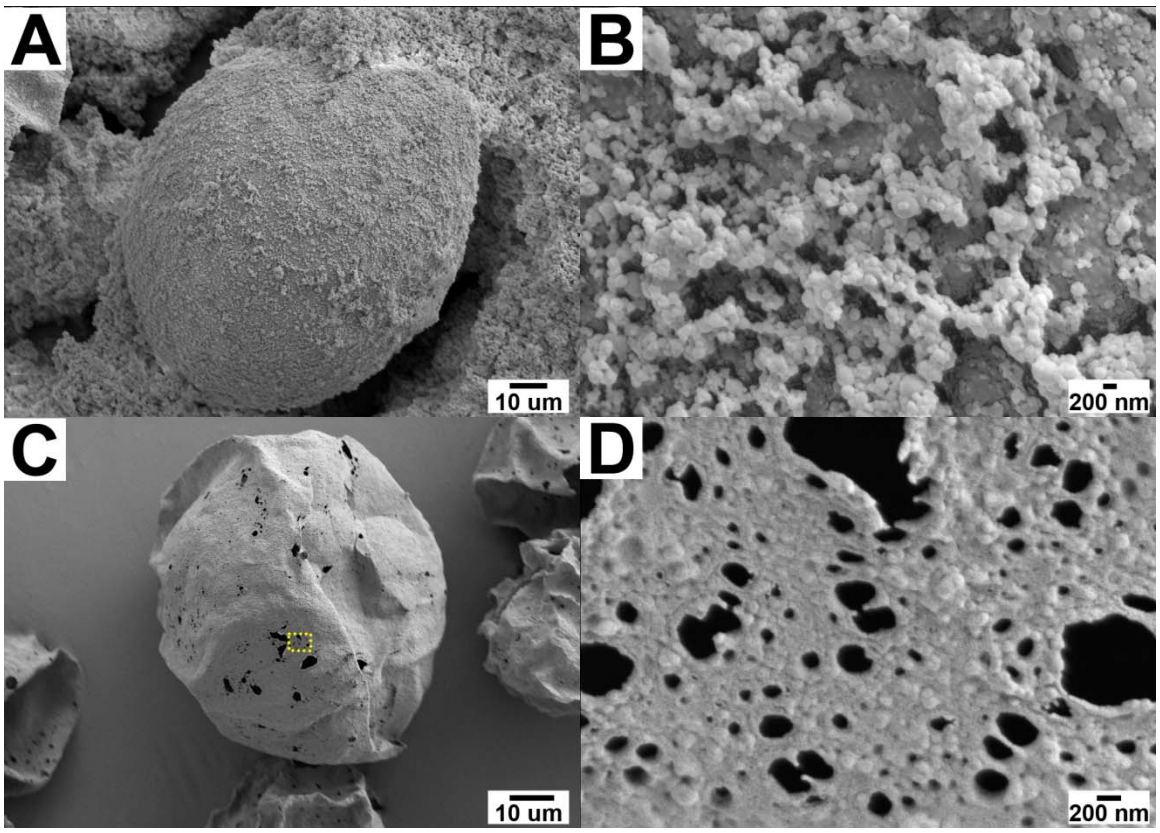

Figure 4.16 SEM images of: (A) particle–PLGA composite capsule, prepared with 14 mg/ml PLGA in the oil phase, (B) surface close-up of A, (C) the same type of capsule after dissolution of the nanoparticles in pH 8 ammonium buffer (''inverse colloidosome''), and (D) close-up of C.

These images suggest that the capsule shell is indeed made up of the polymer with some embedded particles and particle aggregates, although some of the particulate matter seen in the electron micrographs may only have been deposited onto the capsules in the course of the drying process that is part of the sample preparation for SEM imaging. Once the particles are dissolved and washed away, the capsule opens up. Holes can be

clearly seen where some particles have left the polymer shell. Some larger holes appear in the places where particle clusters were embedded. We also note that the composite capsules (before particle dissolution) can tolerate a high vacuum without breaking or collapsing, whereas the highly porous capsules obtained after particle dissolution show a higher tendency to deform when the vacuum is applied.

Different concentrations of PLGA were used and permeability experiments were carried out for each of the resulting capsules; these data are shown in **Figure 4.17**. Clearly, this method is very successful in reducing the permeability, since the average values obtained are the lowest for any of the methods explored in this study. A systematic reduction in capsule permeability with increased concentration of PLGA in the middle emulsion phase is observed.

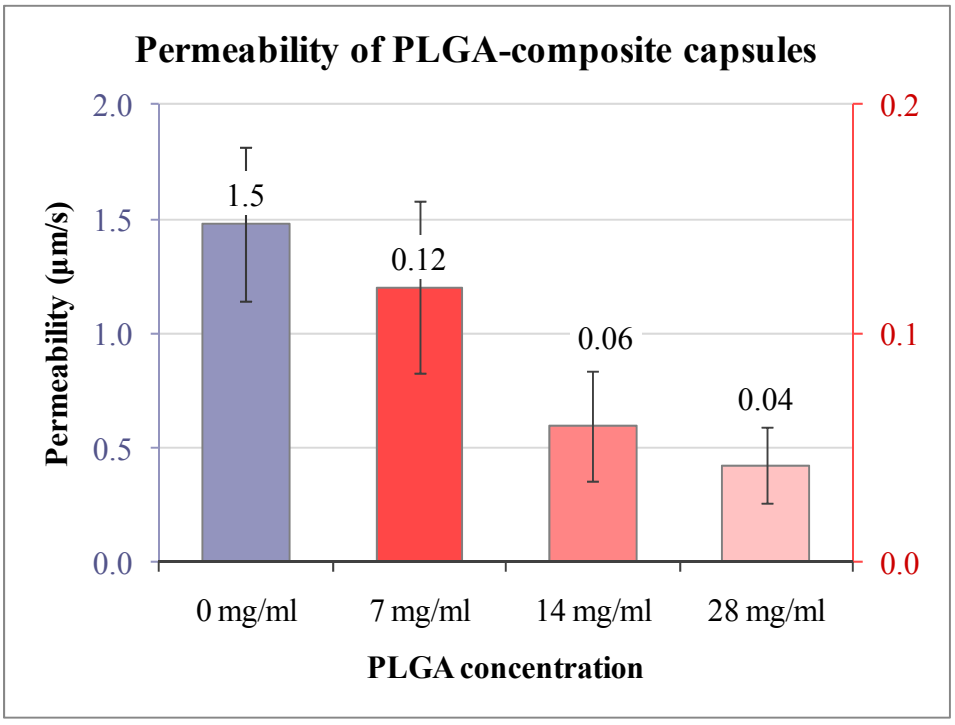

Figure 4.17. Permeability of PLGA-nanoparticle composite capsules and compared to regular dissoluble capsules (0mg/ml). *7, 14 and 28 mg/ml capsules are plotted against the secondary axis.*

As shown in the SEM images, these capsules open up upon raising the pH, but do not dissolve completely. In situ studies of the capsule permeability before and after particle dissolution were again carried out in the microfluidic dialysis cell; the results for three capsules with different PLGA contents are presented in **Figure 4.18**. As expected, a very large permeability jump is triggered when the capsule pH is raised to 8, and the permeability remains high when the pH is reduced back to 6, indicating that the capsule pores stay open. Large permeability differences between the tested capsules prior to particle dissolution are almost certainly linked to the differences in their PLGA content. The significance of capsule-to-capsule variations after particle dissolution, however, is doubtful, since measurements of very high permeabilities are rather imprecise, as previously explained.

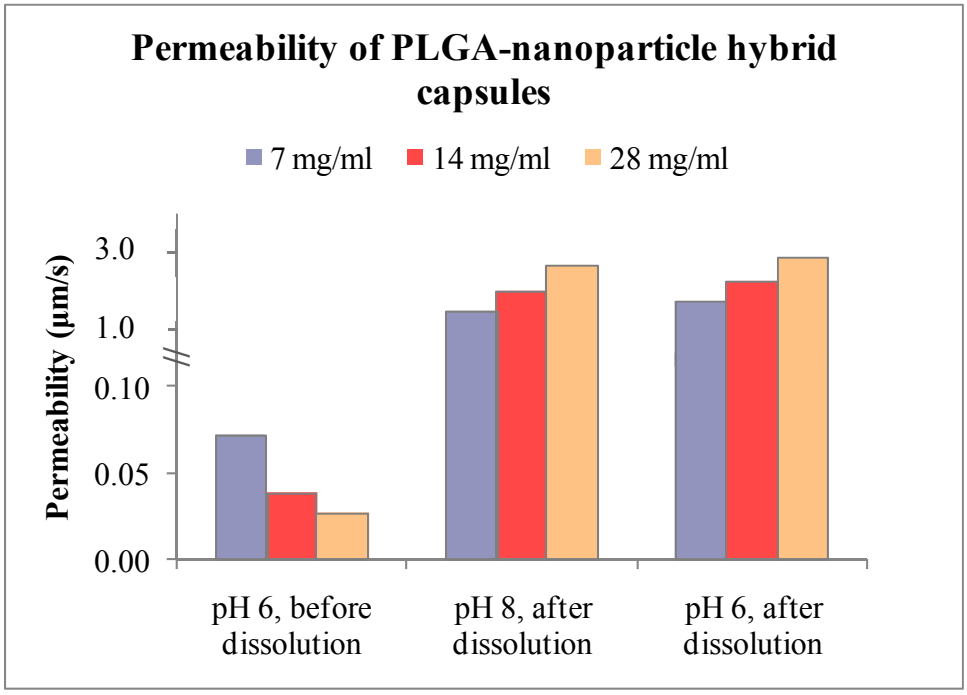

Figure 4.18. Permeability of three individual capsules prepared with different amounts of PLGA at different pH solution conditions, realized in a microfluidic dialysis cell. *Values after dissolution are plotted against secondary axis on the right.*

The pH-responsive hybrid colloidosomes introduced in this approach show very good retention of small molecules until a raise in pH above the particles' dissolution threshold triggers the opening of large pores and thus initiates fast release. Since the double emulsion/solvent extraction method also provides a high capsule yield and excellent encapsulation efficiency, the presented colloidosomes are extremely promising for practical use as delivery vehicles in triggered release applications. The proposed method can be applied to encapsulate active ingredients with a wide range of sizes, since both the particle size and the thickness of the polymer shell can easily be modified. In this way, capsules of different thicknesses and pore sizes can be generated. We suspect that the highly porous capsules obtained after particle dissolution may prove useful in other ways, too. Slurries of these capsules, for instance, could be cast and dried into low weight, biocompatible and biodegradable material with a high porosity defined by two adjustable length scales (the capsule size and capsule pore size). Since these porous materials would be easy to load with any cargo included in the original aqueous capsule cores, they might prove useful e.g. as scaffolds for tissue growth.

4.4. Conclusions

FRAP is a technique that can be applied to measure the permeability of microcapsules. The previous studies developed are only applicable to very small capsules or capsules of very low permeabilities, which would show very efficient photobleaching. A new model has been developed that accounts for two diffusion mechanisms that occur in capsules that are not fully bleached. It has been shown that this model is an excellent fit for recovery curves of very different tracers and of capsules of very different permeabilities. The development of this new model has expanded the applicability of FRAP for permeability measurement of capsules of a wide range of sizes and permeability values. An added advantage of this model comes from the reduction in the intensity recovery time that arises from not requiring precise and complete bleaching of

the capsule interior. Overall, this model seems advantageous over previous models, as it accounts for tracer transport inside and outside of the capsule wall, resulting in a more accurate permeability determination, extending the applicability of FRAP to study the permeability of large microcapsules, and allowing more flexibility in the choice of tracers.

FRAP has been successfully been applied, with the mentioned weighed model, to measure the permeability of the pH-responsive colloidosomes. The originally prepared colloidosomes were found to be unsuitable for efficient encapsulation due to high shell permeability. Three different methods to tune this parameter while preserving the pH-triggered release mechanism have been developed. Responsive high-permeability colloidosomes serving as the base case for our study were generated from a double water-in-oil- in-water Pickering emulsion, from which the oil is extracted to obtain water-in-water colloidosomes. FRAP measurements confirm the reduction of capsule permeability achievable alternatively by ethanol consolidation or layer-by-layer reinforcement of the original capsules, as well as by inclusion of a water-insoluble polymer in the oil phase of the double emulsion droplets from which the capsules are formed. The ethanol consolidation relies on plasticization and partial dissolution of the original colloidosomes by a change in the solvent properties and heat treatment that leads to a fusion of nanoparticles in the capsule shell. In the layer-by-layer reinforcement, alternate layers of dissoluble particles and an oppositely charged polyelectrolyte are adsorbed onto the original capsules; depending on the polyelectrolyte used, the reinforced capsules either dissolve or swell above pH 7.

In the last and arguably most useful method, PLGA is dissolved in the oil phase of the double emulsion, and remains in the capsule shell as the oil is extracted. The resulting hybrid capsules can have very low permeability, yet open up wide pores above the pH threshold for particle dissolution. The double emulsion/solvent extraction method

proposed for creating these colloidosomes allows for high encapsulation efficiency and high capsule yield.

In this way, we arrive at a strategy for encapsulation by colloidosomes that simultaneously satisfies application-driven and notoriously hard-to-reconcile demands with regard to fabrication efficiency, cargo retention and triggered release. By pre-defining the nanoparticle size and the polymer concentration in the middle phase, these microcapsules are very promising as they exhibit well controlled permeability and release kinetics. Furthermore, the incorporation of PLGA with a different lactic acid to glycolic acid ratio can be useful to generate slower or faster degrading capsules. In this way, these capsules could potentially be useful for dual ingredient release. Furthermore, other polymers can be used in substitution for PLGA. Overall, the hybrid nanoparticle-polymer colloidosome approach opens up the possibility for a wide variety of fully-functional colloidosomes with specific material characteristics.

Combinations of the presented methods may potentially allow for further tuning of release profiles, and the highly porous ‘‘inverse colloidosomes’’ formed by dissolution of particles from the PLGA composite capsules are expected to have useful structural properties e.g. for cell encapsulation and tissue scaffolding.

CHAPTER 5

TUNING SURFACE ROUGHNESS OF PARTICLES AND MACROSCOPIC SURFACES

5.1 Introduction

The relation of roughness with wetting has been widely studied on macroscopic surfaces [*80, 82, 84, 86, 90, 92, 96, 99, 100*], where roughness has been shown to have an effect on the contact angle that an equilibrium liquid droplet forms with the surface. Two main models are typically used to describe the wetting regimes: the Wenzel [*99*] and Cassie-Baxter model [*100*]. In general, roughness is expected to accentuate the wetting characteristics of the solid, i.e., a hydrophilic solid will appear more hydrophilic and a hydrophobic solid will appear more hydrophobic with increased roughness, at least in the Wenzel state. The Cassie-Baxter state, for heterogeneous wetting, predicts that the contact angle variation will tend towards 0º or 180º depending on the materials involved. The Wenzel model takes into account only the roughness parameter, r, which relates the real surface area to the projected surface area of the solid. The Cassie-Baxter model also takes into account the solid heterogeneity, which might be due to differences in surface chemistry, or for heterogeneous wetting where air pockets are trapped in the solid grooves between the solid and the liquid droplet. Many more detailed theories have been developed which take into account the geometry of the surface features, such as separation, height-to-width ratio [*92, 103*] and even re-entrant features, where a convex surface feature would allow fluid between the feature and the solid main surface [*82, 96*].

Although this area has been widely studied with many different systems, the study of surface roughness has not yet been expanded to other types of functional surfaces,

such as the surface of microparticles. Surface roughness on particles has been predicted theoretically to influence particles adsorbed at liquid-liquid interfaces by changing contact angle, adsorption energy and by inducing capillary inter-particle attraction [*115-117, 120-122*]. These effects should further translate to the emulsification properties of such particles. Additional aspects of surface roughness might affect Pickering emulsification in unforeseen ways.

With the initial interest of studying the effects that surface roughness on a particle can have on their properties as solid-state stabilizers of emulsions, the first objective is to generate particles with different degrees of surface roughness. Ideally, the changes in wettability with roughness would be studied on the particles themselves. In reality, measuring roughness and contact angles on microparticles can be extremely challenging [*17, 20, 145, 164*]. In order to circumvent these difficulties, macroscopic surfaces with the same surface treatment as the microparticles can serve as models to study roughness and wettability. In this way, the determined characteristics for macroscopic surfaces, such as contact angle and roughness, can be extrapolated to the particles.

5.2 Objective and General Approach

In order to solely study the role of surface roughness in Pickering emulsification, model particles with varying surface roughness should be first developed. The main objective here to generate particles and surfaces with different degrees of surface roughness, but identical surface chemistry.

In Chapter 2, the generation of pH-responsive nanoparticles from enteric coating polymers has been described. As previously mentioned, these materials can dissolve above a certain pH and remain solid below a certain pH. Alternatively, additional solvents such as acetone and ethanol are efficient at plasticizing and dissolving these polymers. In any case, partial particle dissolution should be possible. If these particles are

deposited as a coating material for other substrates, partial dissolution or plasticization can lead to particle fusion. In this way, substrates with different degrees of surface roughness can be generated by controlling the level of particle dissolution and fusion.

The general approach taken to generate surfaces with different degrees of surface roughness can be described in three main steps:

1) Generation of pH-responsive nanoparticles
2) Coating of a substrate material with the pH-responsive nanoparticles
3) Partial dissolution of the particles to tune the degree of surface roughness

This general approach is illustrated in **Figure 5.1.**

The substrates are effectively coated with the negatively charged nanoparticles by irreversible adsorption, which is driven electrostatically by using positively charged substrates, such as polystyrene or silica with amine or amidine surface groups. In the case where negatively charged substrates are used, these can be coated with positively charged polyelectrolytes, as an adhesion layer, or can be chemically modified by covalent attachment of positively charged groups. Ideally, the particles and macroscopic substrates should have the same surface chemistry regardless of the method used for coating with nanoparticles.

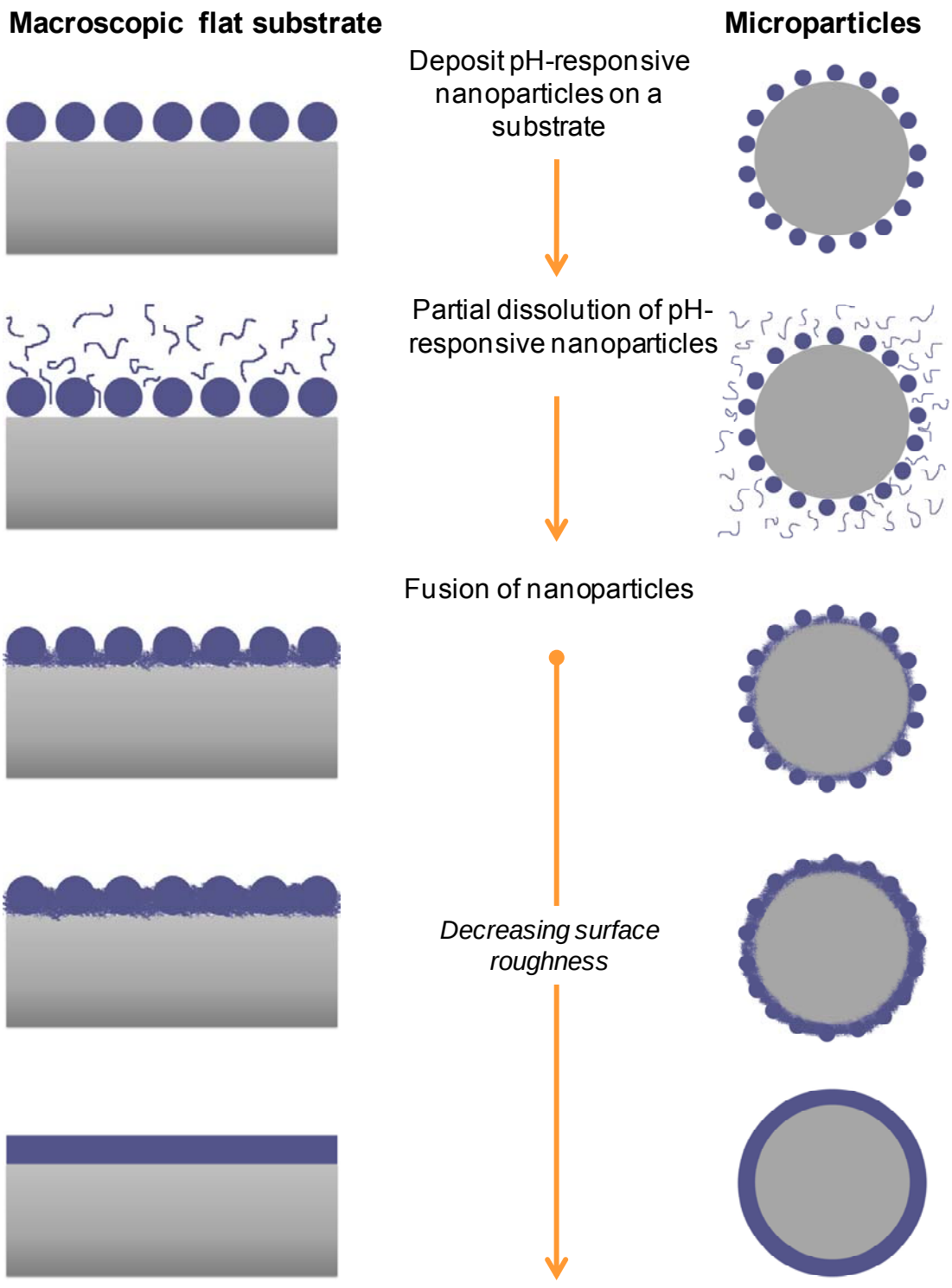

Figure 5.1. General approach for preparing macroscopic surfaces and microparticles with different degrees of surface roughness.

The partial dissolution of the pH-responsive nanoparticle coating should happen without particle detachment, and without complete particle dissolution. This step needs a change in the solvent conditions, for example, a pH approach to the dissolution threshold or the addition of a solvent such as acetone or ethanol. Although the most obvious way to partially dissolve Eudragit particles is via pH; this process is harder to control than the dissolution by exposure to a co-solvent of defined concentration. Moreover, a volatile co-solvent extracts itself and automatically restores the initial solvent conditions.

By using different ratios of the solvent with water, different degrees of dissolution can be accomplished. The different extents of particle dissolution can allow the particles to fuse with each other due to increased polymer chain mobility, but the solvent conditions should be kept below complete particle dissolution. The exposure to a plasticizing or dissolving medium is only a temporary step. Ultimately, the solvents/plasticizers are removed and insoluble coatings with different roughness are obtained.

It is important to mention that the polymer the nanoparticles are made of is a random co-polymer with an average molecular weight of 150,000 Da. This means that in reality there is a distribution of molecular weights in the polymer. Therefore, smaller molecules might completely dissolve in a given ratio of ethanol and water, while larger molecules will remain solid. Although the smallest molecules can completely dissolve in a given solvent mixture, the particles remain as individual, swollen entities, with slightly more mobile chains that can interpenetrate each other. This partial dissolution effect would occur to different extents, until complete melting of the polymer is achieved yielding a completely smooth surface. The substrate will strongly attract the first dissolving polymers; therefore the first effect of partial dissolution will be to coat the exposed substrate surface and prevent the substrate from shining through the adsorbed particle/polymer layer.

One very important aspect of this step is the removal of the solvent. Depending on the method used to remove the solvent, many unwanted results can occur. Fast removal of the solvent, or complete exchange of the water-solvent mixture could result, for example, in removal of the dissolved polymer or of the nanoparticles themselves. Furthermore, fast extraction of the solvent could result in re-precipitation of the dissolved polymer in solution, rather than precipitation of the dissolved polymer onto the fused particle substrate.

It is noteworthy that common charge-stabilized particles have chargeable groups only on the particle surface. These stem from either the initiator of the polymerization reaction (often a persulfate), leaving a single charge at the chain end, or from a surface functionalization of the pre-formed particle. In either case, the particle surface is chemically very different from the interior of the particle. Our Eudragit particles, however, have the same chemistry throughout the particle as they are made from a random co-polymer with methacrylic acid and methyl methacrylate groups along the chain. Therefore, the dissolution, re-precipitation and migration of polymer chains will not change the surface chemistry. In this way, all the generated surfaces will be chemically identical, which is important to study the effects of surface roughness alone.

The suggested approach is a simple method for tuning the surface roughness of macroscopic and particle surfaces to the same extent. Moreover, the generated surfaces and particles will still keep the pH-responsiveness which can be important for applications where a stimulus-response is required. The following sections will describe the results obtained by the aforementioned approach.

5.3 Experimental Methods

5.3.1 Materials

Eudragit S-100 was obtained as a gift from Evonik and used without further purification. Deionized water was obtained from a Barnstead Easy Pure II System, resistivity: 18.2 MΩ cm. Reagent alcohol (BDH 94-96% ethanol/methanol), glacial acetic acid and Alconox detergent were obtained from VWR. NaCl, HCl, NaOH pellets, acetone, toluene and 3-aminopropyltriethoxysilane (APTES) were obtained from Sigma Aldrich and used without further purification. Glass coverslips, no 1.5, were obtained from VWR. Silica particles(0.9 and 0.96 μm in diameter) were purchased from Bangs Laboratories in 10% (wt/v) aqueous dispersions.

5.3.1 Particle synthesis and characterization

Eudragit S-100 particles were synthesized as previously described in Chapter 2 [*123*]. Particles of two different sizes were prepared, one 50 nm and another 182 nm in diameter, as features of different size result in different surface roughness.

For the larger particles, 2 g of Eudragit S-100 are dissolved in 100 ml of hot reagent alcohol (BDH, purchased from VWR). This solution is abruptly added to 200 ml of deionized water and mixed at 400 rpm with a magnetic stirrer. The solution immediately turns turbid, indicating particle precipitation. Alcohol and water are then evaporated under continued mixing at 70°C until the volume is reduced to ~150 ml or less. After passing the particle dispersion through a Whatman Grade 6 qualitative filter, a particle concentration of 1% (w/v) is found by gravimetric analysis. The particle size in diluted samples was measured by Dynamic Light Scattering (DLS) using a goniometer setup (ALV/DLS/SLS-5022F). The (intensity weighted average) size for these particles is 182 nm in diameter with a coefficient of variance (CV) of 8.8%, as determined from a

second order cumulant fit to the measured intensity autocorrelation function. In the case of the smaller particles, 0.5 g of Eudragit S-100 is dissolved in 100 ml of reagent alcohol and this solution is added to 200 ml of deionized water. The dispersion is evaporated at 70°C to ~100 ml. The resulting particle concentration is 0.35% (w/v), with a mean particle diameter of 49.5 nm and a CV of 7.3%.

5.3.2 Covalent attachment of positive groups to silica substrates

5.3.2.1 Macroscopic surfaces

Glass coverslips were used as macroscopic substrates. The surfaces were washed with Alconox detergent and thoroughly rinsed with deionized water. These surfaces were then dipped for 5 minutes at room temperature in a solution containing 50 ml of deionized water, 6 µl of glacial acetic acid and 1 ml of 3-aminopropyltriethoxysilane (APTES). The solution was prepared immediately before dipping the substrates to avoid reaction between APTES molecules in solution. The substrates were then rinsed twice with deionized water and baked at 80° C for 1 hr, to ensure that the covalent bonds between the silane molecules and the silanol groups on the glass had reacted. Finally, the substrates were left to cool at room temperature for ~ 20 minutes.

5.3.2.2 Silica particles

Silica particles were also made positive by covalent attachment of APTES. In this case, to a 0.05% (wt/v) dispersion of particles APTES was added until a concentration of ~ 50 mM (0.012% v/v) was reached, then the mixture was stirred with a magnetic stirrer at 200 rpm for 2 hrs. Lastly, the particle dispersion was washed six times by centrifuging at 2000 rpm for 10 minutes, removing the supernatant and replacing with fresh deionized water in each washing cycle.

5.3.3 Substrate coating with pH-responsive nanoparticles

5.3.3.1 Macroscopic surfaces

A 0.1% (wt/v) dispersion of pH-responsive nanoparticles was prepared at pH 5.3. pH was adjusted with 100 mM HCl or NaOH. Enough salt was then added to the dispersion from a 3M NaCl stock solution to reach a final concentration of 50 mM NaCl, which reduced the pH of the dispersion to ~ 4.8. The positively charged glass substrates were then placed in the dispersion horizontally, with the positively charged side up, for 30 minutes. Afterwards, the surfaces were rinsed by carefully retrieving the substrates with tweezers and dipping it several times in a 1 liter beaker filled with deionized water at pH 5.3, to remove the non-adsorbed particles and NaCl.

5.3.3.2 Silica particle heteroaggregation

The washed, positively charged silica particles were diluted to reach a 0.1% (wt/v) dispersion and the pH was adjusted to 5.3. A separate 0.1% (wt/v) dispersion of the pH-responsive nanoparticles was also prepared at pH 5.3. The two particle dispersions were then mixed (at a 50-50 ratio), to reach a 0.05% (wt/v) concentration of silica particles and 0.05% (wt/v) concentration of Eudragit S-100 nanoparticles. Enough salt was then added from a 3M NaCl solution, to reach a final concentration of 50 mM NaCl, which reduced the pH of the dispersion to ~ 4.8. The sample was stirred to ensure homogeneous mixing and left to rest for at least 3 hrs.

The particle dispersion which now contained silica microparticles with adsorbed polymer nanoparticles was concentrated by centrifuging at 2000 rpm for 10 minutes and removing the supernatant, composed mainly of the pH-responsive nanoparticles. After the sample was concentrated to ~ 0.1% (wt/v), the particles were washed 4 times to

remove the excess nanoparticles and NaCl. This was performed by centrifuging at 2000 rpm for 10 minutes, removing the supernatant and replacing it with water at pH 5.3.

5.3.4 Surface roughness tuning by partial nanoparticle coating dissolution

5.3.4.1 Macroscopic surfaces

Immediately after rinsing, the particle-coated surfaces were dipped in a specific acetone/water solvent mixture (from 10 to 50% acetone) in a tall closed container for 30 minutes. The containers used were 50 ml centrifuge tubes, to which 15 ml of water at pH 5.3 were added. Acetone was then added to reach the desired concentration. The water/acetone mixture was stirred before dipping the substrate to ensure a homogenous solvent quality. The substrate size was small enough that they were completely covered by 15 ml of water. After this treatment time, the containers were opened to allow slow evaporation of the acetone, and were left to rest for at least 4 hrs at room conditions. After this time, the samples were transferred to the hood to continue evaporation. The complete evaporation lasted at least 36 hrs, by the end of which all the containers reached a volume of 15 ml or less. The substrates were then carefully removed from the containers with tweezers and rinsed once in a 1 l beaker filled with pH 5.3 water. Afterwards, the substrates were left to dry at room temperature.

5.3.4.1 Silica particles

5.3.4.1.1 Treatment with acetone

The washed particle dispersions were concentrated to the same starting volume before heteroaggregation, ~ 0.1%(wt/v). 24 ml of this dispersion were added in a 50 ml tall centrifuge tube. Acetone was then added to reach the desired concentration in a range

from 10% to 50%. The dispersion was mixed and left to rest in the closed container for 30 minutes. After this treatment time, the containers were opened to allow slow evaporation of the acetone, and were left to rest for at least 4 hrs at room temperature. After this time, the samples were transferred to the hood to continue evaporation. The complete evaporation lasted for at least 36 hrs, when all the containers reached a volume of 24 ml or less.

The dispersions were washed twice to remove any residual acetone in the sample. The dispersions were centrifuged at 2000 rpm for 10 minutes, the supernatant was removed and replaced with pH 5.3 water for each washing cycle.

5.3.4.1.2 Treatment with ethanol (originally used protocol for controlling roughness, ultimately replaced by the previously described acetone treatment)

The washed particle dispersions were concentrated to the same starting volume before heteroaggregation, ~ 0.1%(wt/v). 12 ml of this dispersion were added in a 30 ml glass centrifuge tube. Ethanol was then added to reach the desired concentration. The dispersion was mixed and left to rest for 30 minutes. After this treatment time, the samples were washed 4 times by centrifuging at 2000 rpm for 10 minutes, removing the supernatant and replacing with water at pH 5.3 each time.

5.3.5 Characterization of particles and macroscopic substrates.

5.3.5.1 Zeta Potential

The zeta potential of the polymer-silica hybrid particles was measured by electrophoresis (Malvern Zetasizer Nano ZS-90) in a 1 mM NaCl background electrolyte, except where noted. The pH of the particle dispersions was adjusted with 1 mM HCl and 1mM NaOH. The zeta potential was evaluated from the measured electropheric mobility

by using the Smoluchowski approximation for large ratios of particle radius to Debye screening length.

5.3.5.2 Scanning Electron Microscopy

SEM images were taken with a Zeiss Ultra 60 SEM at a voltage between 1 and 5 kV. For the particles, a small amount of the dispersion was dried at room conditions on aluminum stubs with carbon tape. For the macroscopic substrates, the samples were dried at room conditions. All samples were then coated with carbon using a Quorum Q150R sputter coater. Macroscopic substrates were imaged in a holder with a ~70° tilt angle to better distinguish the roughness features.

5.3.5.3 Atomic Force Microscopy

The roughness of macroscopic substrates was measured by AFM with a Veeco Dimension 3100 Scanning Probe Microscope. Measurements were made with a Mikromasch silicon NSC14Al probe (typical 10 nm radius of tip curvature and 40° full tip cone, ~ 160 kHz resonant frequency) in non-contact mode. The surface area, projected surface area and root-mean squared (rms) roughness, were obtained with Gwyddion freeware.

5.4 Results and Discussion

5.4.1 Tuning surface roughness of silica particles.

5.4.1.1 Covalent attachment of positive groups on silica particles

The silanization of silica surfaces with positive or hydrophobic groups has been previously used for modifying silicon-based materials, including particles [*165, 166*]. Previous studies for modification of silica particles with silane groups have been performed mainly in toluene [*166*], acetone and water [*165*]. In this case, silanization was carried out in an aqueous environment. Zeta potential measurements before and after silanization of the silica particles corroborate the positive charge on the particles. These data are shown in **Figure 5.2**, where it can be observed that the particles in fact turn positive by the treatment with APTES.

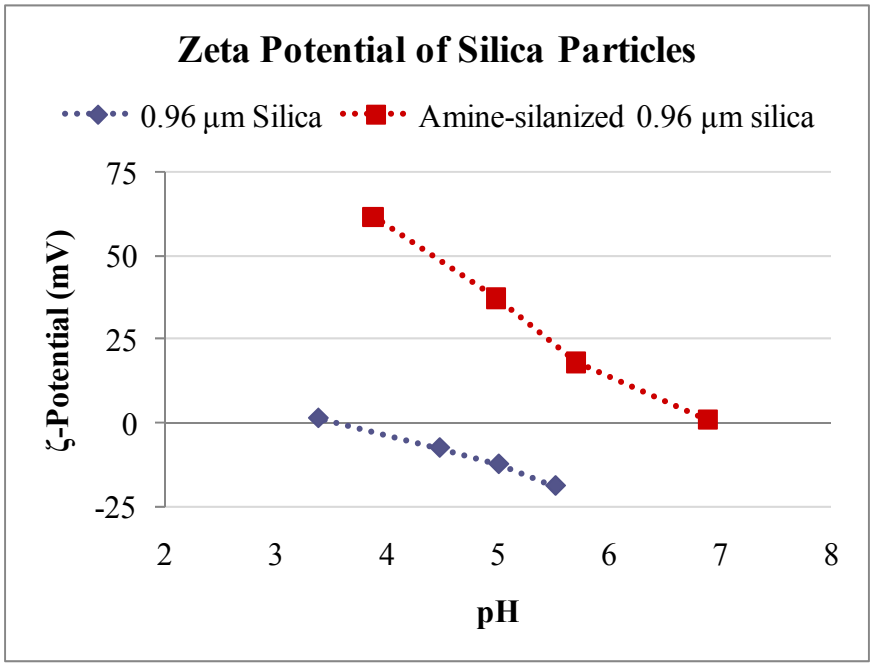

Figure 5.2 Zeta potential of bare and amine-silanized silica particles.

5.4.1.2 Substrate coating with pH-responsive nanoparticles

Positively charged silanized particles were coated with negatively charged pH-responsive nanoparticles by a heteroaggregation procedure. Several important parameters need to be considered in a heteroaggregation experiment, such as the pH and ionic strength of the dispersion, as well as the overall particle concentration and the number ratio of small negative to large positive particles.

Different regimes of heteroaggregation exist [*167*] as shown in **Figure 5.3**, which depend on the aforementioned parameters, as well as on relative particle size. In this case, the objective is to obtain good particle coverage (as in the first regime illustrated in **Figure 5.3**). Unwanted heteroaggregation scenarios can arise such as bridging of silica particles with pH-responsive nanoparticles, or insufficient coverage of the large particles. These problems can occur if the ratio of the small negative to large positive particles is too low. Furthermore, the absolute particle concentration is important; it is intuitive that heteroaggregation in a dilute system, at a high number ratio of small to large particles, will favor good coverage over particle bridging.

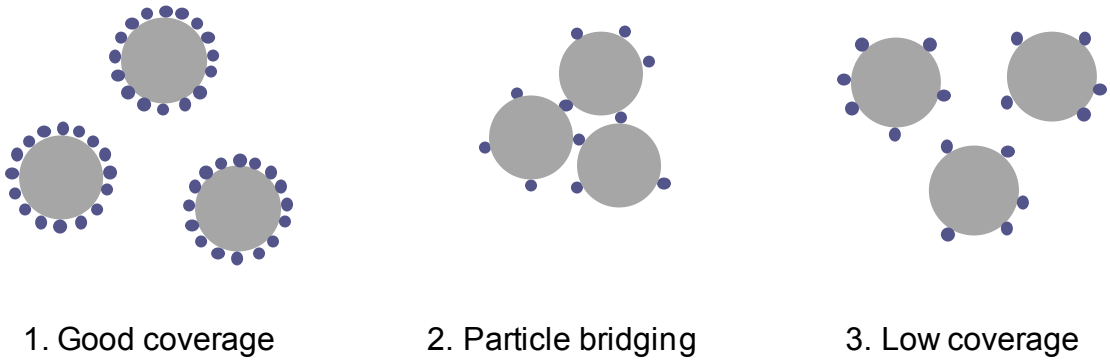

Figure 5.3 Heteroaggregation regimes

Such are the conditions chosen in the experiments in order to avoid unwanted heteroaggregation regimes. The particle ratio was set so that there was an excess number

of small particles, regarding the total surface area of silica particles to be covered. For the 182 nm particles, a 0.05% wt/v concentration represents approximately a 240 to 1 ratio of Eudragit S-100 particles to silica particles (0.96 μm). Theoretically, ~90 polymer particles are required to cover one 0.96 μm silica particle, assuming a hexagonal 2-d packing density of 0.907. The selected concentration represents a ~170% excess in the number of negative particles. In the case of the 50 nm, the small to large particle ratio is of ~11,800 to 1, and ~1200 particles are required to cover one 0.96 μm silica particle, at the same coverage of 0.907. The selected concentration thus represents a 870% negative particle excess.[ii]

The solution conditions were kept in a stable dispersion regime for the pH-responsive nanoparticles, according to the stability diagram shown in **Figure 2.7**. It is expected that a low pH favors complete coverage, as the core particle is highly charged and the small particles are less negatively charged. In this situation a larger number of negative particles are required to obtain charge reversal of the core particles, thus favoring full coverage. Ionic strength conditions were also set to a point where the stability of the pH-responsive nanoparticles was not disturbed, but there was still enough screening to avoid a high lateral repulsion between the negative particles that could work against obtaining full coverage.

To find the appropriate conditions for full coverage, heteroaggregation was carried out at different pH values. **Figure 5.4** shows heteroaggregates generated at pH 4, and **Figure 5.5** shows heteroaggregates formed at pH 5.6.

[ii] Smaller silica particles with a 0.90 μm diameter were also used. For these particles, the excess of small particles is of 150% in the case of 180 nm particles and 800% in the case of 50 nm particles.

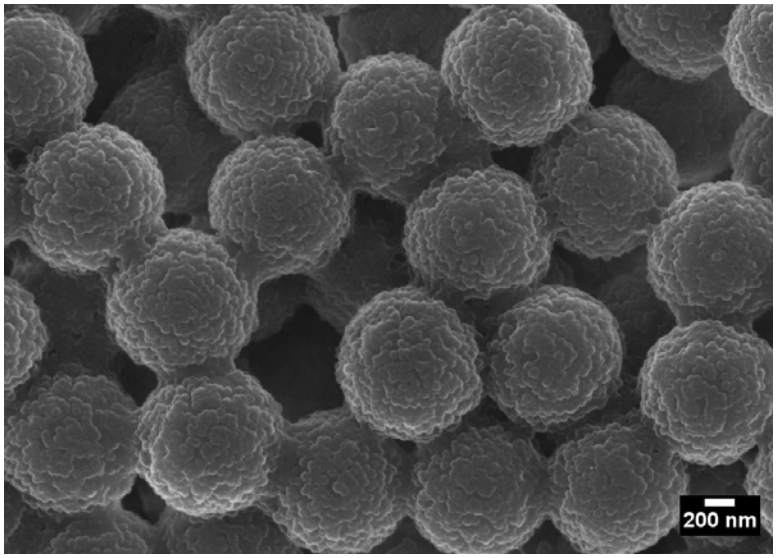

Figure 5.4 Heteroaggregates of 0.96 amine-modified silica and Eudragit S-100 50 nm particles generated at pH 4.

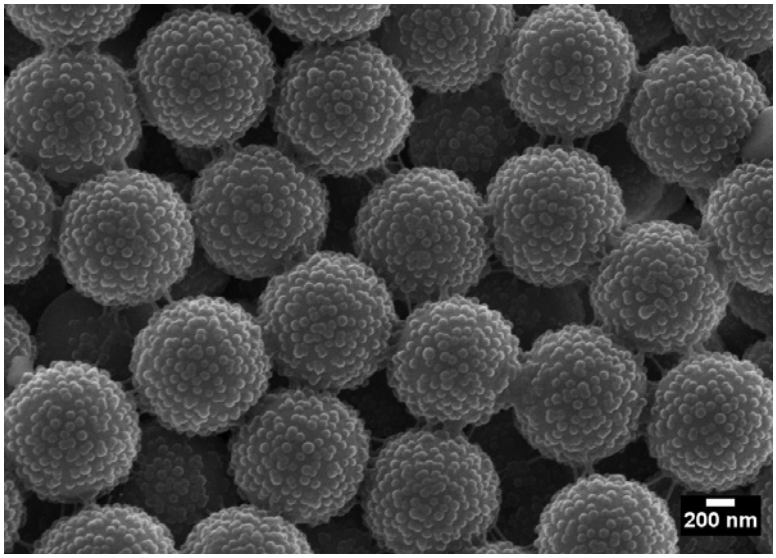

Figure 5.5 Heteroaggregates of 0.96 amine-modified silica and Eudragit S-100 50 nm particles generated at pH 5.6.

As expected, the higher pH induces a higher charging state for the Eudragit S-100 nanoparticles, which produces heteroaggregates with a more widely and evenly spaced coverage due to the inter-particle repulsion. This finding could be interesting to produce heteroaggregates with different degrees of surface covering and inter-particle spacing for other applications. For the present study, the aim is to obtain heteroaggregates with a high degree of surface covering to avoid the substrate positive charges to shine through the nanoparticle coating, while avoiding nanoparticle aggregation. Therefore, the pH for heteroaggregation was maintained at an intermediate value of 4.8.

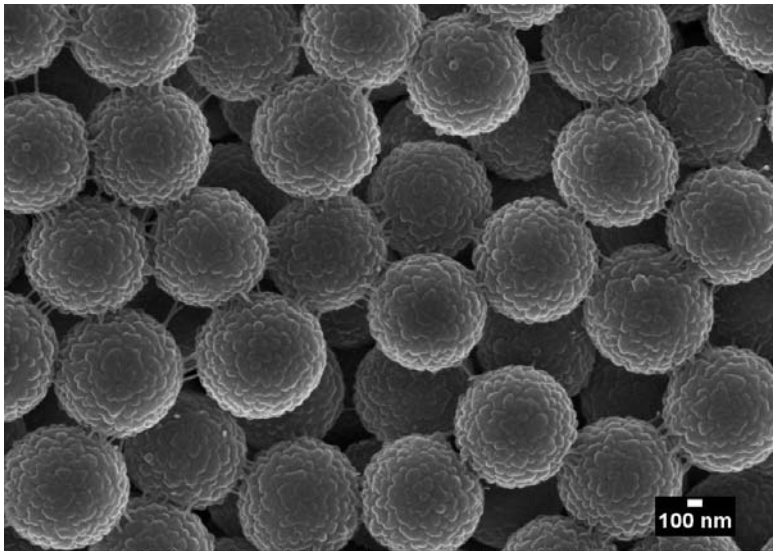

Figure 5.6 Full coverage of 0.90 μm positively charged silica particles by 50 nm Eudragit S-100 nanoparticles at pH 4.8.

At the conditions that heteroaggregation was carried out, efficient coverage of the positive silica particles was obtained with the 50 nm particles, as suggested by the SEM image (**Figure 5.6**).

Heteroaggregation with the 182 nm particles (**Figure 5.7**), on the other hand, resulted in poor coverage of the core silica particles. The reason for this issue can be

attributed to either the size ratio of small to large particles, or to the fact that the heteroaggregation with 182 nm particle was carried out at much lower number concentration of negative nanoparticles, corresponding to an the excess of these particles of only 170%.

It is noteworthy that some heteroaggregation experiments have also been performed with larger (2.2 μm) amidine-functionalized polystyrene latex particles. In this case a 220% negative nanoparticle excess was used under the same solution conditions, which resulted in complete coverage of the latex particles by the Eudragit S-100 nanoparticles. An SEM image of the covered amidine-latex particles is shown in **Figure 5.8.** Comparison between these experiments can provide some insight in the cause for low silica particle coverage.

There are three main differences between the two heteroaggregation experiments: 1) core particle material and surface chemistry, 2) small to large particle number ratio and 3) small to large particle size ratio. The surface chemistry of the amidine latex particles and the amine-functionalized silica particles is different, but the really important parameter in the electrostatic heteroaggregation under the same solution conditions is the surface charge density, which in this case is related to the particle zeta potential. The amidine latex particles have a value of ζ=+30 mV, while the amine-modified silica particles have a value of ζ=+37 at pH 5 and 1mM NaCl. Although these values are slightly different, the positive charge density in both cases should be enough to drive negative particle deposition; a proof of this is the fact that the silica particles are well covered by the 50 nm Eudragit S-100 particles.

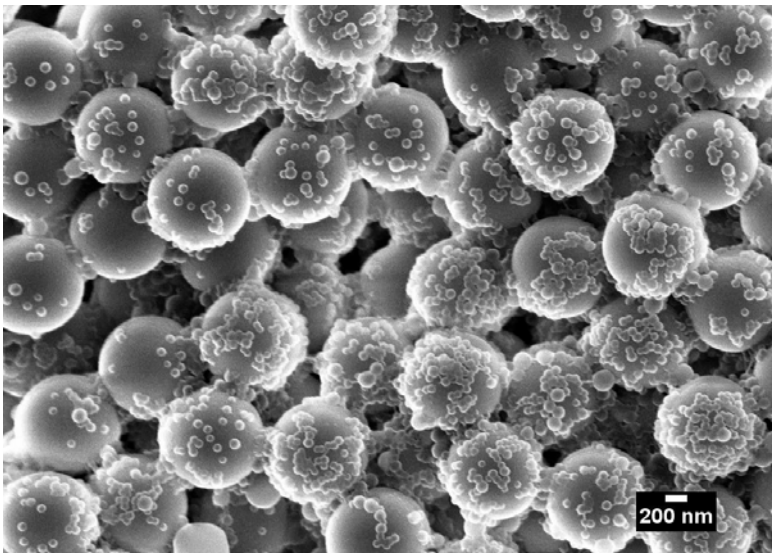

Figure 5.7 Poor coverage of 0.96 μm positively charged silica particle by 182 nm Eudragit S-100 nanoparticles.

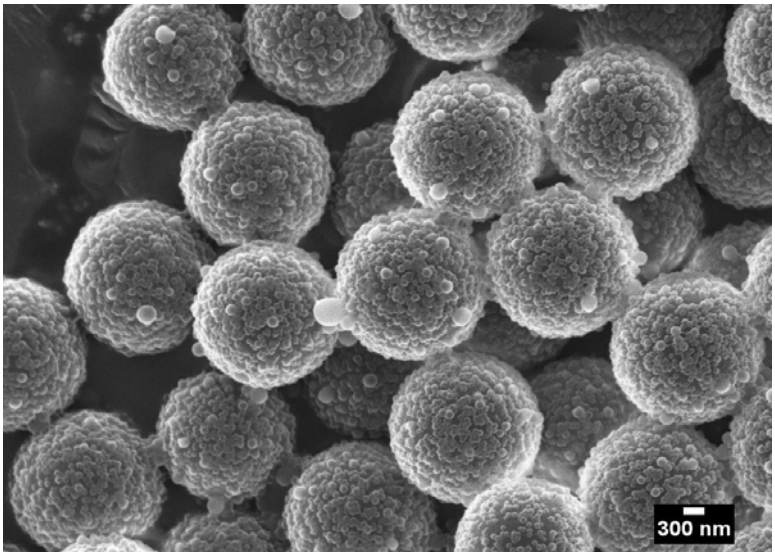

Figure 5.8 Full coverage of 2.2 μm amidine-latex particles by 182 nm Eudragit S-100 nanoparticles.

It is also possible that the factor determining the low coverage of the silica particles by the 182 nm particles is the small to large particle number ratio. However, the difference in excess particle number concentration is small: 142% excess for the latex core and 193% excess for the silica core case. Furthermore, free Eudragit S-100 nanoparticles, not adsorbed to silica particles were observed by SEM imaging. These facts suggest that there were in-fact enough small particles for complete covering of silica particles. Therefore, this factor is not believed to be determining in the poor coverage obtained by the 182 nm particles.

Another factor that might be affecting the coverage is the small to large particle size ratio. In the good coverage cases, the particle radius ratio is of 1:12, for the latex particles covered by 182 nm particles, and 1:18 for the silica particles covered by 50 nm particles. For the low coverage of silica particles by 182 nm particles, this radius ratio is only 1:5.3. From the information provided from these experiments, we believe that the size ratio plays a role in the heteroaggregation regime obtained This problem could easily be solved by using larger core particles. Considering that the ultimate purpose of generating particles with different degrees of roughness is to test them as emulsion stabilizers, larger particles were not generated as they would have undesirable effects in the emulsification stabilization and testing, as will be further described in the next chapter.

5.4.1.3 Tuning surface roughness of silica-Eudragit heteroaggregates by partial dissolution

The heteroaggregates generated by covering amine-functionalized silica particles with 50 nm Eudragit S-100 nanoparticles were used as a starting material to obtain particles with different degrees of surface roughness. As mentioned before, a reduction in surface roughness is expected to occur by partial dissolution of the nanoparticles, which

can be potentially carried out by increasing the pH to above 7, or by using good solvents for the polymer, such as acetone or ethanol.

In the case of pH-driven dissolution there are several issues to be considered. The polymer state depends very sensitively on pH, therefore pH and residence time would have to be manipulated very precisely to obtain good control over the resulting roughness features, which appears to be impractical. Nonetheless, some preliminary tests for pH-driven dissolution were performed on the amidine-latex particles covered with Eudagit nanoparticles. These experiments showed that increasing the pH to different values (7, 7.2, 7.6 and 7.9) did not result in fusion of the particles, but in desorption of the nanoparticles from the core particles instead. This unexpected result is not surprising if one takes into account the fact that pH increase affects not only the charging of the Eudragit polymer chains, but it also affects the charge balance between the core particles and the adsorbed nanoparticles in a way that favors desorption.

Co-solvent mediated partial dissolution of the nanoparticle adsorbate was tested by temporarily diluting the particle dispersion with acetone or ethanol as described above (Section 5.3.4.1) Variation of the co-solvent concentration resulted in particles with different degrees of surface roughness, as can be seen in the SEM images shown in **Figure 5.9** for the acetone treatment and **Figure 5.10** for the ethanol treatment.

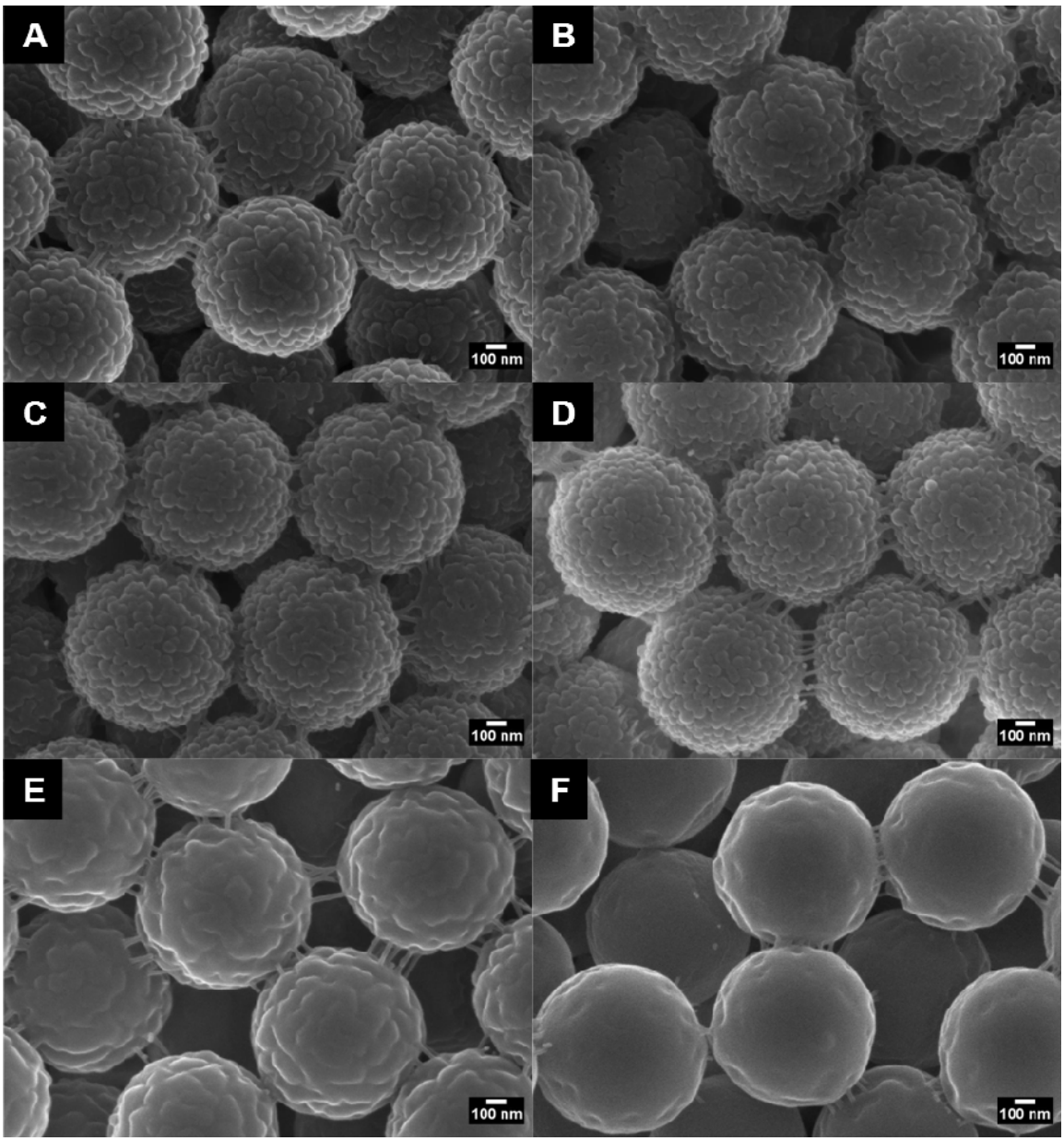

Figure 5.9 Tuning of particle surface roughness of 0.9 µm amine-modified silica particles by acetone treatment of the 50 nm Eudragit S-100 nanoparticle covering. A) No treatment B) 10% acetone C) 20% acetone D) 30% acetone E) 40% acetone F) 45% acetone. *(Acetone percentage represents the volume fraction of acetone in an acetone-water treatment solution)*

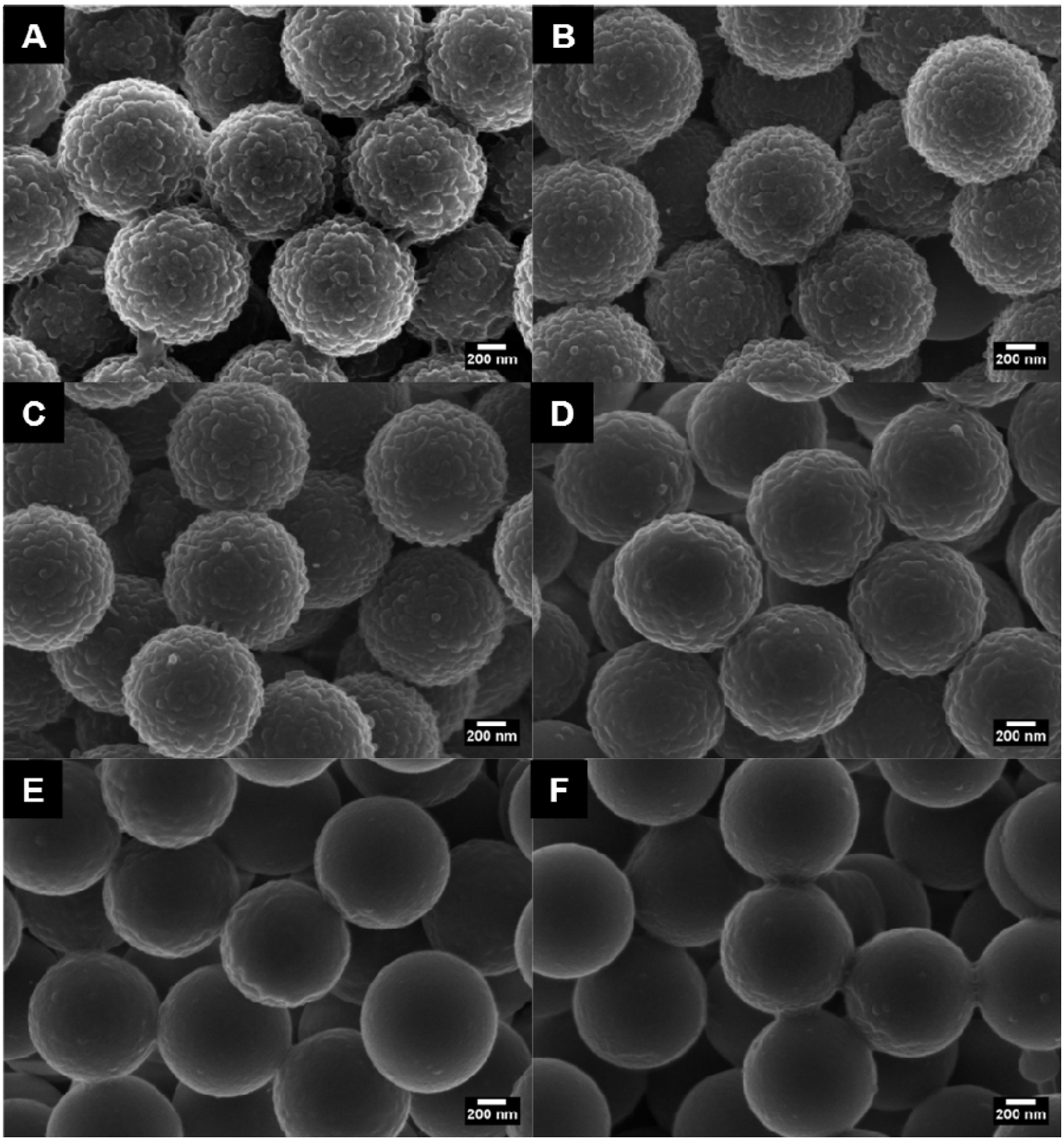

Figure 5.10 Tuning of particle surface roughness of 0.96 μm amine-modified silica particles by ethanol treatment of the 50 nm Eudragit S-100 nanoparticle covering. A) No treatment B) 30% ethanol C) 40% ethanol D) 45% ethanol E) 50% ethanol F) 60% ethanol. *(Ethanol percentage represents the volume fraction of ethanol in an ethanol-water treatment solution)*

As can be observed from the SEM images, both solvents can be used to tune the roughness of the silica-Eudragit heteroaggregates. The acetone protocol appears to be more efficient than the ethanol protocol at reducing the surface roughness, as a smaller amount of acetone is required to achieve a comparable degree of smoothing.

As previously mentioned, the particles with different degrees of surface roughness are intended for use as particulate emulsifiers. In order to assess the role of surface roughness in Pickering emulsification it is very important that variations in the surface roughness be the **only** difference between the tested particles. Although the partial dissolution and plasticization of the polymer does not bring about changes in surface chemistry, the possibility exists that the amine-silanized silica core particle can be exposed if the Eudragit S-100 coating is eroded during the treatment.

In order to investigate how the treatment affects the surface chemistry exposed, the isoelectric point of the particles was determined by zeta potential measurements. While the zeta potential at a randomly chosen pH of rough surfaces might be different from that of smooth surfaces, the isoelectric point should reflect only the balance of chargeable groups, i.e. the surface chemistry. **Figure 5.11** and **Figure 5.12** show the zeta potential dependence with pH obtained for heteroaggregates with different degrees of surface treatment with acetone and ethanol.

As can be seen from these figures, there is a displacement of the zeta potential vs pH line with ethanol treatment, while with acetone treatment all the lines fall roughly on top of each other. These data suggest that the ethanol treatment erodes the Eudragit S-100 coating and the positive charges from the amine groups bonded to the silica are exposed. The data obtained for zeta potential can be used to estimate isoelectric point of each particle type. **Figure 5.13** shows the isoelectric points obtained by extrapolation or interpolation.

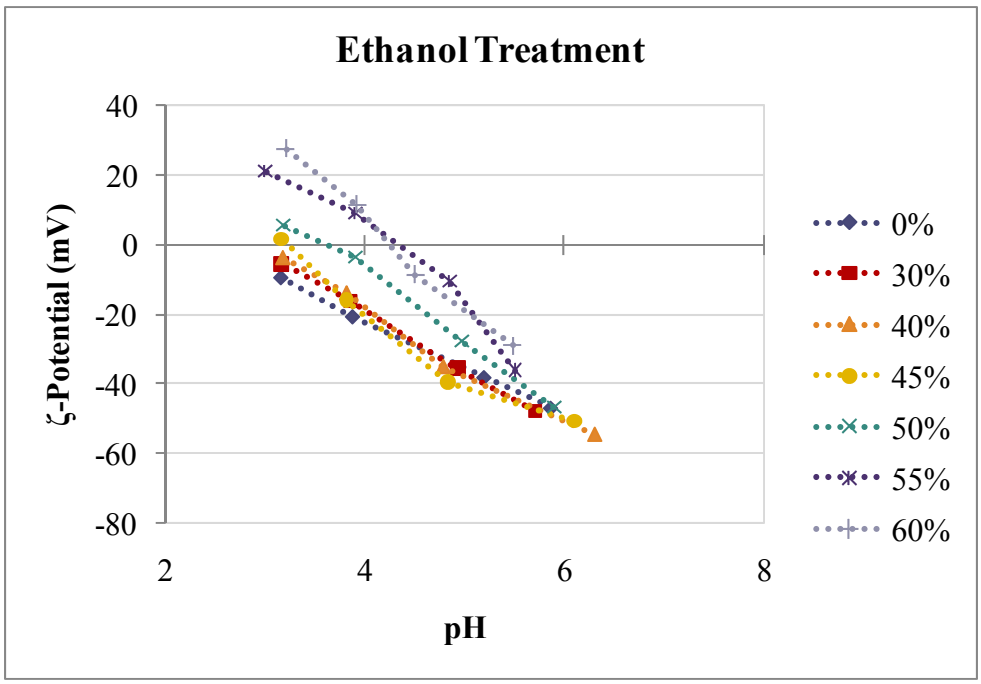

Figure 5.11 Zeta Potential at 1mM NaCl for silica/Eudragit S-100 heteroaggregates treated at different ethanol concentrations for reducing surface roughness.

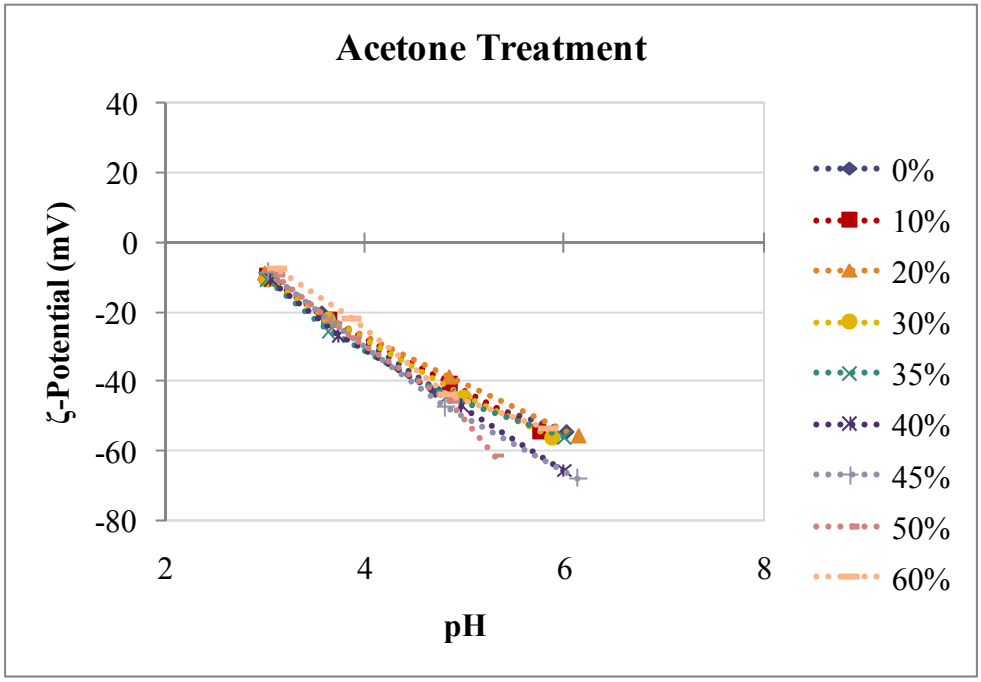

Figure 5.12 Zeta Potential at 1mM NaCl for silica/Eudragit S-100 heteroaggregates treated at different acetone concentrations for reducing surface roughness.

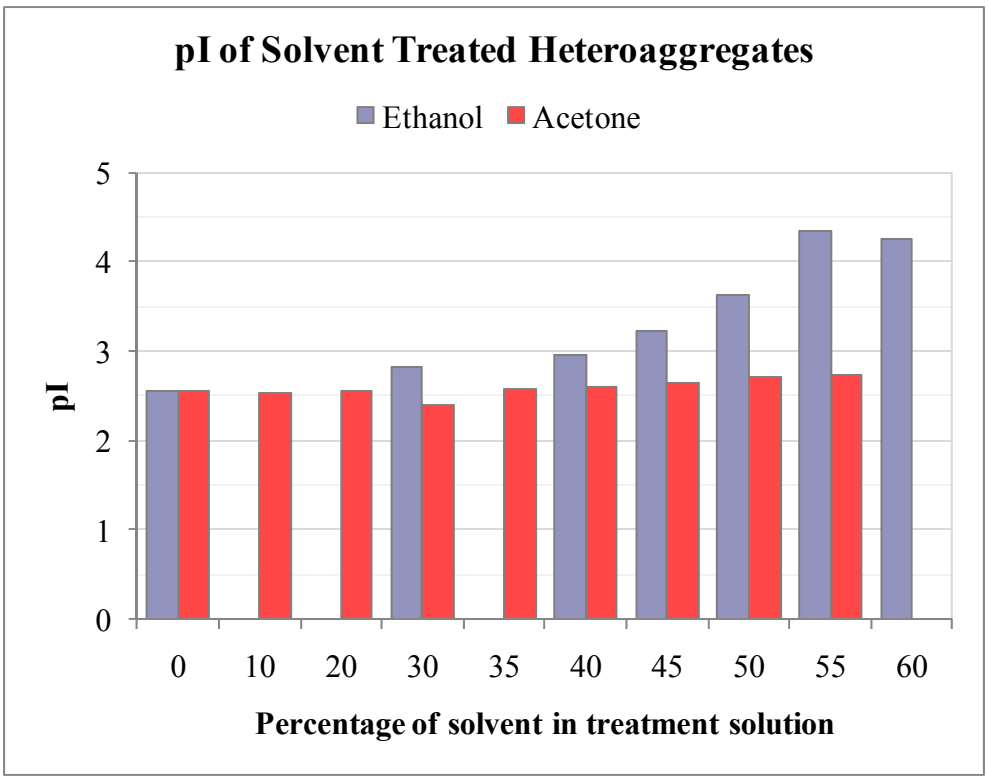

Figure 5.13 Isoelectric Point of silica/Eudragit S-100 heteroaggregates treated with acetone and ethanol.

As the pI represents the pH at which the substrate has no net charge, it is a good indicator of changes in the particle's surface chemistry caused by the solvent treatments. From **Figure 5.13**, a clear systematic increase in pI is observed with increasing exposure to ethanol. This trend is a clear indicator that ethanol treatment is not producing particles with the same surface chemistry, but rather that the positive silica surface shines through the Eudragit S-100 nanoparticle coating. In contrast, acetone treatment shows no significant change in the pI of heteroaggregates treated to varying extents.

The reason for the change in pI with ethanol treatment can be attributed to erosion of Eudragit S-100 from the silica particle surface. The removal of material is believed to occur due to the washing procedure after treatment and not due to the solvent quality

itself. From SEM images, it in fact appears that acetone is a better solvent than ethanol since a smaller concentration of acetone is required to reduce the surface roughness.

Ethanol removal after treatment was carried out by removing the supernatant of the centrifuged sample, and consecutive washing cycles. This method of solvent removal is the likely reason for removal of dissolved Eudragit S-100. Acetone, on the other hand, is a solvent with a higher volatility than ethanol (Vapor pressure = 231 mm Hg vs 44.4 mm Hg, respectively), and thus allows using evaporation as a much milder and gradual method for solvent removal. The slow evaporation process can allow any completely dissolved molecules to re-adsorb onto the heteroaggregates.

Clearly, the acetone treatment is a better approach for generating particles with different degrees of surface roughness while maintaining the same surface chemistry. These particles are an excellent model to study the effect of particle roughness on the particles' performance as stabilizers of Pickering emulsions.

Ideally these particles would be thoroughly characterized with respect to their surface roughness and contact angle. Quantitative measurements of the surface roughness and three-phase contact angle for micron-sized particles, however, present a formidable challenge. Therefore, macroscopic models for the particle surfaces are generated from flat substrates with the exact same surface treatment as the particles. These are used as particle models for the purpose of characterizing surface roughness and contact angle. The generation of such surfaces and their characterization is described in the following section.

5.4.2 Tuning surface roughness of macroscopic glass substrates.

5.4.2.1 Coating macroscopic glass substrates with Eudragit S-100 nanoparticles.

The effect of surface roughness on wettability has been extensively studied, as previously mentioned. Nevertheless, the attention has been focused mainly on hydrophobic materials [*82, 86-91*]. Macroscopic surfaces with different degrees of surface roughness that resemble the described particles are not only interesting as models for the characterization of the rough particles, but also as hydrophilic surfaces with tunable roughness and wettability, yet fixed surface chemistry.

Since the main goal of the macroscopic surfaces is to function as models for the previously described particles, these should be as similar as possible to the particles they represent. Therefore, the exact same method of surface preparation was adopted for both particles and flat substrates. Glass was used as the substrate material, which was positively modified by covalently boding APTES to its surface. Coating of the positively charged surfaces with Eudragit S-100 nanoparticles was carried out at the same solution conditions as the heteroaggregation of silica particles and Eudragit S-100 nanoparticles. These conditions appeared to be appropriate to obtain good coverage of the glass substrates. In this case, poor coverage could also be obtained if the screening between the nanoparticles was reduced, for example by coating the surfaces in the absence of NaCl, as shown in **Figure 5.14** and **Figure 5.15**. This shows that the same solution conditions are required for coating of the macroscopic surfaces and the particles, thus suggesting that the mechanism for both is the same, i.e., electrostatic attraction.

Surfaces covered with 50 nm and 180 nm particles were prepared this way, as different particle size would produce different degree of surface roughness. Although the 50 nm covered surfaces are to be used as models for the silica heteroaggregates, the 180 nm covered surfaces can be very interesting to show differences in roughness and wetting produced by having features of different size.

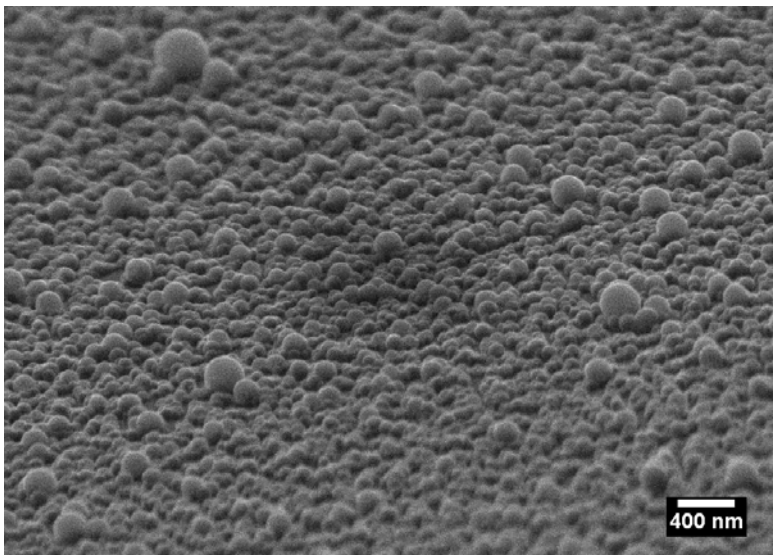

Figure 5.14. Full coverage of an amine-modified glass substrate by 180 nm Eudragit S-100 nanoparticles. *The image was taken at a tilt angle of ~ 70º, which facilitates the recognition of roughness features and explains the out-of-focus regions at the top and bottom of the image.*

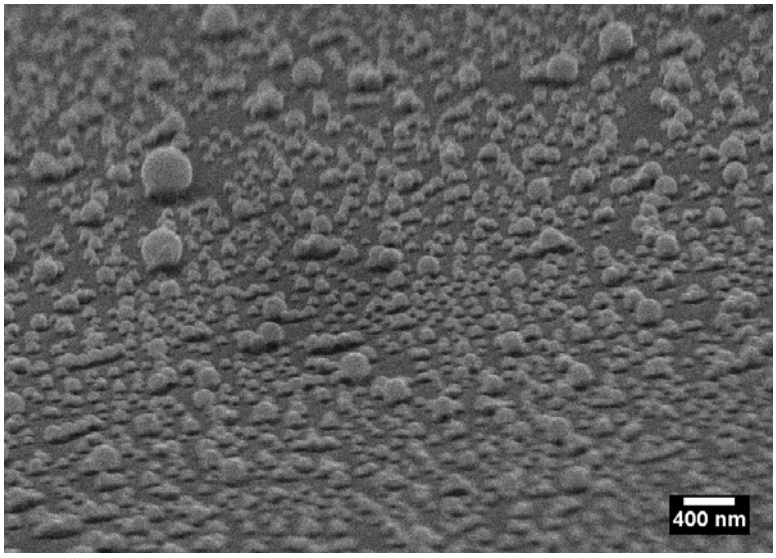

Figure 5.15. Low coverage of an amine-modified glass substrate by 180 nm Eudragit S-100 nanoparticles in the absence of NaCl. *Tilt angle: ~ 70°.*

5.4.2.2 Tuning surface roughness of macroscopic glass substrates coated Eudragit S-100 nanoparticles by partial dissolution.

The macroscopic substrates coated with Eudragit S-100 nanoparticles were subject to the same treatment as the particle heteroaggregates, with an acetone/water at pH 5.3 solvent mixture. The resulting substrates, as expected, show a decreasing surface roughness as the acetone percentage is increased. SEM images of the treated substrates coated with 50 nm and 200 nm particles are shown in **Figure 5.16** and **Figure 5.17.**

From the images, it appears that a treatment with 40% acetone produces fairly smooth surfaces, which is in agreement to the results obtained for the acetone-treated silica heteroaggregates, and suggest that these substrates should indeed be good models for the heteroaggregated particles.

In order to fully characterize the level of roughness produced by treating the nanoparticle-coated glass substrates, AFM measurements were performed which provide quantitative information of the roughness as measured by the difference in surface area and in projected surface area; as well as root-mean squared roughness, Rms, which includes information about the height of the sample. A typical AFM scan of a rough and a smooth surface is shown in **Figure 5.18.**

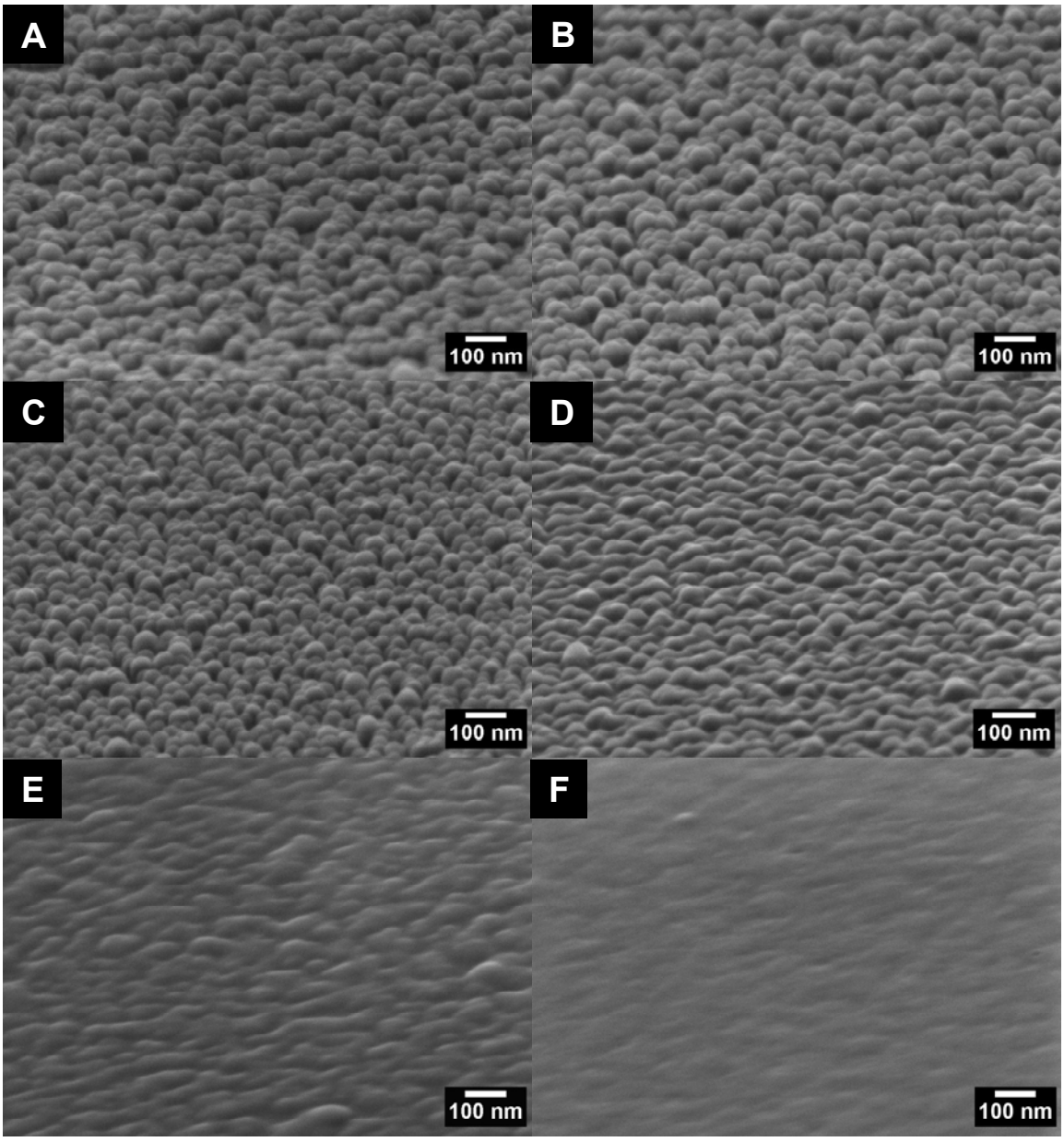

Figure 5.16. SEM images of macroscopic glass surfaces coated with 50 nm Eudragit S-100 nanoparticles and treated with acetone at A) 0%, B) 10%, C) 20%, D) 30%, E) 35%, F) 40% in the treatment solution. *Imaging was done on a tilted holder at ~ 70°.*

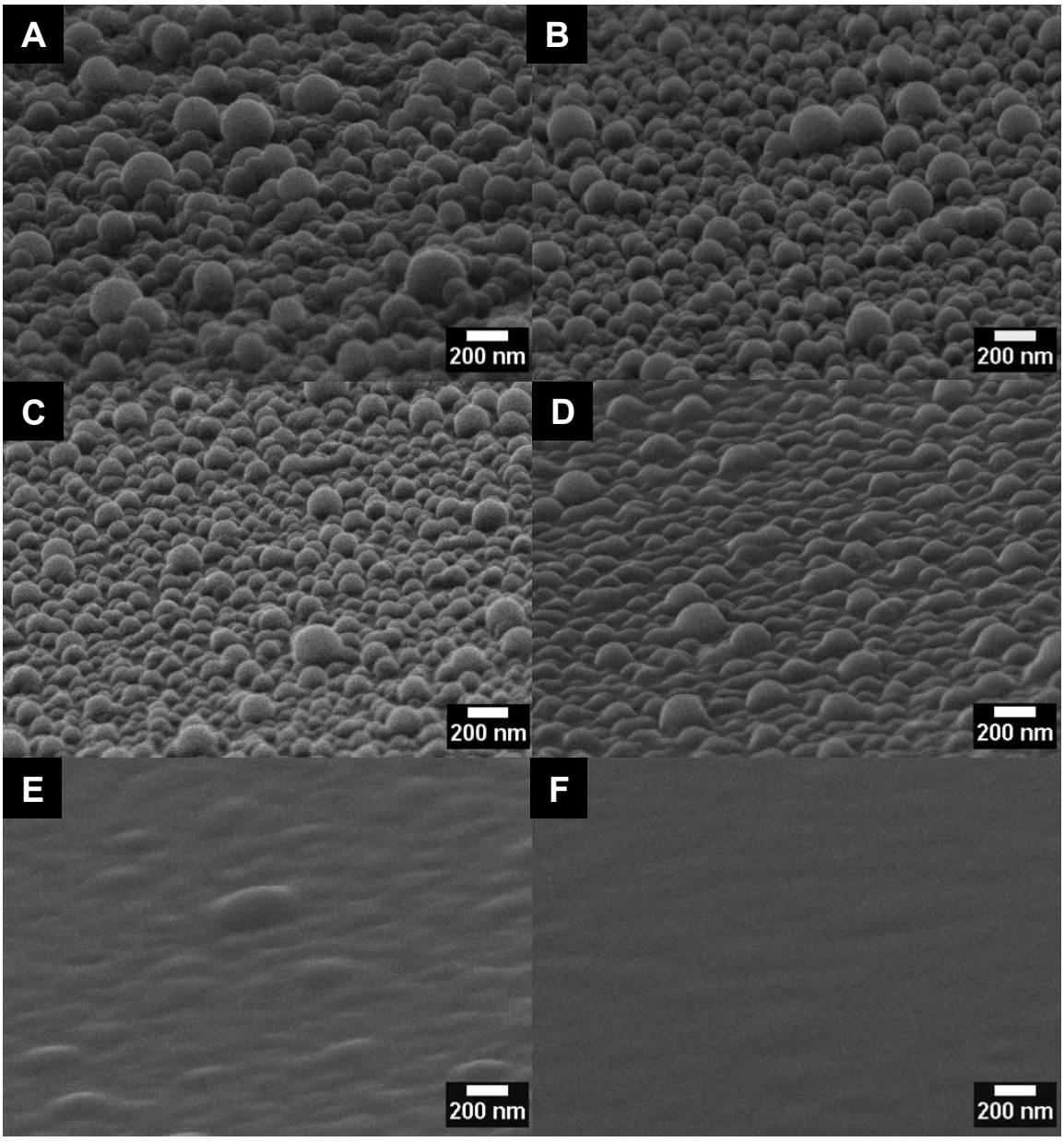

Figure 5.17. SEM images of macroscopic glass surfaces coated with 180 nm Eudragit S-100 nanoparticles and treated with ethanol at A) 0%, B) 20%, C) 30%, D) 35%, E) 40%, F) 45% in the treatment solution.

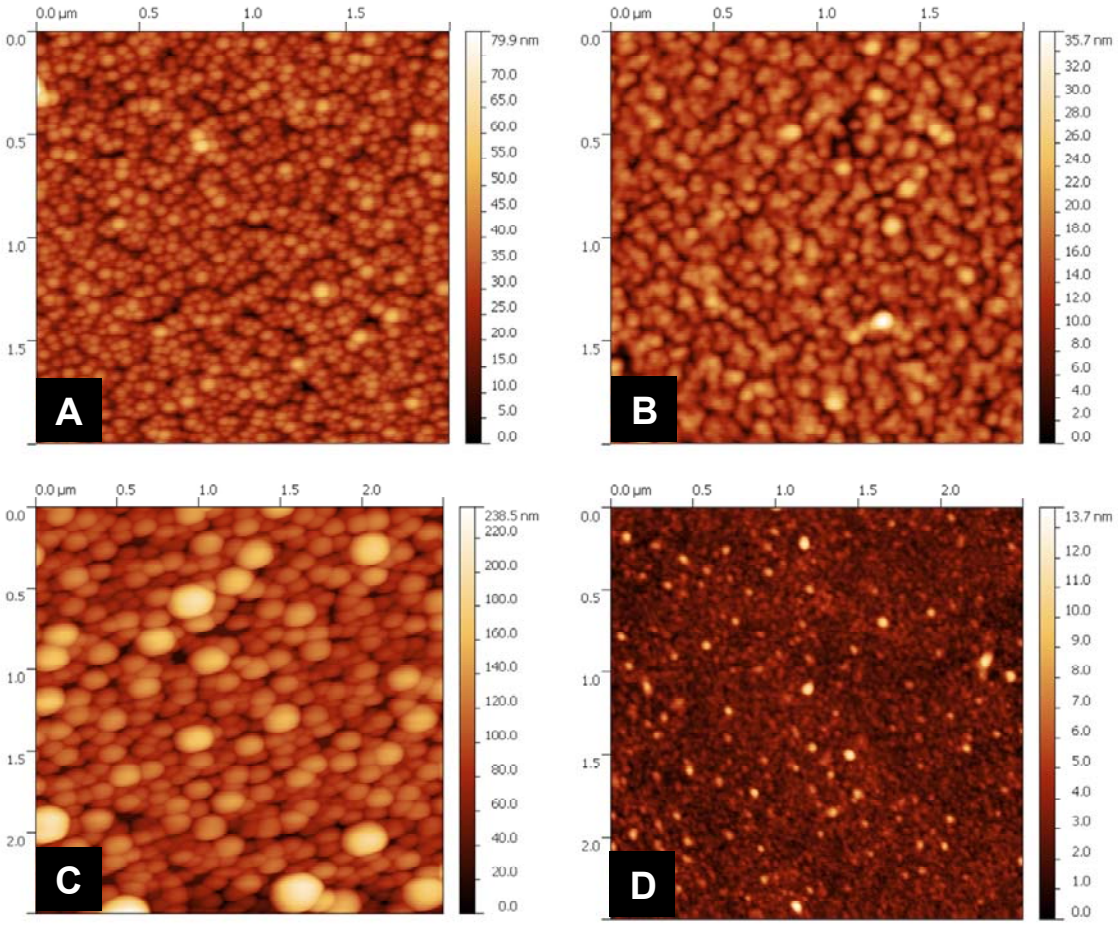

Figure 5.18. AFM Scans of macroscopic substrates coated with Eudragit S-100 and treated with acetone A) 50 nm particles, 10% treatment, B) 50 nm particles, 35% treatment, C) 200 nm particles, no treatment, D) 200 nm particles, 60% treatment.

Roughness data can be extracted from the AFM scans, and are shown in **Figure 5.19** and **Figure 5.20.** Two different parameters for quantifying roughness are shown: r refers to the ratio of the measured surface area to the projected surface area, Rms refers to the root-mean squared average of the height values obtained. Typically, the roughness effect on wettability has been studied by the roughness parameter r, in the Wenzel state.

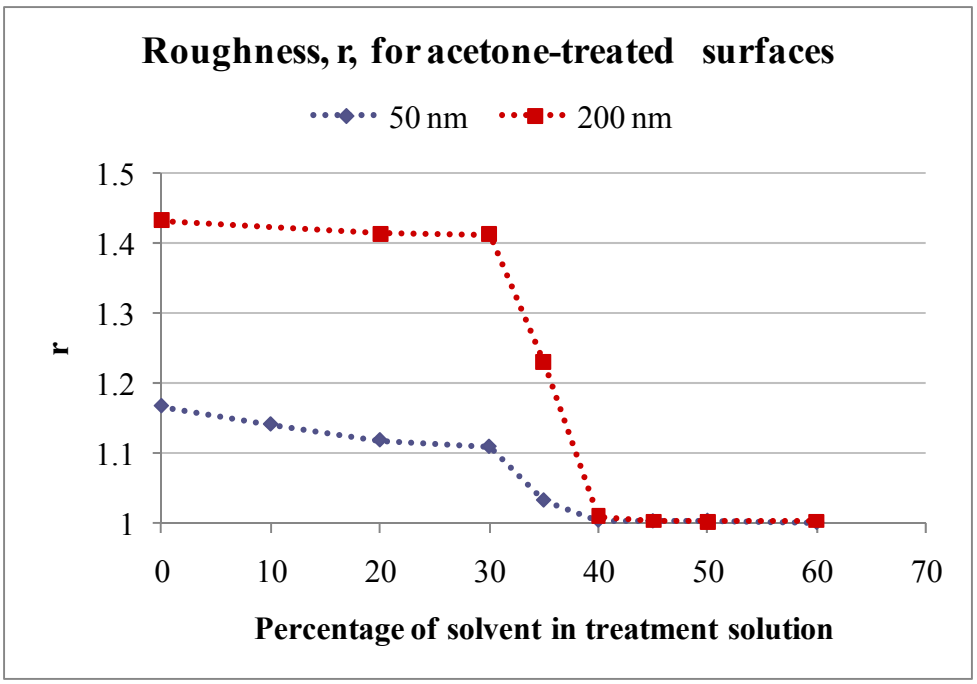

Figure 5.19. Roughness, r, for Eudragit S-100 nanoaprticle coated surfaces treated with acetone.

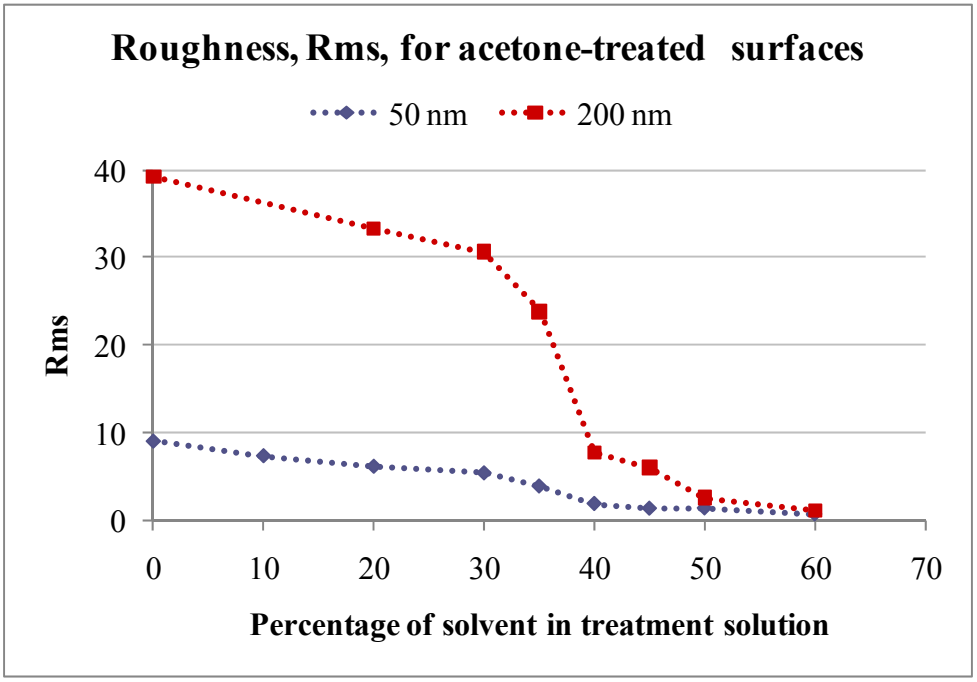

Figure 5.20. Roughness, Rms, for Eudragit S-100 nanoaprticle coated surfaces treated with acetone.

Due to the size of the features, and the configuration of the AFM probe, the image obtained is expected to be a convolution of the real surface and the tip shape. In this case, the parameter r would be affected to a larger extent than the parameter Rms. This is due to the fact that Rms only takes into consideration height information, while r accounts for the perceived surface area, which is bound to grossly underestimate the real area of a surface, especially one exhibiting re-entrant features. Nonetheless, both parameters show a clear effect of the treatment solution in the degree of surface roughness.

As is to be expected, coatings with larger particles produce a higher degree of surface roughness than those obtained with smaller particles. In the case of large particles, a sharp transition in roughness is obtained between 30% and 40% acetone in the treatment solution, which agrees with the SEM images shown. In the case of the smaller particles, a more gradual decrease in roughness is observed with increasing acetone percentage in the treatment solution.

Although the difference in roughness for the mildest treatment is not discernible with SEM, the quantitative roughness data confirms that even at low treatment there is an effective decrease in roughness. This decrease in roughness might not be observable with SEM as it might be a reduction in the re-entrance space between the particles and the substrate. This change would certainly not be observable with SEM but the Rms should reflect it, since a reduction in height would be expected as is the case for the data shown.

5.5 Conclusions

pH-responsive nanoparticles have been applied as coating for amine-silanized silica substrates including spherical micron-sized particles and flat glass slides. These nanoparticles form uniform coatings which can be partially dissolved by treatment with a solvent/water solution. Roughness is gradually reduced until a virtually smooth surface is obtained. In this way, hydrophilic surfaces with various degrees of roughness can be

generated. Due to the composition of the polymer used for the nanoparticle coating and the treatment method, surface chemistry can be kept constant for surfaces while varying the roughness.

Roughness of the flat substrates can be predefined by the size of the adsorbed particles and tuned by the degree of solvent treatment. Additionally, the surfaces generated are pH-responsive, allowing for the coatings to be dissolved by raising the pH above a moderate threshold value (~pH 7). These surfaces can potentially be used for applications where a stimulus-responsive surface with a defined roughness and wettability is required.

The generated surface coatings provide excellent opportunities to study wettability on hydrophilic rough substrates, as well as Pickering emulsification with rough and smooth particles. These are topics of high relevance for many applications including emulsion-based functional materials as well as anti-fog and oil-repellant surfaces. The following chapter deals with basic studies of wettability of these rough surfaces, as well as emulsification with particles of systematically varied surface roughness.

CHAPTER 6

THE ROLE OF PARTICLE SURFACE ROUGHNESS IN PICKERING EMULSIFICATION

6.1 Introduction

The effect of surface roughness on particle entrapment at the interface and on emulsification is a topic where information is scarce and conflicting ideas co-exist.

It has been suggested that particle roughness-induced contact angle hysteresis is the reason for the tendency of an emulsion to have the phase where the particles are initially dispersed as the continuous phase [*19*]. Furthermore, it has been shown theoretically that roughness-induced contact angle hysteresis is beneficial for emulsion stability by increasing the maximum capillary pressure for rupture of emulsion films [*41*]. On the other hand, Vignati et al. [*112*] found that particle roughness decreases emulsion stability as well as droplet coverage. They also suggested that the roughness affects the kinetics of adsorption to the interface [*112*] as an explanation for decreased droplet coverage. However, this study was performed with only 2 particle types where surface chemistry was not shown to be constant.

More fundamental theoretical studies have shown that roughness on a particle will affect the energy of particle adsorption to the interface as well as the equilibrium contact angle [*120-122*] and even induce capillary attraction [*115-118*].

In macroscopic flat substrates, surface roughness is expected to change the contact angle and induce some contact angle hysteresis, as has been described in the first chapter. The same effect is expected for particles at a liquid-liquid interface. The mentioned theoretical studies predict that the contact angle of the particles at the

interface, as well as the adsorption energy, will change and that the dependence of this change with roughness will be related to the wetting regime: Wenzel or Cassie-Baxter [*120-122*]. For particles in the Wenzel wetting regime, the inherent hydrophilicity or hydrophobicity of the particles [*121*] should be enhanced. For extremely rough surfaces, the existence of a Cassie-Baxter regime will depend mainly on the initial liquid the particle is immersed in [*120*].

For the sake of better understanding the true importance of surface roughness in particle adsorption, the heteroaggregates with various degrees of surface roughness described in the previous chapter are used as models to study emulsification properties. In this case, the wettability of the macroscopic rough surfaces described in the previous chapters will be determined. This data and the quantitative roughness information will be correlated to the emulsification experiments performed with rough particles.

6.2 Wettability of hydrophilic surfaces with various degrees of surface roughness

The surfaces generated with various degrees of roughness should show different wettability. Quantifying it by measuring contact angle is important not only to serve as models for the wettability of rough and smooth particles at liquid-liquid interfaces, but also since the wettability of hydrophilic surfaces is not as widely explored as that of hydrophobic surfaces. Several contact angle measurements were taken, using the same liquids to be analyzed in emulsification experiments. Since contact angle hysteresis can be important, the three-phase contact angles were measured for pending oil drops in water. In this way the solid phase could be in contact with an aqueous environment initially, as is the case also of the particles used for emulsification from an aqueous dispersion.

6.2.1 Contact Angle Measurement Experimental Details

The contact angle of macroscopic substrates was measured less than 48 hrs after sample preparation in a Ramé Hart goniometer. Contact angle measurements of sessile water drops in air were done by depositing a drop of 1mM aqueous NaCl solution at pH 5 on the substrate. Pending oil drop contact angle measurements were carried out in a water- filled quartz-cell, at pH 5 and 1mM NaCl. The substrates were submerged in the quartz cell and suspended upside down by polycarbonate holders. A drop of octanol or decane was then deposited from below on the substrate with a 22 gauge inverted needle. Images were taken after the drop spread and reached equilibrium, typically 10 sec – 4 minutes depending on the substrate and drop phase. Contact angles were measured with NIS-Elements imaging software (Nikon). Reported values are an average of at least 3 drops with both sides measured. The reported contact angles are always measured through the water phase.

6.2.2 Wettability of rough and smooth surfaces as determined by contact angle measurements

Figure 6.1 shows the results obtained from the contact angle measurements for surfaces treated with acetone to various extents.

As can be seen from these data, the contact angles change by anywhere from 20° to 90° with an increasingly intensive treatment. The smallest change is exhibited by the contact angle of a sessile water drop in air and a pending air bubble submerged in water.

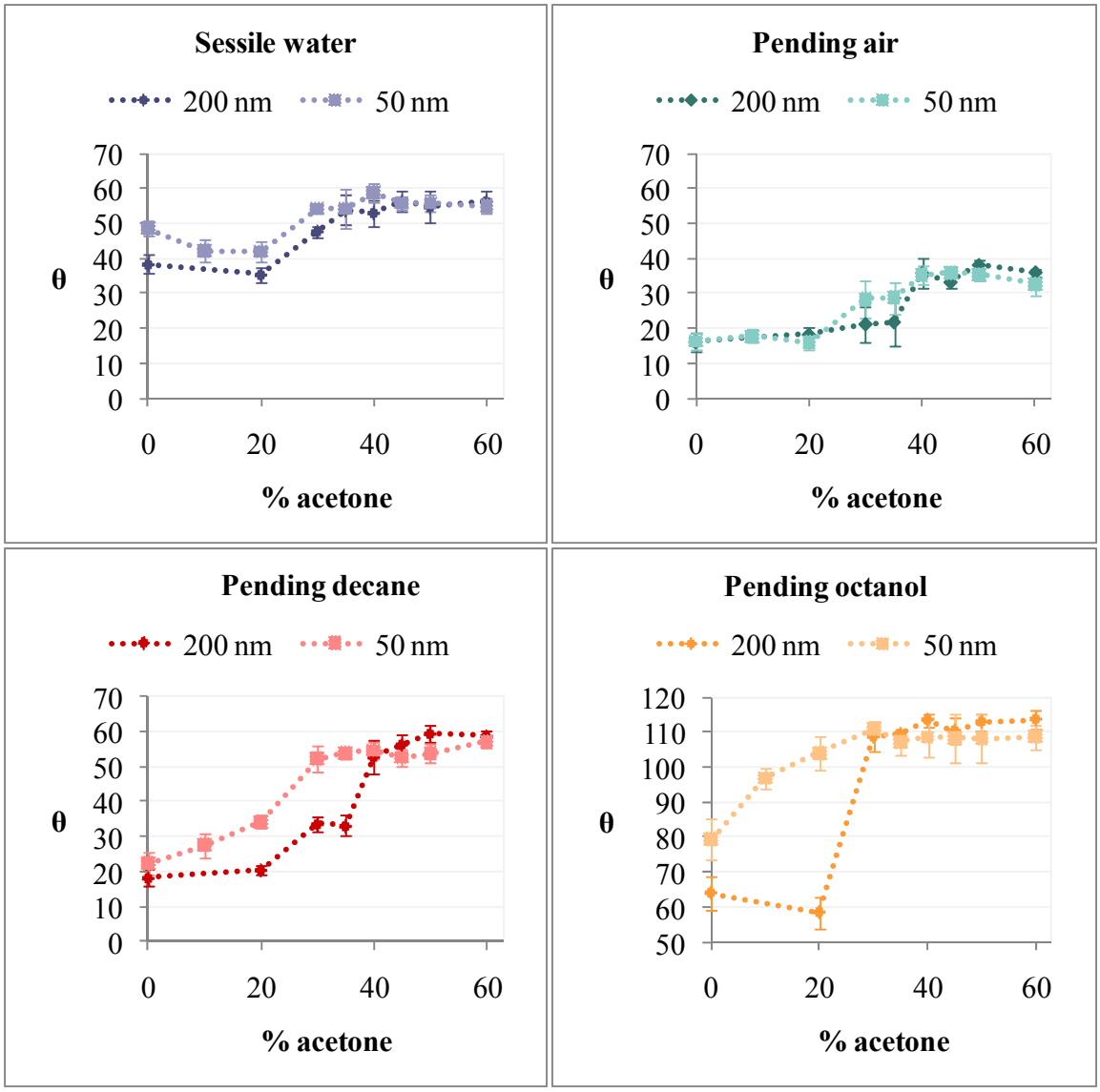

Figure 6.1. Contact angles for Eudragit S-100 nanoparticle coated macroscopic flat surfaces as a function of percentage of acetone in treatment solution. *Pending drop measurements done in water. Water at pH 5 with 1 mM NaCl.*

For an ideal surface, that follows Young's equation, the contact angle measured through water for the pending air drop and the sessile water drop should be identical. Clearly this is not the case here, which is explained by the fact that these surfaces are far from ideal, and are exposed to the fluid phases in different order. Furthermore, it is important to mention that the presence of gravitational deformation of the sessile water

and pending air droplets has an effect on the measured contact angles, which could also explain this difference. The comparison of the two is a clear indicator that the wettability of these surfaces depends on the liquid it is first in contact with. Both sessile water and pending air measurements show a reduced hydrophilicity as the treatment is increased. This is to be expected, as the higher degree of treatment produces smoother surfaces. Therefore, this indicates that roughness is in fact enhancing the inherent hydrophilicity of the material.

From the graphs shown in **Figure 6.1** it appears as if there is not a large difference between the 50 nm and 200 nm particle-coated surfaces, in terms of wettability change with degree of treatment for sessile water and pending air. This difference is increased in the case of pending octanol and decane drops. In every case, wettability seems to be similar for both surfaces at high treatment, which is expected as this is where the smoothest surfaces are generated (according to SEM and AFM data shown in the previous chapter).

Since surface roughness is the reason for the change in wettability, this would be better described by correlating contact angle measurements with the surface's quantified roughness. **Figure 6.2** shows data represented in this way, which exhibits a previously unseen difference between the surfaces generated with 50 nm and 200 nm particles. It is clear from the graphs, that at the same levels of root-mean-squared roughness, the wettability of the surfaces is different for 200 and 50 nm particle-coated substrates. Although this might seem surprising at first, in reality surfaces with different feature geometry and size, but same Rms, are not expected to have the same wettability.

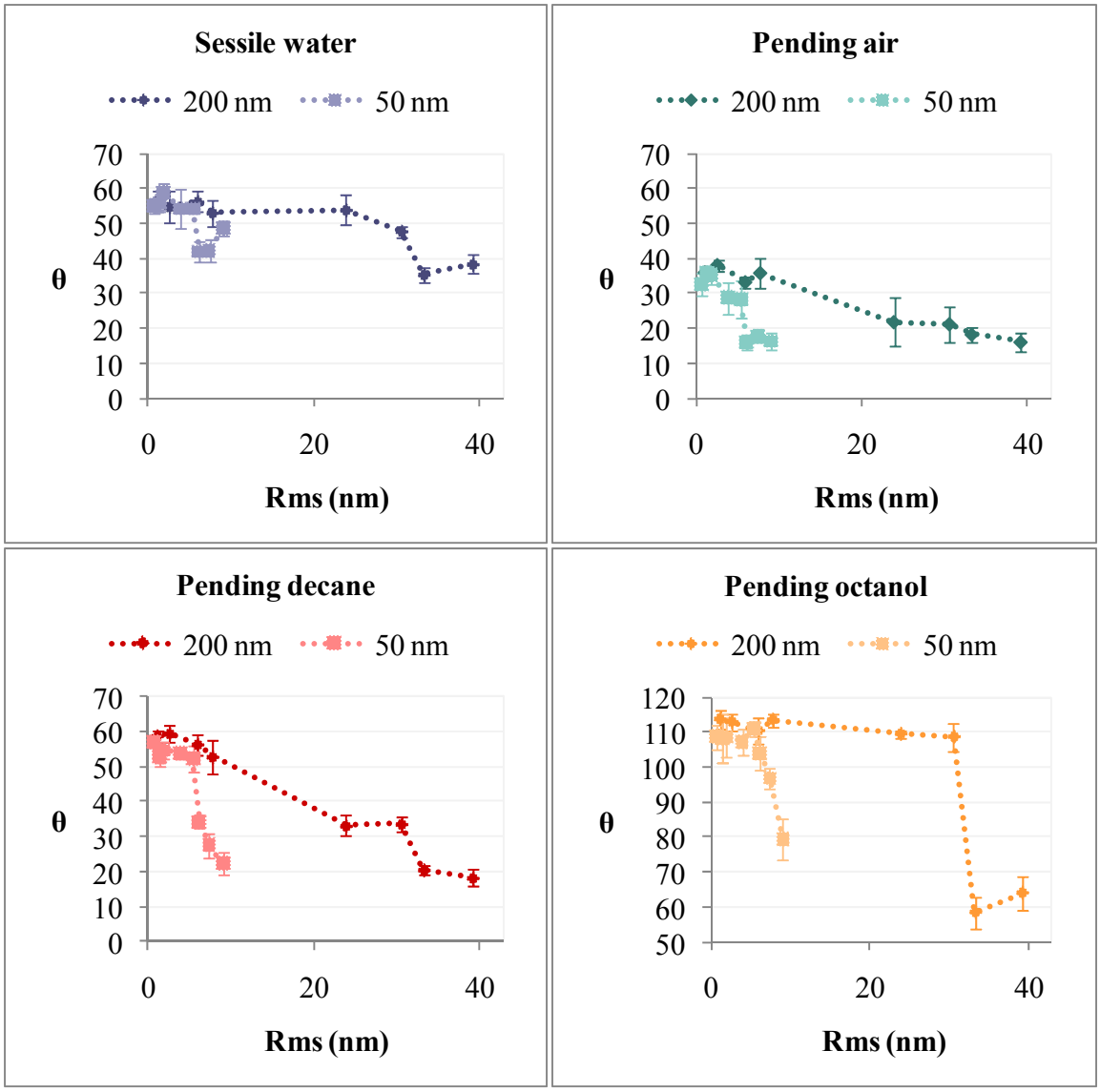

Figure 6.2. Contact angles for Eudragit S-100 nanoparticle coated macroscopic flat surfaces as a function of root-mean-squared roughness, Rms. *Pending drop measurements done in water. Water at pH 5 with 1 mM NaCl.*

If these surfaces were in an ideal Wenzel state, then the wettability should be the same at the same roughness parameter, r, which is difficult to accurately determine by AFM for the reasons previously stated. Here, the roughness correlated with wettability only describes the root-mean-squared average height of the sample, which is a good indicator of surface roughness in this case. However, two surfaces with different r can

have the same Rms. For instance, the surface area for perfectly circular features and for a 2-d sinusoidal wave-like surface with the same Rms would certainly produce a different r value. Even in the case where a precise value for r can be measured, these surfaces could still differ in contact angle at the same r value due to possible heterogeneous wetting, overhanging or re-entrant features.

Clearly, the size of the nanoparticles that serve as roughness-producing coatings is a very useful parameter to tune the surface wettability. Using particles of different size will cause a change in the root-mean-squared roughness and surface area; furthermore, due to their difference in curvature, it will form potential re-entrant sites which could favor heterogeneous wetting. The dimensions of such re-entrant sites will be related to the particle size. Upon solvent-treatment, the size change of such sites, or their complete disappearance, will be determined by the treatment intensity. Furthermore, tuning the roughness of the starting nanoparticle-coated substrate can lead to wave-like surfaces of different wavelength, which at the same Rms and surface chemistry can have different wettability. Therefore, the particle size is a very useful parameter to tune wettability, beyond the Rms it can produce.

Typically, the Wenzel wetting regime theory predicts that the surface wettability will be more greatly enhanced the farther the contact angle for the smooth surface is from 90°. As can be seen from the data, this is certainly not the case for these surfaces. For the 200 nm particle coating, both the sessile water drop and the pending decane drop have a value around 60° for the smoothest surface. Nonetheless, the increase in hydrophilicity is of around 20° in one case and 40° in the other. Meanwhile, the pending octanol drop, with a starting value of around 110° decreases about 50°. However, octanol appears to be a special case which will be discussed separately.

It is important to note that the roughness effect on wettability when the two fluids under consideration are liquids has not yet been shown experimentally. Although, theoretically the previously described wetting regimes should also apply to this case, to

the best of our knowledge the effect of roughness on liquid-liquid-solid contact angles has never been studied.

At first, it might seem surprising that the octanol contact angles at high roughness levels are very hydrophilic, around 60°, and upon a reduction of surface roughness these values turn hydrophobic, with contact angles above the 90° threshold. This transition can be an indication of heterogeneous wetting. Typically the Cassie-Baxter regime for a liquid drop in an air environment predicts that the surface should become more hydrophobic as the roughness is increased, regardless of the contact angle of the smooth material. This is caused by a change in the parameter *f*, which accounts for the fraction of surface area in contact with the liquid drop. As the roughness is increased, this parameter *f*, should be reduced due to pockets of air trapped in the features below the water drop. In the case presented here, as the surface is hydrophilic, and first immersed in water, the features would be filled with water under the octanol droplet. It is clear how an increase in roughness would reduce the factor *f*, which would mean a higher fraction of area taken up by the water pockets. This in turn would result in a more hydrophilic surface, regardless of the contact angle of the smooth material, which is precisely the case here.

It is noteworthy that in all surfaces the deposited droplets first spread on the surface until equilibrium is reached. Although all the data presented is for equilibrium contact angles, the time to reach equilibrium seems to be relevant, especially in the octanol case. This time ranged from ~10 sec to ~4 min, and was assessed by taking consecutive droplet images approximately 1 sec apart until no visible difference in the droplet shape was observed. This time to reach equilibrium was generally longer for rougher surfaces, as could be expected, and especially for octanol droplets. A significant contact angle change with time was observed for octanol droplets. For rougher surfaces, the deposited octanol drops always started with a value below 90°. From the data, it can be seen that the two roughest surfaces found an equilibrium value below this threshold. However, the next surfaces in degree of roughness reached values above 90°, although

also starting below this value. This is a very significant observation that will become relevant in the emulsification studies to be described in the following section.

6.3 Emulsification with particles with various degrees of surface roughness

Although several theoretical studies have been performed regarding the equilibrium positions of rough and smooth particles at interfaces and their stabilization of emulsion droplets [*41, 120-122*], the effect of surface roughness on Pickering emulsification is far from understood, and greatly lacking experimental evidence. In this section, particle roughness as a tunable parameter for Pickering emulsification is studied.

For the sake of isolating the effects of surface roughness, particles of the same size, density and surface chemistry but varying degrees of roughness have been used as stabilizers of emulsions with polar and non-polar oils. Emulsification studies were carried out with amine-modified silica particles coated with 50 nm Eudragit S-100 nanoparticles, and treated by acetone to different extents, which are described in detail in the previous chapter.

Several different factors are typically used to characterize emulsions: emulsion type, average droplet size, percentage of creamed or sedimented phase and, in some cases, the oil or water fraction for catastrophic phase inversion. While the aforementioned indicators are certainly useful to describe the emulsions at their initial state, they do not provide information about long-term stability.

In order to cover all potential effects of particle surface roughness on emulsification, the emulsion type and average droplet size were determined. An even more telling parameter shown is the maximum capillary pressure, P_C^{max}, which is an indicator for long-term emulsion stability.

As has been discussed in the introductory chapter, Pickering emulsion stabilization has been described by the well-known equation that relates particle radius and contact angle to the energy of adsorption at the interface, ΔG_{int}, which predicts that larger particles with contact angles close to 90º are better emulsion stabilizers (Eq.1). In reality, to avoid droplet coalescence the particles need to stabilize the film formed by the continuous phase between two approaching droplets. Therefore, the capillary pressure required to break the emulsion film between two approaching droplets also needs to be taken into account, which is a stabilization mechanism sometimes overlooked in the Pickering emulsion literature. The stability of these films, has been described by various authors [*21, 35-39, 41*] in terms of the maximum capillary pressure, P_C^{max}. This parameter represents the maximum pressure that a film stabilized by particles can be subjected to before breaking. The most general expression to describe the maximum capillary pressure, previously shown (Eq. 2) has been developed by Kaptay [*21*] and takes the form:

$$P_C^{max} = \pm p \frac{2\gamma_{ow}}{r} \cos(\theta \pm z) \qquad \textit{Eq. (2)}$$

where p and z are parameters describing the arrangement and packing of the particle layers; these values are typically constant for a specific situation (i.e., a range of contact angles and mono- or bi-layer of particles). The positive sign in is applied for o/w emulsions and the – sign is applied for w/o emulsions.

Beyond theoretical detail, the interesting fact of this stabilization parameter is that it predicts more stable films when smaller particles are used, and when the contact angles are further from 90º. This difference between the two equations describing emulsion stabilization (particle adsorption energy and maximum capillary pressure) comes from the fact that they describe different emulsion failure modes: particle detachment, and film breakage respectively.

The relevance of the aforementioned stabilization mechanisms lies in the fact that in order to study long-term stability, the thinning film stability needs to be taken into account. Emulsion coalescence is thus a result of such film ruptures. It is therefore logical to use P_C^{max} as an indicator for film stability, and hence for emulsion stability. It turns out that P_C^{max} is easily quantifiable by centrifugation experiments, as has been previously shown by Tcholakova et al. [*35, 36*]. When an emulsion is subjected to a centrifugal force, the dispersed droplets with a density difference, Δρ, to the continuous phase will be pushed together, as centrifugation causes an effective amplification of gravity. The force exerted on the droplets increases in the direction of acceleration (gravity) for $\Delta\rho > 0$ and in the opposite direction for $\Delta\rho < 0$, and results, for sufficiently large acceleration, in the coalescence of droplets into a phase-separated liquid volume of height H_{REL} at the bottom ($\Delta\rho > 0$) or top ($\Delta\rho < 0$) of the vial. The pressure at the interface of the released liquid and the emulsion is exactly the maximum pressure that the film between an emulsion droplet and the released volume can withstand. This pressure is of course identical to P_C^{max}; the maximum pressure a film between two emulsion droplets can withstand before breaking, and can be easily calculated. For an o/w emulsion, the measurement the amount of oil released after centrifugation, can be related to the P_C^{max} by [*36*]:

$$P_C^{max} = \Delta\rho g_c (H_{OIL} - H_{REL}) \qquad \textit{Eq. (12)}$$

where Δρ is the density difference between the dispersed and the continuous medium, g_c is the centrifugal field, H_{oil} is the height of the oil phase if all the oil is separated, $H_{oil} = V_{oil}/A$ (A = cross-sectional area of the vial), and H_{REL} is the height of oil released.

The maximum capillary pressure becomes more important in the case where particle surface roughness is under study, as theoretical approaches have suggested it affects the maximum capillary pressure [*41*], wherein a higher contact angle hysteresis due to roughness or heterogeneities increases the maximum capillary pressure. In this study, the long term stability of Pickering emulsions is thus assessed by P_C^{max}, and correlated with the particle surface roughness.

The experimental details and results obtained for decane/water and octanol/water emulsions will be presented next.

6.3.1 Experimental Methods

Emulsions of decane/water or octanol/water systems were studied as model for emulsions of a non-polar and polar oils. A 50:50 mixture of oil and water at pH 5 and 1 mM NaCl was homogenized at 13,000 rpm in a IKA T10 homogenizer for 20 sec in the octanol case and for 40 sec in the decane case. The particles used were amine-silanized silica particles coated with 50 nm Eudragit S-100 nanoparticles and treated to different extents with an acetone/water solution, as described in the previous chapter. The particle concentration was determined by gravimetric analysis. In the decane case the particles used were 0.90 μm at a 3.2% (wt/v); in the octanol case the particles were 0.96 μm at 2.5% (wt/v). Emulsions were prepared in long glass tubes to increase the accuracy of released phase height after centrifugation.

25 μl of the emulsion phase were removed after preparation for microscopic observation, which was performed on a Nikon Eclipse 50i upright microscope with a 10x air objective. Droplet radius measurements were performed on 170 drops with NIS-Elements Nikon software. Images were also taken with a 60x oil objective for the observation of particle packing at the droplet interface.

The emulsions were centrifuged in the closed glass vials, in an Eppendorf 5702 centrifuge. Digital photographs of the emulsions next to a linear scale were taken for height measurements of each fluid phase. Octanol emulsions were centrifuged at 1,000 rpm for 1 hr. Decane emulsions were centrifuged twice at 4,400 rpm for 1 hr each time. Photographs were taken after each centrifugation cycle.

The height of each fluid phase, and the linear scale, were measured in pixels with ImageJ software, with an accuracy of ~ 6 px, which represents a 0.11 to 0.19 mm error (where the total emulsion height is typically 18 mm).

6.3.2. Decane as a model for a non-polar oil

The decane/water emulsions stabilized with rough and smooth particles were all oil-in-water, as is to be expected according to the contact angles for the flat substrates, which are all below 90º for this system. Homogenization resulted in a single emulsion phase, which creamed after a few minutes, with no visible difference among the samples. In all the emulsions observed, complete surface coverage was observed, with a hexagonal packing arrangement, as shown in **Figure 6.3**.

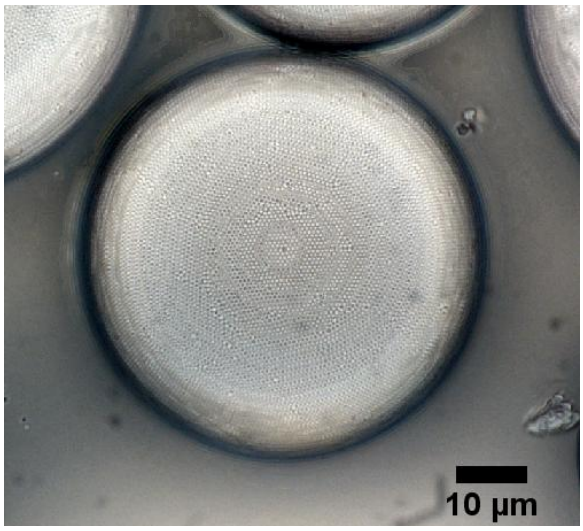

Figure 6.3. Micrograph of a decane-in-water droplet stabilized by rough particles. *Focused image reconstruction by imaging different focal planes, thus the appearance of circular discontinuities.*

Furthermore, the droplet radius obtained did not vary significantly between samples, as shown in **Figure 6.4**. The plot shows the number-averaged radius (R_N), as well as the mean volume-surface averaged radius (R_{32}). Both R_N and R_{32} are obtained from histogram classes and weighed as: $R_N = \frac{\sum N_i \cdot R_i}{N}$, where Ni is the number of droplets and Ri the radius of each class, N is the total number of droplets measured. R_N is different from the unweighed average in the sense that number density becomes a relevant factor, where the presence of a large number of smaller droplets, for example, would result in a R_N smaller than R.

R_{32} is weighed by the volume-surface area ratio, and is defined as $R_{32} = \frac{\sum N_i \cdot R_i^3}{\sum N_i \cdot R_i^2}$. Volume-surface averaged numbers are larger as larger droplets weigh more heavily than in the number-averaged size.

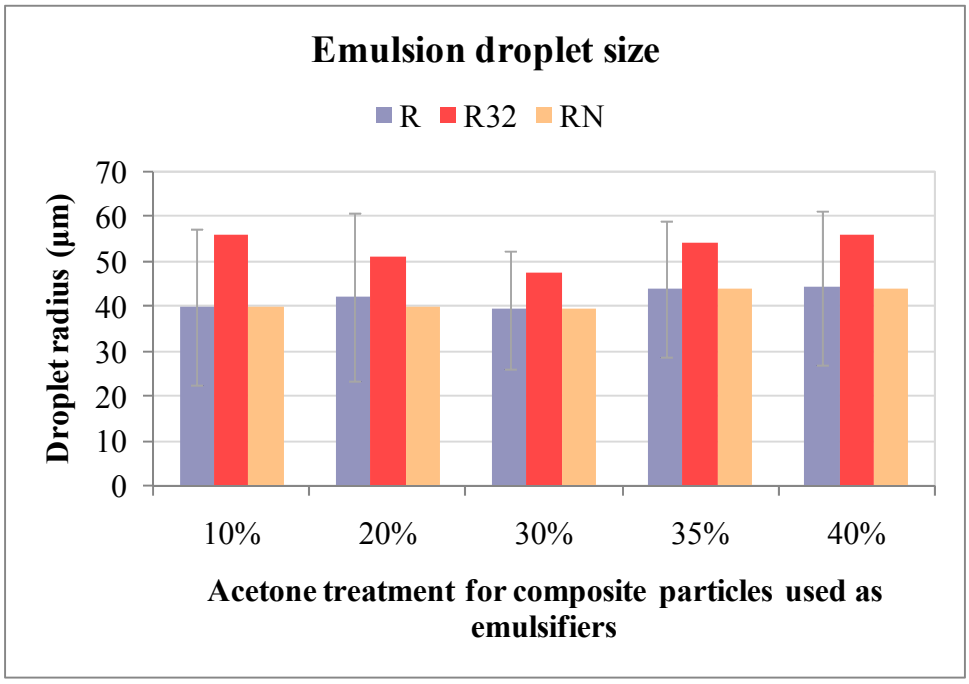

Figure 6.4. Mean droplet radius of decane/water emulsions stabilized with 0.90 µm particles with different degrees of surface roughness. R=unweighed average, R32=volume-surface average, RN=number average.. *Error bars for un-weighed drop size average represent the standard deviation.*

From these experiments, it appears as if the surface roughness has no effect on the percentage of creaming, type of emulsion or droplet size. The centrifugation experiments, related to long-term emulsion stability, on the other hand, provided interesting information where a clear difference between emulsions stabilized with rough and smooth particles, as shown in **Figure 6.5**.

Visual examination of the emulsions after centrifugation show a clear difference between the samples, where it appears that, up to certain extent, the rougher the particle surface, the better the particle is at stabilizing the emulsion.

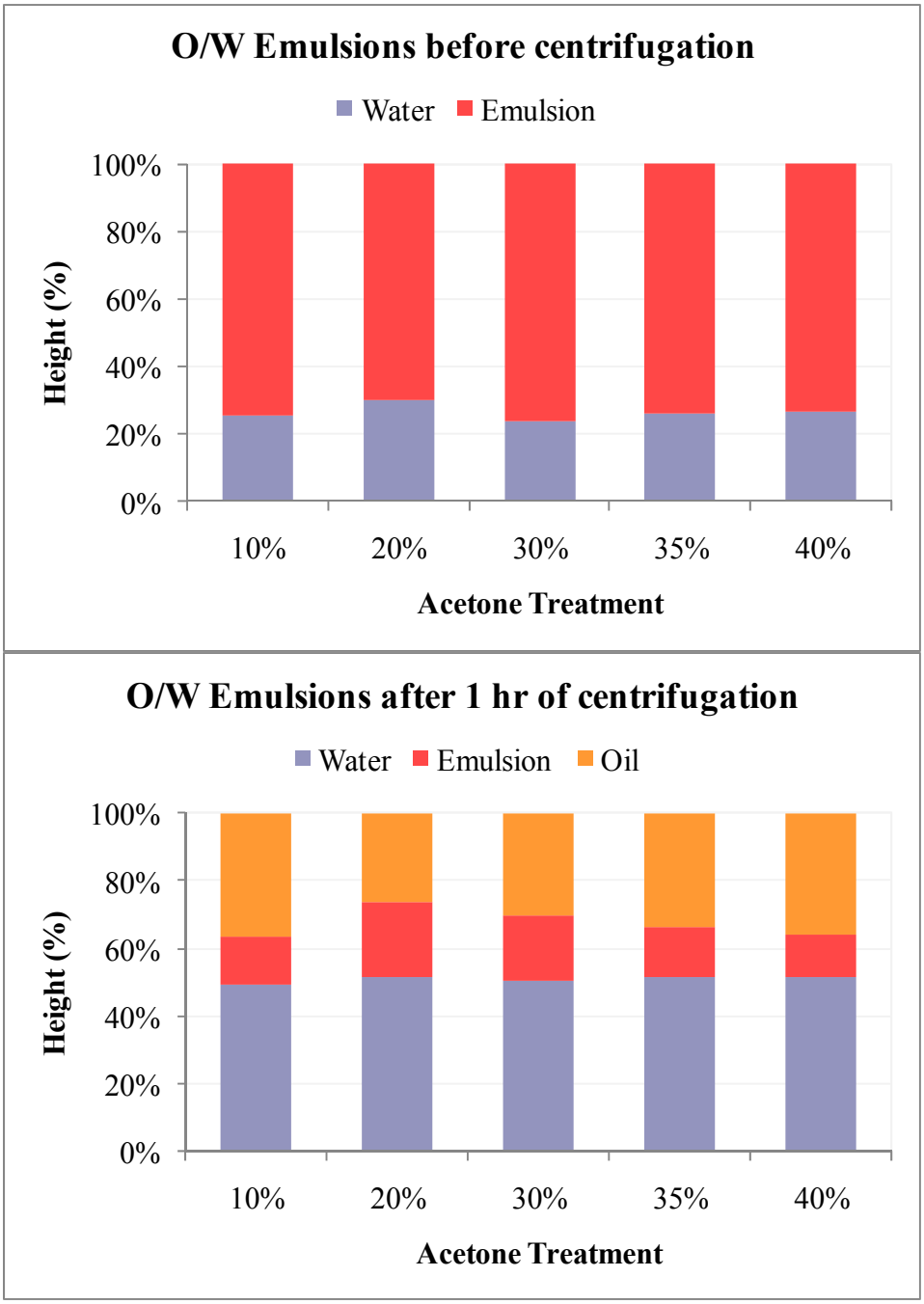

Figure 6.5. Height of water, emulsion and oil phases of decane/water emulsions stabilized with 0.9 µm particles with different degrees of surface roughness. *Top: Emulsions before centrifugation. Bottom: Emulsions after 1 hr centrifugation at 4400 rpm.*

In order to better visualize the differences among samples after centrifugation, the fraction of emulsion remaining is established as $\Phi = \frac{V_{em}}{V_T - V_{em}}$, which represents the ratio of emulsion to non-emulsion phase after centrifugation. The results of centrifugation experiments are plotted this way in **Figure 6.6**, which also shows Φ as a function of expected root-mean-squared roughness, Rms, and the expected particle contact angle. The expected Rms and contact angle are those obtained for a macroscopic flat substrate with the same treatment as the particles, as described in the previous chapter. This figure also shows the results obtained after an additional hour of centrifugation. The values show that after 1 hr of centrifugation the emulsions prepared with rough particles have not yet reached equilibrium with the centrifugal force applied. Nonetheless, it is clear that the dynamics of emulsion de-stabilization are different for the samples, as the emulsions with smooth particles reached equilibrium after only 1 hour of centrifugation.

Although the parameter Φ allows easier visualization of the differences between emulsions, it is not a value that relates to a physical characteristic about emulsion stability. The maximum capillary pressure is, and can therefore serve as a quantitative measure of emulsion stability. The values for P_C^{max} of the decane/water emulsions are calculated from the height of oil released after 2 hours of centrifugation, and are shown in **Figure 6.7,** where typical values range from 15 to 23 kPa.

From either representation of emulsion stability, Φ or P_C^{max}, it can be seen that except for the roughest particles tested (10% treatment), the results show a clear trend where the emulsions stabilized with rougher particles (with higher degree of surface treatment) are more stable to coalescence, as has been suggested by the literature [*19*], but in contradiction of the experimental results by Vignati et al. [*112*].

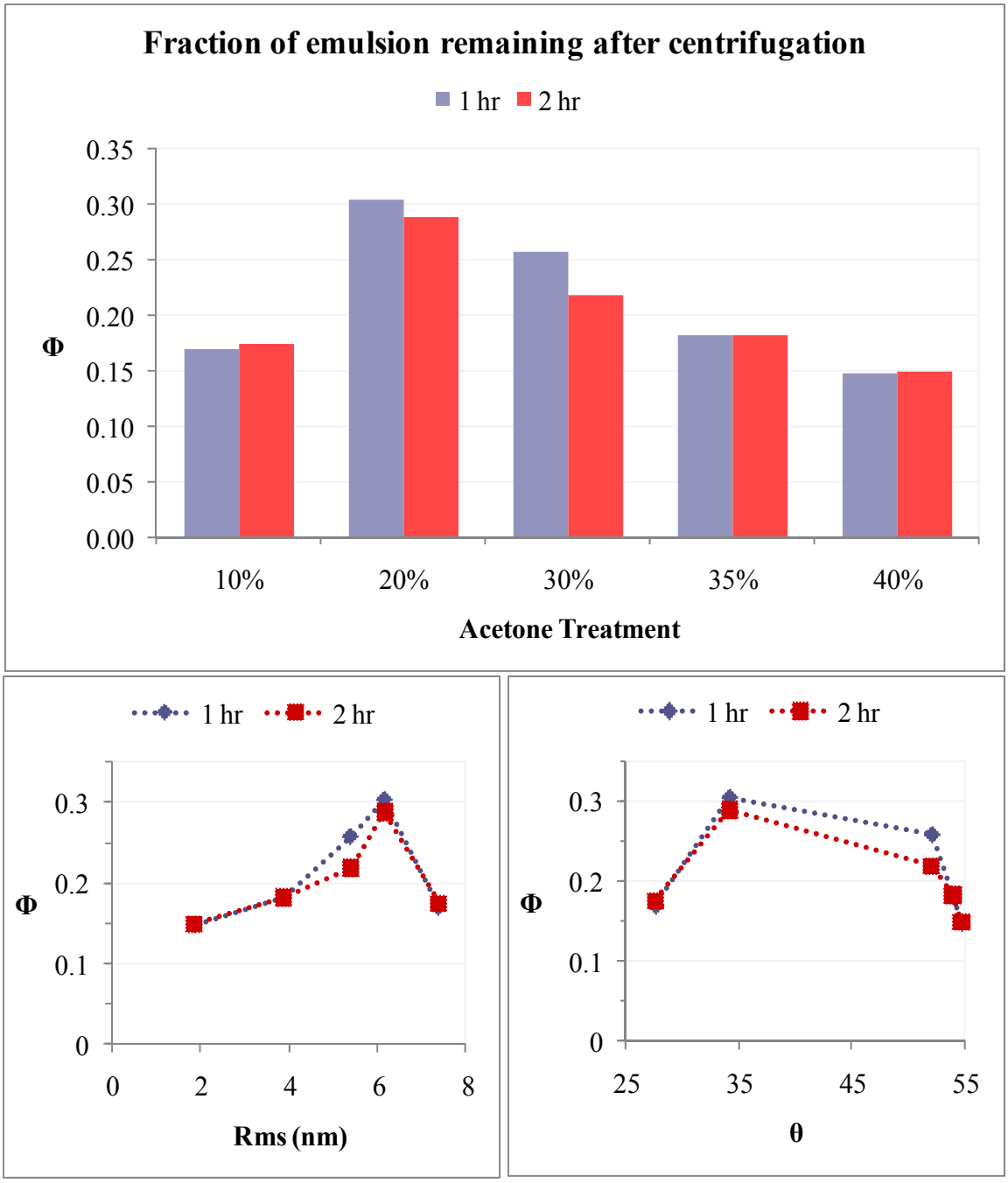

Figure 6.6. Fraction of emulsion phase remaining after centrifugation for 1 or 2 hrs at 4400 rpm. *Emulsions are decane/water, stabilized with 0.90 μm particles with different degrees of surface roughness. Surface roughness and contact angles are those obtained for macroscopic surfaces coated with the same surface treatment as the particles used for stabilization.*

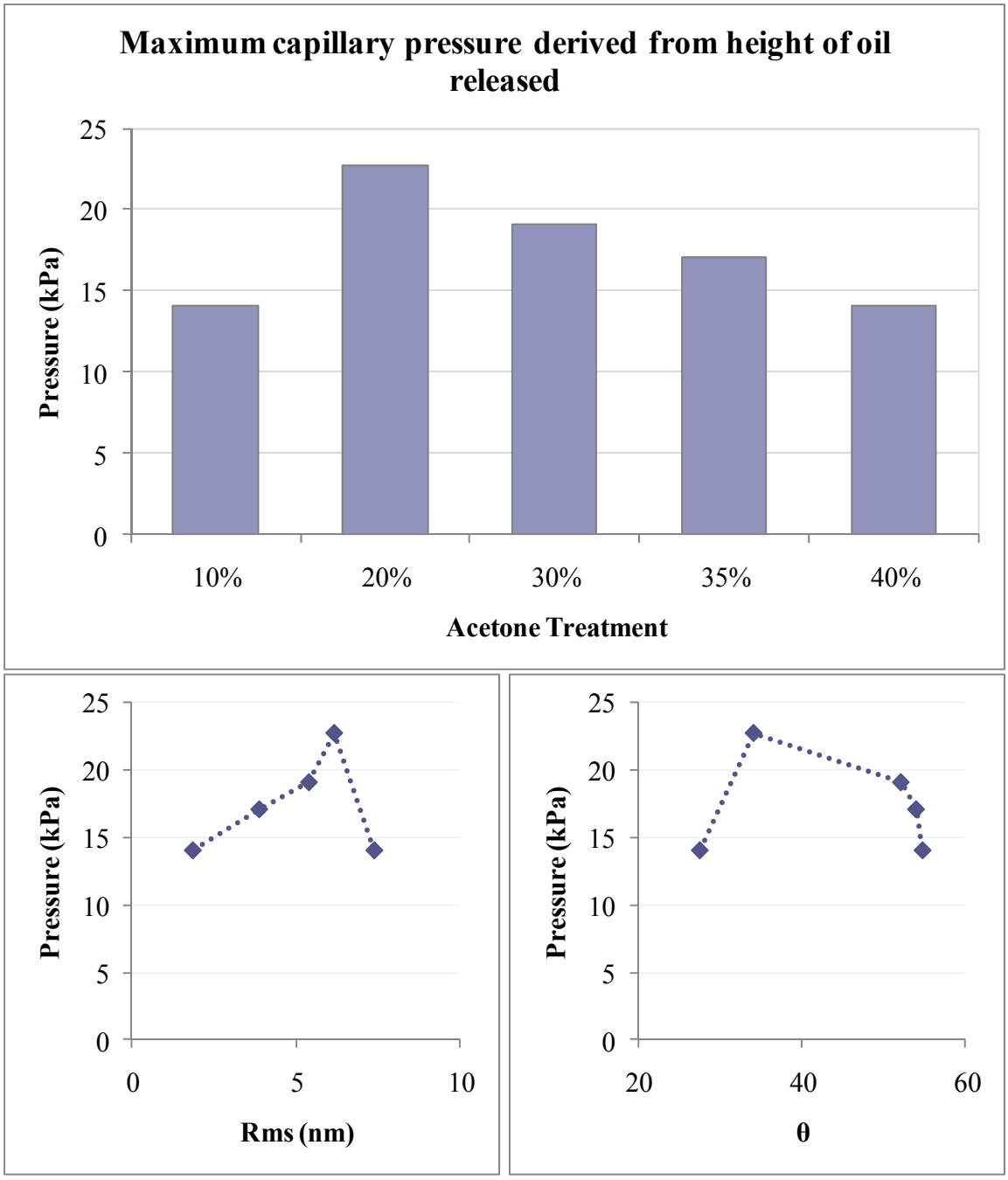

Figure 6.7. Maximum capillary pressure of emulsions stabilized with particles with different degree of surface roughness. *Emulsions are decane/water, stabilized with 0.9 μm particles. Surface roughness and contact angles are those obtained for macroscopic surfaces coated with the same surface treatment as the particles used for stabilization.*

Surprisingly, the roughest particle with only 10% acetone in the treatment solution, (with an Rms of 7.4 nm for the equivalent flat surface), produces much less stable emulsions than most other particles, reaching almost the same value as the smoothest particle tested (40% acetone treatment, 1.9 Rms for the equivalent flat surface). Furthermore, this trend-breaking behavior does not seem to be related to a change in contact angle, as shown from the images. It is noteworthy that this deviating point was tested twice and complete qualitative behavior has been reproduced with a batch of 0.96 μm particles.

One possible explanation for the difference observed with this roughest particle type is that potentially it is in a Cassie-Baxter wetting regime. It is expected that the least solvent treated particles will have larger re-entrant features, as there will be some space between a deposited spherical particles and the substrate due to the particle curvature, as illustrated in **Figure 6.8**. These "re-entrant" sites, or "overhangings" have been shown to favor heterogeneous wetting [*82, 96*].

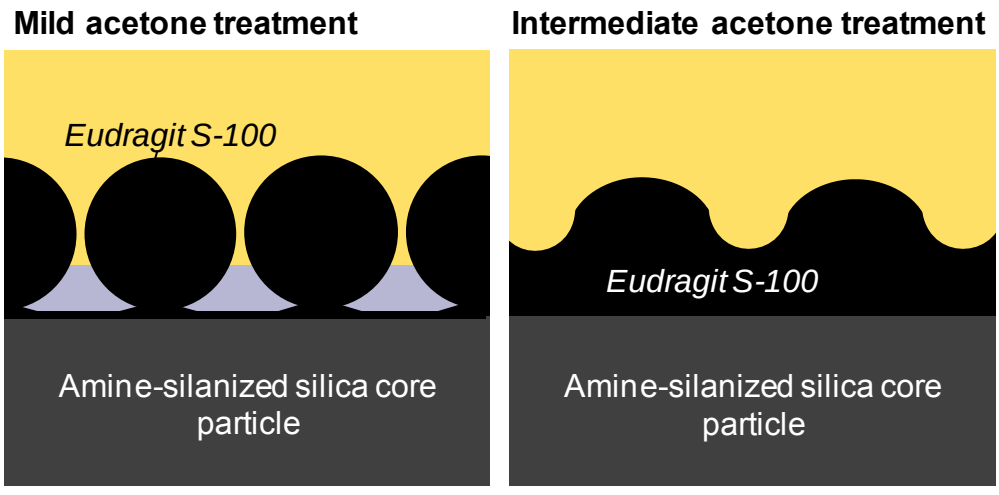

Figure 6.8. Proposed wetting schemes for Eudragit S-100 – silica heteroaggregates with different degrees of surface roughness at the decane-water interface. *For the mild treatment case, re-entrant features that favor Cassie-Baxter wetting are shown.*

This suggests the particles treated with 10% acetone, could be in a heterogeneous wetting regime, where the re-entrant sites are filled with water, therefore making the particles appear overall more hydrophilic as would be expected for a heterogeneous wetting regime where the initial fluid in contact with the surface is water. Although contact angle data does not show a big change with 10% treated particles, the values are already very low (~ 27 °), and therefore cannot be evidence for the existence of heterogenous wetting. Furthermore, the re-entrant sites created by deposited particles on flat and spherical substrates could be different, possibly larger for spherical substrates. If this is the case, in this specific sample, the contact angle of the flat substrate might not adequately represent the contact angle of the particle at the liquid-liquid interface.

In any case, if the 10% treatment particles were in fact in a heterogeneous wetting regime, stability of the emulsions would be expected to be reduced, since a smaller degree of "effective" roughness relevant for film breakage is present. Furthermore, desorption of particles to the aqueous fluid phase should be less costly if a fraction of the surface area is already in contact with water.

In summary, surface roughness in Pickering emulsification appears to enhance the emulsion stability of o/w emulsion of a non-polar oil, up to a certain extent. Heterogeneous wetting is suggested as one potential cause for loss of emulsion stability for the roughest particles, but in this case, the effect of roughness on stabilization should depend on the initial state of the system. The particle wetting regime should be explored further as it appears to be crucial in the effect of particle roughness on emulsion stability.

6.3.3. Octanol as model for a polar oil

The results of emulsification experiments with octanol/water systems with rough and smooth particles are much more complicated than those for the decane/water system. In the first place, the emulsion type was not the same for the different particles tested. By

a simple drop test, the type of the main emulsion phase was determined as o/w for the roughest particles (10% treatment) and w/o for all the rest. Microscopic observation of the emulsions showed the existence of both types of emulsions in most samples, but to a larger extent with rougher particles.

As previously mentioned, the contact angle measurements of octanol were taken with an equilibrated drop. However, it is important to mention that the octanol drops usually took the longest to equilibrate (~ 4 min), and for the rougher surfaces started at values clearly below 90°. This might be relevant, as the emulsification time has been only 20 sec, thus particle adsorption should occur before an equilibrium position is reached. It is suggested, that the contact angle of the particles in the octanol/water systems show a higher degree of hysteresis, where initially the particles have lower contact angles which change over time, thus producing both types of emulsions, especially since the 90° threshold is crossed.

The droplets observed were typically completely covered by the particles, and showed some deformation due to shear. The emulsions before and after centrifugation are shown in **Figure 6.9.** As can be seen from this image, the emulsion prepared with 10% treated particles has an o/w emulsion phase between the water and oil after centrifugation, while for all the rest, it appears that the w/o emulsion gets transferred through the interface into water, thus producing a network of particle-covered water droplets and aggregates.

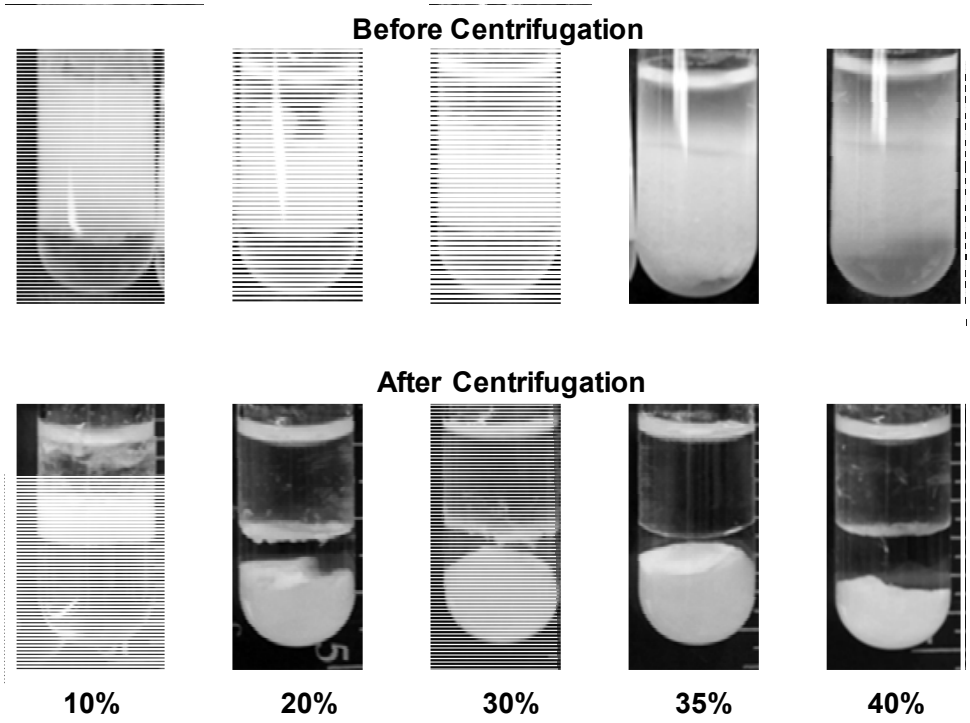

Figure 6.9. Images of octanol/water emulsions stabilized with particles of different degrees of surface roughness. *Top: Before centrifugation. Bottom: After 1 hr centrifugation at 1000 rpm.*

Clearly, these results are very difficult to analyze in order to elucidate the role of surface roughness for emulsification of a non-polar oil, and quantitative information is therefore not presented. Nonetheless, it is evident that the particle surface roughness has clear effect on emulsification, which might be related to contact angle hysteresis and the dynamics of spreading and emulsification.

6.4 Conclusions

From the presented data, it can be concluded that the generated nanoparticle-coated surfaces can be tuned to different degrees of surface roughness and wettability. Coating nanoparticle size is an important parameter to determine surface roughness and wettability beyond this sole parameter. Furthermore, the surfaces can behave as

hydrophilic or hydrophobic depending on the system under study, and on the degree of roughness.

Particles with different degree of surface roughness have been applied to study the effect of particle surface roughness on Pickering emulsification with a decane/water system. Particles of different surface roughness showed no effects on emulsion droplet size and surface coverage, thus discarding the previously suggested idea that rough particles produce low coverage droplets due to adsorption kinetics effects [*112*]. Although the timescale for reaching an equilibrium position at the interface (i.e. contact angle) is expected to vary, the potential differences in the particle's Brownian motion timescale due to roughness do not seem to be important for emulsification purposes.

Although roughness does not appear to have an effect on the emulsion type, or average droplet size, in the decane/water system, it appears to be important in the long-term emulsion stability. Centrifugation has been used to characterize long-term emulsion stability by the maximum capillary pressure at which an emulsion breaks. The results show that up to a certain extent rougher particles are better stabilizers of emulsions than smooth particles. Nontheless, the roughest particles tested are an outlier for this trend, suggesting heterogeneous wetting regime which in this case reduces the stabilization capability of the particles. From the rest of the data shown, believed to be in the homogeneous wetting regime, it is suggested that surface roughness does enhance emulsion stability. Therefore, it appears as if the wetting regime of the particles at the liquid-liquid interface is important to determine the surface roughness effect on emulsification.

CHAPTER 7

CONCLUSIONS AND FUTURE OUTLOOK

Microcapsules generated from Pickering emulsion templates, i.e., colloidosomes, have been suggested as an ideal microencapsulation technology due to the advantages that come from using solid particles as building blocks for a microcapsule shell. Nonetheless, colloidosomes produced with high encapsulation efficiency and yield, and which integrate a mild stimulus-triggered release as well as a tunable permeability had not been shown before. This work focuses on two main areas: a thorough application-oriented study for the generation of fully functional colloidosomes, and some fundamental studies regarding the stability of Pickering emulsions, which is crucial for their use as microcapsule templates.

pH-responsive nanoparticles, synthesized from enteric coating polymers by a simple nanoprecipitation method, can be successfully applied as building blocks of stimulus-responsive colloidosomes with a triggered dissolution above pH 7. These colloidosomes are prepared by a double emulsion-solvent extraction method, thus ensuring high yield and encapsulation efficiency. Furthermore, the permeability of these colloidosomes prior to dissolution can be efficiently measured by FRAP with a newly developed model, suitable for capsules of any size and permeability value.

The permeability of pH-responsive colloidosomes can be further tuned by one of three shown methods: 1) ethanol consolidation, 2) layer-by-layer assembly and 3) hybrid PLGA-nanoparticle colloidosome generation. The various types of colloidosomes produced result in a different stimulus-response to a slight pH increase. Moreover, the permeability before and after a release triggering can be assessed, thus providing many options for generating functional colloidosomes with pre-defined stimulus response and

permeability that can be adjusted to the desired values depending on the application. This work is thus very relevant as microencapsulation techniques and especially colloidosome-based microcapsules become increasingly important in many different areas. This work provides a basis for future application of colloidosomes as efficient microencapsulation vehicles, with different materials and stimulus-response. Still, an additional parameter which can be further improved is the colloidosome size uniformity, by applying microfluidics or membrane emulsification to the generation of such colloidosomes.

As the initial pH-responsive colloidosomes were realized, many simultaneous requirements had to be met. Clearly, fully understanding the role of each parameter at a fundamental level is a much larger undertaking, beyond the scope of this dissertation. In turn, one specific issue is studied at the fundamental level, regarding the generation of stable Pickering emulsions, which is a crucial requirement for colloidosome generation.

Although several studies have been focused on Pickering emulsion stabilization with particle wettability, concentration and oil type, among others, the role of particle surface roughness in Pickering emulsification is far from understood and greatly lacking experimental evidence. In order to elucidate one specific fundamental aspect for Pickering emulsification, which greatly lacks experimental evidence, the role of particle surface roughness on emulsion stabilization has been studied. This aspect was selected for in-depth studies as the pH-responsive nanoparticles generated provide an experimental basis for systematic studies of particles with various degrees of surface roughness but identical surface chemistry

These pH-responsive nanoparticles have been applied as coatings for flat and spherical substrates, thus generating rough surfaces. By treating such particle-coated substrates via partial dissolution, the surface roughness can be effectively tuned while keeping the surface chemistry constant.

Such spherical substrates have been applied as Pickering emulsifiers in order to study the effect of surface roughness on stabilization. Additionally, the wettability and roughness of the flat substrates has been determined and taken as indicative of the spherical substrate characteristics. These emulsification studies suggest that particle surface roughness is in fact relevant for emulsion stability, quantified by the maximum capillary pressure obtained by centrifugation. The results show that rougher particles are better stabilizers up to a certain extent, where potential heterogeneous wetting regimes come into play and are detrimental for emulsion stability in this specific system. These results thus appear to corroborate the theoretical predictions that particle roughness enhances emulsion stability. The work developed in this regard is of high importance since controlled experimental corroboration of some theoretical studies was previously unavailable. Nevertheless, there are still many open questions. Mainly, the wetting regime seems to be important, and thus exploring this in relation with Pickering emulsification might help to improve the so-far studied scheme of roughness and Pickering emulsification.

This work can be the starting point of a series of experimental works on roughness as a new parameter for Pickering emulsion stabilization. The heteroaggregates developed with different degrees of surface roughness could be applied to experimental studies of inter-particle capillary interactions at liquid-liquid interfaces, for example.

Furthermore, the generated rough and smooth flat substrates can prove useful as hydrophilic surfaces with a tunable wettability and a pH-response, or for testing the influence of roughness on electric surface conductance. Additionally, the generated particles with different degrees of surface roughness could potentially be applied as coatings to generate hierarchical structures with different levels of roughness.

APPENDIX A

PUBLICATIONS AND SCIENTIFIC PRESENTATIONS

A.1 Peer-Reviewed Publications

1. **A. San Miguel**, S. H. Behrens: Permeability Control in Stimulus-Responsive *Colloidosomes*, Soft Matter **7**, 1948 – 1956 (2011).
2. **A. San Miguel**, J. Scrimgeour, J. E. Curtis, **S**. H. Behrens: *Smart Colloidosomes with a Dissolution Trigger*, Soft Matter **6**, 3163-3166 (2010).
3. J. Rubin, **A. San Miguel**, A. S. Bommarius, S. H. Behrens: *Correlating Aggregation Kinetics and Stationary Diffusion in Protein – Sodium Salt Systems Observed with Dynamic Light Scattering*, J. Phys. Chem. B **114**, 4383 – 4387 (2010).
4. J. Scrimgeour, **A. San Miguel**, S.H. Behrens, J.E. Curtis: *FRAP as a measurement tool for microcapsule permeability* (in preparation)
5. **A. San Miguel**, S.H. Behrens: *The role of particle surface roughness in Pickering emulsion stability* (in preparation)

A.2 Other Publications

6. **A. San Miguel and S.H. Behrens**, *Microcapsules with Controlled Porosity for Triggered Release Applications and Tissue Scaffolding*, GT Invention Disclosure 5383 (2010).
7. **A. San Miguel**, J. Scrimgeour, J.E. Curtis, S.H. Behrens: *pH-Responsive Microcapsules from Double Pickering Emulsions* Smart Polymer Systems, 2010, iSmithers. *Conference Proceeding.*

A.3 Scientific Presentations

1. **A. San Miguel**, J. Scrimgeour, J.E. Curtis, S.H. Behrens. November 2009 AIChE Annual Meeting, Nashville, TN. *pH-Responsive microcapsules from Pickering emulsion templates.*

2. **A. San Miguel**, S.H. Behrens. December 2010. Atlanta Colloid & Soft Matter Bag Lunch Seminar, Atlanta, GA. *Colloidosomes with a dissolution trigger.*
3. **A. San Miguel**, S.H. Behrens. April 2010 ChBE Graduate Student Symposium, Georgia Tech, Atlanta, GA. *pH-Responsive microcapsules from Pickering emulsion templates.*
4. **A. San Miguel**, S.H. Behrens. August 2010 Universidad Autónoma de San Luis Potosí, SLP, México. Invited seminar speaker. *Coloidosomas sensibles a estímulos*. (Stimulus-sensitive colloidosomes)
5. **A. San Miguel,** J. Rubin, A. Bommarius and S.H. Behrens. October 2010. IBB Industry Partners Symposium, Georgia Tech, *Prediction and Accelerated Test of Protein Aggregation*,
6. **A. San Miguel**, S.H. Behrens. October 2010. Ziegler Award Presentation, ChBE Seminar Series. Georgia Institute of Technology *Functional colloidosomes: tunable permeability and stimulus-responsive release*
7. **A. San Miguel**, S.H. Behrens. November 2010. AIChE Annual Meeting, Salt Lake City, UT, *Emulsion Stabilization with Rough and Smooth Particles: The role of surface Roughness for Pickering Emulsification*.
8. **A. San Miguel**, S.H. Behrens. April 2011. Atlanta Colloid & Soft Matter Bag Lunch Seminar, Atlanta, GA. *Surfaces with tunable roughness studied by AFM and contact angle measurements.*

A.4 Poster Presentations

9. **A. San Miguel**, S.H. Behrens. November 2010. AIChE Annual Meeting, Salt Lake City, UT, *pH-Responsive Nanoparticles, Colloidosomes and Hybrid Microcapsules: Triggered Release and Tunable Permeability*.
10. **A. San Miguel**, S.H. Behrens. February 2011. Georgia Tech Research and Innovation Conference. *pH-Responsive Nanoparticles, Colloidosomes and Hybrid Microcapsules*.

REFERENCES

1. Gibbs, B. F., Kermasha, S., Alli, I., and Mulligan, C. N. Encapsulation in the food industry: a review, *Int. J. Food Sci. Nutr.,* **50**, 213-224, (1999).
2. Hemsley, A. R., and Griffiths, P. C. Architecture in the microcosm: biocolloids, self-assembly and pattern formation, *Philos. Trans. R. Soc. Lond. Ser. A-Math. Phys. Eng. Sci.,* **358**, 547-564, (2000).
3. Jain, R. A. The manufacturing techniques of various drug loaded biodegradable poly(lactide-co-glycolide) (PLGA) devices, *Biomaterials,* **21**, 2475-2490, (2000).
4. Rossier-Miranda, F. J., Schroen, C., and Boom, R. M. Colloidosomes: Versatile microcapsules in perspective, *Colloids and Surfaces A: Physicochemical and Engineering Aspects,* **343**, 43-49, (2009).
5. Kamen, M. E., Bernstein, P., and Rivero, R. T. Method of Encapsulating Pigment Particles Useful in the Manufacturing of Cosmetic Products and the Products Thereof, *5,234,711,* (1993).
6. Yow, H. N., and Routh, A. F. Formation of liquid core-polymer shell microcapsules, *Soft Matter,* **2**, 940-949, (2006).
7. Hawlader, M. N. A., Uddin, M. S., and Khin, M. M. Microencapsulated PCM thermal-energy storage system, *Applied Energy,* **74**, 195-202, (2003).
8. Chu, L.-Y., Park, S.-H., Yamaguchi, T., and Nakao, S.-i. Preparation of Micron-Sized Monodispersed Thermoresponsive Core-Shell Microcapsules, *Langmuir,* **18**, 1856-1864, (2002).
9. Peyratout, C. S., and Dahne, L. Tailor-made polyelectrolyte microcapsules: From multilayers to smart containers, *Angew. Chem.-Int. Edit.,* **43**, 3762-3783, (2004).
10. Goosen, M. F. A., Oshea, G. M., Gharapetian, H. M., Chou, S., and Sun, A. M. Optimization of Microencapsulation Parameters - Semipermeable Microcapsules as a Bioartificial Pancreas, *Biotechnol. Bioeng.,* **27**, 146-150, (1985).
11. Velev, O. D., Furusawa, K., and Nagayama, K. Assembly of latex particles by using emulsion droplets as templates .1. Microstructured hollow spheres, *Langmuir,* **12**, 2374-2384, (1996).
12. Dinsmore, A. D., Hsu, M. F., Nikolaides, M. G., Marquez, M., Bausch, A. R., and Weitz, D. A. Colloidosomes: Selectively permeable capsules composed of colloidal particles, *Science,* **298**, 1006-1009, (2002).

13. Hsu, M. F., Nikolaides, M. G., Dinsmore, A. D., Bausch, A. R., Gordon, V. D., Chen, X., Hutchinson, J. W., and Weitz, D. A. Self-assembled shells composed of colloidal particles: Fabrication and characterization, *Langmuir,* **21**, 2963-2970, (2005).

14. Ramsden, W. "Separation of solids in the surface-layers of solutions and 'Suspensions' (Observations on surface-membranes, bubbles, emulsions, and mechanical coagulation). Preliminary Account.", *Proc. R. Soc. London,* **72**, 156-164, (1903).

15. Pickering, S. U. Emulsions, *Journal of the Chemical Society,* **91**, 2001-2021, (1907).

16. Levine, S., Bowen, B. D., and Partridge, S. J. Stabilization of Emulsions by Fine Particles.1.Partitioning of Particles between Continuous Phase and Oil-Water Interface, *Colloids and Surfaces,* **38**, 325-343, (1989).

17. Binks, B. P. Particles as surfactants - similarities and differences, *Curr. Opin. Colloid Interface Sci.,* **7**, 21-41, (2002).

18. Bancroft, W. D. The theory of emulsification, V, *J. Phys. Chem.,* **17**, 501-519, (1913).

19. Aveyard, R., Binks, B. P., and Clint, J. H. Emulsions stabilised solely by colloidal particles, *Adv. Colloid Interface Sci.,* **100**, 503-546, (2003).

20. Binks, B. P., and Lumsdon, S. O. Effects of oil type and aqueous phase composition on oil-water mixtures containing particles of intermediate hydrophobicity, *PCCP Phys. Chem. Chem. Phys.,* **2**, 2959-2967, (2000).

21. Kaptay, G. On the equation of the maximum capillary pressure induced by solid particles to stabilize emulsions and foams and on the emulsion stability diagrams, *Colloid Surf. A-Physicochem. Eng. Asp.,* **282**, 387-401, (2006).

22. Lin, Y., Boker, A., Skaff, H., Cookson, D., Dinsmore, A. D., Emrick, T., and Russell, T. P. Nanoparticle assembly at fluid interfaces: Structure and dynamics, *Langmuir,* **21**, 191-194, (2005).

23. Lin, Y., Skaff, H., Emrick, T., Dinsmore, A. D., and Russell, T. P. Nanoparticle assembly and transport at liquid-liquid interfaces, *Science,* **299**, 226-229, (2003).

24. Binks, B. P., and Lumsdon, S. O. Catastrophic phase inversion of water-in-oil emulsions stabilized by hydrophobic silica, *Langmuir,* **16**, 2539-2547, (2000).

25. Kralchevsky, P. A., Ivanov, I. B., Ananthapadmanabhan, K. P., and Lips, A. On the thermodynamics of particle-stabilized emulsions: Curvature effects and catastrophic phase inversion, *Langmuir,* **21**, 50-63, (2005).

26. Ngai, T., Auweter, H., and Behrens, S. H. Environmental responsiveness of microgel particles and particle-stabilized emulsions, *Macromolecules,* **39**, 8171-8177, (2006).

27. Read, E. S., Fujii, S., Amalvy, J. I., Randall, D. P., and Armes, S. P. Effect of varying the oil phase on the behavior of pH-responsive latex-based emulsifiers: Demulsification versus transitional phase inversion, *Langmuir,* **20**, 7422-7429, (2004).

28. Binks, B. P., and Lumsdon, S. O. Influence of particle wettability on the type and stability of surfactant-free emulsions, *Langmuir,* **16**, 8622-8631, (2000).

29. Binks, B. P., and Rodrigues, J. A. Inversion of emulsions stabilized solely by ionizable nanoparticles, *Angew. Chem.-Int. Edit.,* **44**, 441-444, (2005).

30. Marinova, K. G., Alargova, R. G., Denkov, N. D., Velev, O. D., Petsev, D. N., Ivanov, I. B., and Borwankar, R. P. Charging of oil-water interfaces due to spontaneous adsorption of hydroxyl ions, *Langmuir,* **12**, 2045-2051, (1996).

31. Leunissen, M. E., van Blaaderen, A., Hollingsworth, A. D., Sullivan, M. T., and Chaikin, P. M. Electrostatics at the oil-water interface, stability, and order in emulsions and colloids, *Proc. Natl. Acad. Sci. U. S. A.,* **104**, 2585-2590, (2007).

32. Golemanov, K., Tcholakova, S., Kralchevsky, P. A., Ananthapadmanabhan, K. P., and Lips, A. Latex-particle-stabilized emulsions of anti-Bancroft type, *Langmuir,* **22**, 4968-4977, (2006).

33. Menon, V. B., and Wasan, D. T. (1983) *Encyclopedia of Emulsion Technology.* , Vol. 2, Dekker.

34. Gautier, F., Destribats, M., Perrier-Cornet, R., Dechezelles, J. F., Giermanska, J., Heroguez, V., Ravaine, S., Leal-Calderon, F., and Schmitt, V. Pickering emulsions with stimulable particles: from highly- to weakly-covered interfaces, *PCCP Phys. Chem. Chem. Phys.,* **9**, 6455-6462, (2007).

35. Tcholakova, S., Denkov, N. D., and Lips, A. Comparison of solid particles, globular proteins and surfactants as emulsifiers, *PCCP Phys. Chem. Chem. Phys.,* **10**, 1608-1627, (2008).

36. Tcholakova, S., Denkov, N. D., Ivanov, I. B., and Campbell, B. Coalescence in beta-lactoglobulin-stabilized emulsions: Effects of protein adsorption and drop size, *Langmuir,* **18**, 8960-8971, (2002).

37. Nushtayeva, A. V., and Kruglyakov, P. M. Capillary pressure in a thinning emulsion film stabilised by spherical solid particles, *Mendeleev Commun.*, 235-237, (2001).

38. Nushtaeva, A. V., and Kruglyakov, P. M. Capillary pressure in thinning emulsion film stabilized with solid spherical particles, *Colloid J.,* **65**, 341-349, (2003).

39. Kruglyakov, P. M., Nushtayeva, A., and Vilkova, N. G. Experimental investigation of capillary pressure influence on breaking of emulsions stabilized by solid particles, *Journal of Colloid and Interface Science,* **276**, 465-474, (2004).

40. Hunter, T. N., Pugh, R. J., Franks, G. V., and Jameson, G. J. The role of particles in stabilising foams and emulsions, *Adv. Colloid Interface Sci.,* **137**, 57-81, (2008).

41. Denkov, N. D., Ivanov, I. B., Kralchevsky, P. A., and Wasan, D. T. A POSSIBLE MECHANISM OF STABILIZATION OF EMULSIONS BY SOLID PARTICLES, *Journal of Colloid and Interface Science,* **150**, 589-593, (1992).

42. Barthel, H., Binks, B. P., Dyab, A., and Fletcher, P. Multiple Emulsions, *US Patent 2003/0175317 A1,* (2003).

43. Lee, D., and Weitz, D. A. Double emulsion-templated nanoparticle colloidosomes with selective permeability, *Adv. Mater.,* **20**, 3498-3503, (2008).

44. Velev, O. D., and Nagayama, K. Assembly of latex particles by using emulsion droplets .3. Reverse (water in oil) system, *Langmuir,* **13**, 1856-1859, (1997).

45. Velev, O. D., Furusawa, K., and Nagayama, K. Assembly of latex particles by using emulsion droplets as templates .2. Ball-like and composite aggregates, *Langmuir,* **12**, 2385-2391, (1996).

46. Yow, H. N., and Routh, A. F. Release Profiles of Encapsulated Actives from Colloidosomes Sintered for Various Durations, *Langmuir,* **25**, 159-166, (2009).

47. Cayre, O. J., Noble, P. F., and Paunov, V. N. Fabrication of novel colloidosome microcapsules with gelled aqueous cores, *J. Mater. Chem.,* **14**, 3351-3355, (2004).

48. Noble, P. F., Cayre, O. J., Alargova, R. G., Velev, O. D., and Paunov, V. N. Fabrication of "hairy" colloidosomes with shells of polymeric microrods, *Journal of the American Chemical Society,* **126**, 8092-8093, (2004).

49. Ao, Z., Yang, Z., Wang, J. F., Zhang, G. Z., and Ngai, T. Emulsion-Templated Liquid Core-Polymer Shell Microcapsule Formation, *Langmuir,* **25**, 2572-2574, (2009).

50. Sander, J. S., and Studart, A. R. Monodisperse Functional Colloidosomes with Tailored Nanoparticle Shells, *Langmuir,* **27**, 3301-3307, (2011).

51. Caruso, F., Caruso, R. A., and Mohwald, H. Nanoengineering of inorganic and hybrid hollow spheres by colloidal templating, *Science,* **282**, 1111-1114, (1998).

52. Shilpi, S., Jain, A., Gupta, Y., and Jain, S. K. Colloidosomes: An emerging vesicular system in drug delivery, *Crit. Rev. Ther. Drug Carr. Syst.,* **24**, 361-391, (2007).

53. Lawrence, D. B., Cai, T., Hu, Z., Marquez, M., and Dinsmore, A. D. Temperature-responsive semipermeable capsules composed of colloidal microgel spheres, *Langmuir,* **23**, 395-398, (2007).

54. Kim, J.-H., and Lee, T. R. Thermo- and pH-Responsive Hydrogel-Coated Gold Nanoparticles, *Chem. Mat.,* **16**, 3647-3651, (2004).

55. Shah, R. K., Kim, J. W., and Weitz, D. A. Monodisperse Stimuli-Responsive Colloidosomes by Self-Assembly of Microgels in Droplets, *Langmuir,* **26**, 1561-1565, (2010).

56. Cejková, J., Hanus, J., and Stepánek, F. Investigation of internal microstructure and thermo-responsive properties of composite PNIPAM/silica microcapsules, *Journal of Colloid and Interface Science,* **346**, 352-360,

57. Bivas-Benita, M., Romeijn, S., Junginger, H. E., and Borchard, G. PLGA-PEI nanoparticles for gene delivery to pulmonary epithelium, *Eur. J. Pharm. Biopharm.,* **58**, 1-6, (2004).

58. Wang, J. J., Chua, K. M., and Wang, C. H. Stabilization and encapsulation of human immunoglobulin G into biodegradable microspheres, *Journal of Colloid and Interface Science,* **271**, 92-101, (2004).

59. Vrancken, M. N., and Claeys, D. A. Process for Encapsulating Water and Compounds in Aqueous Phase by Evaporation, (1970).

60. Ogawa, Y., Yamamoto, M., Okada, H., Yashiki, T., and Shimamoto, T. A New Technique to Efficiently Entrap Leuprolide Acetate into Microcapsules of Polylactic Acid or Copoly(Lactic Glycolic) Acid, *Chem. Pharm. Bull.,* **36**, 1095-1103, (1988).

61. El-Kamel, A. H., Sokar, M. S., Al Gamal, S. S., and Naggar, V. F. Preparation and evaluation of ketoprofen floating oral delivery system, *International Journal of Pharmaceutics,* **220**, 13-21, (2001).

62. Sato, Y., Kawashima, Y., Takeuchi, H., and Yamamoto, H. In vitro evaluation of floating and drug releasing behaviors of hollow microspheres (microballoons) prepared by the emulsion solvent diffusion method, *Eur. J. Pharm. Biopharm.,* **57**, 235-243, (2004).

63. Lee, J. H., Park, T. G., and Choi, H. K. Effect of formulation and processing variables on the characteristics of microspheres for water-soluble drugs prepared

by w/o/o double emulsion solvent diffusion method, *International Journal of Pharmaceutics,* **196**, 75-83, (2000).

64. Cayre, O. J., and Biggs, S. Hollow microspheres with binary porous membranes from solid-stabilised emulsion templates, *J. Mater. Chem.,* **19**, 2724-2728, (2009).

65. Yow, H. N., and Routh, A. F. Colloidal buckets formed via internal phase separation, *Soft Matter,* **4**, 2080-2085, (2008).

66. Squillante, E., Morshed, G., Bagchi, S., and Mehta, K. A. Microencapsulation of beta-galactosidase with Eudragit L-100, *Journal of Microencapsulation,* **20**, 153-167, (2003).

67. Kilicarslan, M., and Baykara, T. Effects of the permeability characteristics of different polymethacrylates on the pharmaceutical characteristics of verapamil hyhdrochloride-loaded microspheres, *Journal of Microencapsulation,* **21**, 175-189, (2004).

68. Jain, D., Majumdar, D. K., and Panda, A. K. Insulin loaded Eudragit L100 microspheres for oral delivery: Preliminary in vitro studies, *Journal of Biomaterials Applications,* **21**, 195-211, (2006).

69. Jain, D., Panda, A. K., and Majumdar, D. K. Eudragit S100 entrapped insulin microspheres for oral delivery, *AAPS PharmSciTech,* **6**, (2005).

70. Schonhoff, M. Self-assembled polyelectrolyte multilayers, *Curr. Opin. Colloid Interface Sci.,* **8**, 86-95, (2003).

71. Qiu, X. P., Leporatti, S., Donath, E., and Mohwald, H. Studies on the drug release properties of polysaccharide multilayers encapsulated ibuprofen microparticles, *Langmuir,* **17**, 5375-5380, (2001).

72. Caruso, F., Trau, D., Mohwald, H., and Renneberg, R. Enzyme encapsulation in layer-by-layer engineered polymer multilayer capsules, *Langmuir,* **16**, 1485-1488, (2000).

73. Bon, S. A. F., and Colver, P. J. Pickering Miniemulsion Polymerization Using Laponite Clay as a Stabilizer, *Langmuir,* **23**, 8316-8322, (2007).

74. Colver, P. J., Chen, T., and Bon, S. A. F. Supracolloidal Structures through Liquid-Liquid Interface Driven Assembly and Polymerization, *Macromolecular Symposia,* **245-246**, 34-41, (2006).

75. Antonietti, M., and Forster, S. Vesicles and liposomes: A self-assembly principle beyond lipids, *Adv. Mater.,* **15**, 1323-1333, (2003).

76. Discher, B. M., Won, Y. Y., Ege, D. S., Lee, J. C. M., Bates, F. S., Discher, D. E., and Hammer, D. A. Polymersomes: Tough vesicles made from diblock copolymers, *Science,* **284**, 1143-1146, (1999).

77. Ngai, T., Behrens, S. H., and Auweter, H. Novel emulsions stabilized by pH and temperature sensitive microgels, *Chemical Communications*, 331-333, (2005).

78. Fujii, S., Read, E. S., Binks, B. P., and Armes, S. P. Stimulus-responsive emulsifiers based on nanocomposite microgel particles, *Adv. Mater.,* **17**, 1014-+, (2005).

79. Kim, J. W., Fernandez-Nieves, A., Dan, N., Utada, A. S., Marquez, M., and Weitz, D. A. Colloidal assembly route for responsive colloidosomes with tunable permeability, *Nano Lett.,* **7**, 2876-2880, (2007).

80. Marmur, A. The Lotus Effect: Superhydrophobicity and Metastability, *Langmuir,* **20**, 3517-3519, (2004).

81. Barthlott, W., and Neinhuis, C. Purity of the sacred lotus, or escape from contamination in biological surfaces, *Planta,* **202**, 1-8, (1997).

82. Herminghaus, S. Roughness-induced non-wetting, *Europhysics Letters,* **52**, 165-170, (2000).

83. Gao, X. F., and Jiang, L. Water-repellent legs of water striders, *Nature,* **432**, 36-36, (2004).

84. Nosonovsky, M., and Bhushan, B. Biologically inspired surfaces: Broadening the scope of roughness, *Advanced Functional Materials,* **18**, 843-855, (2008).

85. Patankar, N. A. Mimicking the lotus effect: Influence of double roughness structures and slender pillars, *Langmuir,* **20**, 8209-8213, (2004).

86. Dorrer, C., and Ruhe, J. Some thoughts on superhydrophobic wetting, *Soft Matter,* **5**, 51-61, (2009).

87. Roach, P., Shirtcliffe, N. J., and Newton, M. I. Progess in superhydrophobic surface development, *Soft Matter,* **4**, 224-240, (2008).

88. Erbil, H. Y., Demirel, A. L., Avci, Y., and Mert, O. Transformation of a simple plastic into a superhydrophobic surface, *Science,* **299**, 1377-1380, (2003).

89. Balu, B., Kim, J. S., Breedveld, V., and Hess, D. W. Tunability of the Adhesion of Water Drops on a Superhydrophobic Paper Surface via Selective Plasma Etching, *J. Adhes. Sci. Technol.,* **23**, 361-380, (2009).

90. Marmur, A. Wetting on hydrophobic rough surfaces: To be heterogeneous or not to be?, *Langmuir,* **19**, 8343-8348, (2003).

91. Patankar, N. A. On the modeling of hydrophobic contact angles on rough surfaces, *Langmuir,* **19**, 1249-1253, (2003).

92. Martines, E., Seunarine, K., Morgan, H., Gadegaard, N., Wilkinson, C. D. W., and Riehle, M. O. Superhydrophobicity and superhydrophilicity of regular nanopatterns, *Nano Lett.,* **5**, 2097-2103, (2005).

93. Abdelsalam, M. E., Bartlett, P. N., Kelf, T., and Baumberg, J. Wetting of Regularly Structured Gold Surfaces, *Langmuir,* **21**, 1753-1757, (2005).

94. Burton, Z., and Bhushan, B. Hydrophobicity, Adhesion, and Friction Properties of Nanopatterned Polymers and Scale Dependence for Micro- and Nanoelectromechanical Systems, *Nano Lett.,* **5**, 1607-1613, (2005).

95. Bico, J., Thiele, U., and Quere, D. Wetting of textured surfaces, *Colloid Surf. A-Physicochem. Eng. Asp.,* **206**, 41-46, (2002).

96. Tuteja, A., Choi, W., Ma, M. L., Mabry, J. M., Mazzella, S. A., Rutledge, G. C., McKinley, G. H., and Cohen, R. E. Designing superoleophobic surfaces, *Science,* **318**, 1618-1622, (2007).

97. Marmur, A. Underwater Superhydrophobicity: Theoretical Feasibility, *Langmuir,* **22**, 1400-1402, (2006).

98. Motornov, M., Sheparovych, R., Lupitskyy, R., MacWilliams, E., and Minko, S. Responsive colloidal systems: Reversible aggregation and fabrication of superhydrophobic surfaces, *Journal of Colloid and Interface Science,* **310**, 481-488, (2007).

99. Wenzel, R. N. Resistance of solid surfaces to wetting by water, *Industrial and Engineering Chemistry,* **28**, 988-994, (1936).

100. Cassie, A. B. D., and Baxter, S. Wettability of porous surfaces, *Transactions of the Faraday Society,* **40**, 0546-0550, (1944).

101. Israelachvili, J. N., and Gee, M. L. CONTACT ANGLES ON CHEMICALLY HETEROGENEOUS SURFACES, *Langmuir,* **5**, 288-289, (1989).

102. Quere, D., Lafuma, A., and Bico, J. Slippy and sticky microtextured solids, *Nanotechnology,* **14**, 1109-1112, (2003).

103. Oner, D., and McCarthy, T. J. Ultrahydrophobic surfaces. Effects of topography length scales on wettability, *Langmuir,* **16**, 7777-7782, (2000).

104. Barbieri, L., Wagner, E., and Hoffmann, P. Water wetting transition parameters of perfluorinated substrates with periodically distributed flat-top microscale obstacles, *Langmuir,* **23**, 1723-1734, (2007).

105. Lau, K. K. S., Bico, J., Teo, K. B. K., Chhowalla, M., Amaratunga, G. A. J., Milne, W. I., McKinley, G. H., and Gleason, K. K. Superhydrophobic Carbon Nanotube Forests, *Nano Lett.,* **3**, 1701-1705, (2003).

106. Suh, K. Y., and Jon, S. Control over Wettability of Polyethylene Glycol Surfaces Using Capillary Lithography, *Langmuir,* **21**, 6836-6841, (2005).

107. Leroy, F., and Muller-Plathe, F. Rationalization of the Behavior of Solid-Liquid Surface Free Energy of Water in Cassie and Wenzel Wetting States on Rugged Solid Surfaces at the Nanometer Scale, *Langmuir,* **27**, 637-645, (2011).

108. Kwon, Y., Patankar, N., Choi, J., and Lee, J. Design of Surface Hierarchy for Extreme Hydrophobicity, *Langmuir,* **25**, 6129-6136, (2009).

109. Israelachvili, J. N. (2011) *Intermolecular and Surface Forces*, 3rd ed., Academic Press.

110. Ran, C. B., Ding, G. Q., Liu, W. C., Deng, Y., and Hou, W. T. Wetting on nanoporous alumina surface: Transition between Wenzel and Cassie states controlled by surface structure, *Langmuir,* **24**, 9952-9955, (2008).

111. Netz, R. R., and Andelman, D. Roughness-induced wetting, *Physical Review E,* **55**, 687-700, (1997).

112. Vignati, E., Piazza, R., and Lockhart, T. P. Pickering emulsions: Interfacial tension, colloidal layer morphology, and trapped-particle motion, *Langmuir,* **19**, 6650-6656, (2003).

113. Tadros, T. V., and Vincent, B. (1983) *Encyclopedia of Emulsion Technology.* , Vol. 1, Dekker.

114. Briggs, T. R. Emulsions with Finely Divided Solids, *Journal of Industrial & Engineering Chemistry,* **13**, 1008-1010, (1921).

115. Stamou, D., Duschl, C., and Johannsmann, D. Long-range attraction between colloidal spheres at the air-water interface: The consequence of an irregular meniscus, *Physical Review E,* **62**, 5263-5272, (2000).

116. Danov, K. D., Kralchevsky, P. A., Naydenov, B. N., and Brenn, G. Interactions between particles with an undulated contact line at a fluid interface: Capillary multipoles of arbitrary order, *Journal of Colloid and Interface Science,* **287**, 121-134, (2005).

117. Lucassen, J. Capillary forces between solid particles in fluid interfaces, *Colloids and Surfaces,* **65**, 131-137, (1992).

118. Kralchevsky, P. A., and Denkov, N. D. Capillary forces and structuring in layers of colloid particles, *Curr. Opin. Colloid Interface Sci.,* **6**, 383-401, (2001).

119. Oettel, M., Dominguez, A., and Dietrich, S. Effective capillary interaction of spherical particles at fluid interfaces, *Physical Review E,* **71**, (2005).

120. Nonomura, Y., and Komura, S. Surface activity of solid particles with extremely rough surfaces, *Journal of Colloid and Interface Science,* **317**, 501-506, (2008).

121. Nonomura, Y., Komura, S., and Tsujii, K. Adsorption of microstructured particles at liquid-liquid interfaces, *Journal of Physical Chemistry B,* **110**, 13124-13129, (2006).

122. Nonomura, Y., Komura, S., and Tsujii, K. Surface-active particles with microstructured surfaces, *Langmuir,* **21**, 9409-9411, (2005).

123. San Miguel, A., Scrimgeour, J., Curtis, J. E., and Behrens, S. H. Smart colloidosomes with a dissolution trigger, *Soft Matter,* **6**, 3163-3166, (2010).

124. San Miguel, A., and Behrens, S. H. Permeability control in stimulus-responsive colloidosomes, *Soft Matter,* **7**, 1948-1956, (2011).

125. Qiu, Y., and Park, K. Environment-sensitive hydrogels for drug delivery, *Adv. Drug Deliv. Rev.,* **53**, 321-339, (2001).

126. Alarcon, C. D. H., Pennadam, S., and Alexander, C. Stimuli responsive polymers for biomedical applications, *Chem. Soc. Rev.,* **34**, 276-285, (2005).

127. Abu-Lail, N. I., Kaholek, M., LaMattina, B., Clark, R. L., and Zauscher, S. Micro-cantilevers with end-grafted stimulus-responsive polymer brushes for actuation and sensing, *Sens. Actuator B-Chem.,* **114**, 371-378, (2006).

128. Suzuki, H. Stimulus-responsive gels: Promising materials for the construction of micro actuators and sensors, *J. Intell. Mater. Syst. Struct.,* **17**, 1091-1097, (2006).

129. Galaev, I. Y., and Mattiasson, B. 'Smart' polymers and what they could do in biotechnology and medicine, *Trends Biotechnol.,* **17**, 335-340, (1999).

130. Chuang, C.-Y., Don, T.-M., and Chiu, W.-Y. Synthesis and properties of chitosan-based thermo- and pH-responsive nanoparticles and application in drug release, *Journal of Polymer Science Part A: Polymer Chemistry,* **47**, 2798-2810, (2009).

131. Lu, A. H., Salabas, E. L., and Schuth, F. Magnetic nanoparticles: Synthesis, protection, functionalization, and application, *Angew. Chem.-Int. Edit.,* **46**, 1222-1244, (2007).

132. Evonik. (2007) Eudragit L100 and Eudragit S100 Specifications, In *http://www.pharma-polymers.com/pharmapolymers/en/eudragit/*.

133. BASF. (2009) Kollicoat MAE grades Technical information, In *http://www.pharma-ingredients.basf.com/*.

134. Aubry, J., Ganachaud, F., Addad, J. P. C., and Cabane, B. Nanoprecipitation of Polymethylmethacrylate by Solvent Shifting: 1. Boundaries, *Langmuir,* **25**, 1970-1979, (2009).

135. Ganachaud, F., and Katz, J. L. Nanoparticles and nanocapsules created using the Ouzo effect: Spontaneous emulsification as an alternative to ultrasonic and high-shear devices, *ChemPhysChem,* **6**, 209-216, (2005).

136. Vitale, S. A., and Katz, J. L. Liquid droplet dispersions formed by homogeneous liquid-liquid nucleation: "The ouzo effect", *Langmuir,* **19**, 4105-4110, (2003).

137. Fessi, H., Devissaguet, J., Puisieux, F., and Theis, C. Process for the preparation of dispersible colloidal systems of a substance in the form of nanoparticles. , *US Patent 5,118,528,* (1992).

138. Galindo-Rodriguez, S., Allemann, E., Fessi, H., and Doelker, E. Physicochemical parameters associated with nanoparticle formation in the salting-out, emulsification-diffusion, and nanoprecipitation methods, *Pharm. Res.,* **21**, 1428-1439, (2004).

139. Nguyen, C. A., Konan-Kouakou, Y. N., Allemann, E., Doelker, E., Quintanar-Guerrero, D., Fessi, H., and Gurny, R. Preparation of surfactant-free nanoparticles of methacrylic acid copolymers used for film coating, *AAPS PharmSciTech,* **7**, 7, (2006).

140. Provencher, S. W. A CONSTRAINED REGULARIZATION METHOD FOR INVERTING DATA REPRESENTED BY LINEAR ALGEBRAIC OR INTEGRAL-EQUATIONS, *Computer Physics Communications,* **27**, 213-227, (1982).

141. Wypych, G. (2008) Knovel Solvents - A Properties Database, (Publishing, C., Ed.).

142. BASF. (2004) Technical Bulletin. Pluronic F127, In *http://worldaccount.basf.com/*.

143. BASF. (2004) Technical bulletin. Pluronic 25R2, In *http://worldaccount.basf.com/*.

144. Cohen, S., Yoshioka, T., Lucarelli, M., Hwang, L. H., and Langer, R. CONTROLLED DELIVERY SYSTEMS FOR PROTEINS BASED ON POLY(LACTIC GLYCOLIC ACID) MICROSPHERES, *Pharm. Res.,* **8**, 713-720, (1991).

145. Binks, B. P., and Clint, J. H. Solid wettability from surface energy components: Relevance to pickering emulsions, *Langmuir,* **18**, 1270-1273, (2002).

146. Yaws, C. L., (Ed.) (2003) *Yaws' Handbook of Thermodynamic and Physical Properties of Chemical Compounds*, Knovel.

147. Green, D. W. P., Robert H., (Ed.) (2008) *Perry's Chemical Engineers' Handbook*, 8th ed., McGraw-Hill.

148. Speight, J., (Ed.) (2005) *Lange's Handbook of Chemistry.*, 16th ed., McGraw-Hill.

149. Sun, G. Q., Li, Z. F., and Ngai, T. Inversion of Particle-Stabilized Emulsions to Form High-Internal-Phase Emulsions, *Angew. Chem.-Int. Edit.,* **49**, 2163-2166, (2010).

150. Aveyard, R., Beake, B. D., and Clint, J. H. Wettability of spherical particles at liquid surfaces, *J. Chem. Soc.-Faraday Trans.,* **92**, 4271-4277, (1996).

151. Shah, R. K., Shum, H. C., Rowat, A. C., Lee, D., Agresti, J. J., Utada, A. S., Chu, L. Y., Kim, J. W., Fernandez-Nieves, A., Martinez, C. J., and Weitz, D. A. Designer emulsions using microfluidics, *Materials Today,* **11**, 18-27, (2008).

152. Shum, H. C., Lee, D., Yoon, I., Kodger, T., and Weitz, D. A. Double emulsion templated monodisperse phospholipid vesicles, *Langmuir,* **24**, 7651-7653, (2008).

153. Ibarz, G., Dahne, L., Donath, E., and Mohwald, H. Controlled permeability of polyelectrolyte capsules via defined annealing, *Chem. Mat.,* **14**, 4059-4062, (2002).

154. Lopez, A., Dupou, L., Altibelli, A., Trotard, J., and Tocanne, J. F. Fluorescence recovery after photobleaching (FRAP) experiments under conditions of uniform disk illumination. Critical comparison of analytical solutions, and a new mathematical method for calculation of diffusion coefficient D, *Biophysical Journal,* **53**, 963-970, (1988).

155. Soumpasis, D. M. Theoretical Analysis of Fluorescence Photobleaching Recovery Experiments, *Biophysical Journal,* **41**, 95-97, (1983).

156. Axelrod, D., Koppel, D. E., Schlessinger, J., Elson, E., and Webb, W. W. Mobility measurement by analysis of fluorescence photobleaching recovery kinetics, *Biophysical Journal,* **16**, 1055-1069, (1976).

157. Gribbon, P., and Hardingham, T. E. Macromolecular diffusion of biological polymers measured by confocal fluorescence recovery after photobleaching, *Biophysical Journal,* **75**, 1032-1039, (1998).

158. Sato, J., and Breedveld, V. Transient rheology of solvent-responsive complex fluids by integrating microrheology and microfluidics, *Journal of Rheology,* **50**, 1-19, (2006).

159. Caruso, F., Lichtenfeld, H., Giersig, M., and Mohwald, H. Electrostatic self-assembly of silica nanoparticle - Polyelectrolyte multilayers on polystyrene latex particles, *Journal of the American Chemical Society,* **120**, 8523-8524, (1998).

160. Caruso, F. Nanoengineering of particle surfaces, *Adv. Mater.,* **13**, 11-+, (2001).

161. Hammond, P. T. Form and Function in Multilayer Assembly: New Applications at the Nanoscale, *Adv. Mater.,* **16**, 1271-1293, (2004).

162. Goedel, W. A. A simple theory of particle-assisted wetting, *Europhysics Letters,* **62**, 607-613, (2003).

163. Xu, H., and Goedel, W. A. From particle-assisted wetting to thin free-standing porous membranes, *Angew. Chem.-Int. Edit.,* **42**, 4694-4696, (2003).

164. Paunov, V. N. Novel method for determining the three-phase contact angle of colloid particles adsorbed at air-water and oil-water interfaces, *Langmuir,* **19**, 7970-7976, (2003).

165. Xiao, H. N., and Cezar, N. Organo-modified cationic silica nanoparticles/anionic polymer as flocculants, *Journal of Colloid and Interface Science,* **267**, 343-351, (2003).

166. Kulkarni, S. A., Ogale, S. B., and Vijayamohanan, K. P. Tuning the hydrophobic properties of silica particles by surface silanization using mixed self-assembled monolayers, *Journal of Colloid and Interface Science,* **318**, 372-379, (2008).

167. Islam, A. M., Chowdhry, B. Z., and Snowden, M. J. Heteroaggregation in colloidal dispersions, *Adv. Colloid Interface Sci.,* **62**, 109-136, (1995).